Solid-state NMR structure studies of polyisocyanodipeptides and functionalized polyisocyanides

Solid-state NMR structure studies of polyisocyanodipeptides and functionalized polyisocyanides

Proefschrift

ter verkrijging van de graad van doctor
aan de Radboud Universiteit Nijmegen
op gezag van de rector magnificus prof. mr. S.C.J.J Kortmann,
volgens besluit van het college van decanen
in het openbaar te verdedigen
op vrijdag 03 mei 2013 om 13:00 uur precies

Chandrakala Mariswamy Gowda

geboren op 27 december 1979
te Bangalore, India

Promotor

Prof. dr. Arno P. M. Kentgens

Copromotor

Dr. Ernst R. H. van Eck

Manuscriptcommissie

Prof. Dr. Roeland J. M. Nolte

Dr. ir. Gilles A. de Wijs

Prof. dr. Matthias Ernst (ETH Zurich)

Solid-state NMR structure studies of polyisocyanodipeptides and functionalized polyisocyanides

Chandrakala Mariswamy Gowda

PhD Thesis, Radboud University Nijmegen, The Netherlands

This research has been financially supported by the "Nederlandse Organisatie voor Wetenschappelijk Onderzoek (NWO)"

ISBN: 978-94-6191-674-7
Printed by: Ipskamp Drukkers B.V., Enschede

voor mijn lieve ouders,

Table of Contents

Chapter 1

Introduction

1.1 Introduction to polyisocyanides

New synthetic materials and synthetic polymers are envisioned to be applied in various fields such as bio-medicine, biosensing, catalysis, opto-electronics to mention a few. Natural macromolecular systems such as DNA, RNAs, proteins and photosynthetic systems which possess extraordinary stability in structure and can perform complex tasks with extreme efficiency have inspired the design of synthetic polymers. The development of systems in which chromophores are ordered in a well-defined manner is of great interest for chemistry and material science.[1, 2] The coupling of the exciton interactions between the organized neighbouring dyes gives rise to unique photophysical and electronic properties. The research and development of new chromophoric arrays has been inspired by chromophoric systems commonly found in nature such as light harvesting antenna and photosynthetic centres used by green plants.[3] A delicate balance of local and long-range interactions defines the structure and functional properties of such supra- and macromolecular constructs. Synthetic chromophores are often self-organized by means of one or multiple interactions such as π–π stacking, hydrogen bonding, metal-ligand interactions, or electrostatic interactions.[4] However, self-organized systems are often very photo sensitive and are also influenced by factors such as solvent concentration, temperature etc.[5] Physisorption is an example of a technique that had been explored to organize the self-assembly of molecules on a surface.[5] An alternative method is to use rigid and stable polymers as structural scaffolds to covalently link the functional moieties. Polyguanidines,[6, 7] polycarbodiimides,[8] and polyisocyanides[9, 10] are some of the example of the polymers that have been explored for this purpose.

Polyisocyanides also known as polyisocyanonitriles or polyiminomethylene are one of the earliest of the polymers to have known to possess a stable helical conformation. The polyisocyanides have attracted interest in the research community due to their stability and rigid rod like helical structure.[9, 11, 12] Since the polymer helices are chiral in nature they have been used as enantiomer selective groups in chromatography and as

enantio-selective catalysts.[13] The basic molecular skeleton of the polyisocyanides can be represented as shown in Figure 1.1a. The structure allows that variety of chemical groups can be substituted as -R groups leading to the synthesis of a variety of polymers with different properties. The side chains (–R) when sufficiently bulky, lock the helix conformation due to steric interactions. The polyisocyanides with bulky side chains are thus associated with a high helix inversion barrier. With an aim of creating more stable and rigid polyisocyanides which can possess well defined secondary structure Cornelissen et al. synthesized peptide derived polyisocyanides.[14, 15] Inspired by the natural molecules such as the proteins and biomolecules they incorporated a similar design into the polyisocyanides. Amino acids such as alanine and glycine were used to form peptide derived polyisocyanides.[15] These are also called polyisocynaopeptides. Prefixes such as *–di*, *-tri* etc., are used to specify a single peptide bond, a double peptide bond etc., respectively as in *polyisocynaodipeptides* and *polyisocynaotripeptides*. The monomer unit L-isocyanoalanyl-D-alanine methyl ester (L,D-IAA), is shown in Figure 1.1b, and the corresponding polymer is shown in Figure 1.1c. The amino acids are chiral in nature. These chiral monomeric units bias the polymerization process leading to preferential formation of polymers of one screw sense over the other.[14] The introduction of amino acids resulted in N-H---C=O hydrogen bonding between the ‘n’ and ‘n+4’ sidechains of the polymer thus stabilizing the helix.[14, 16]

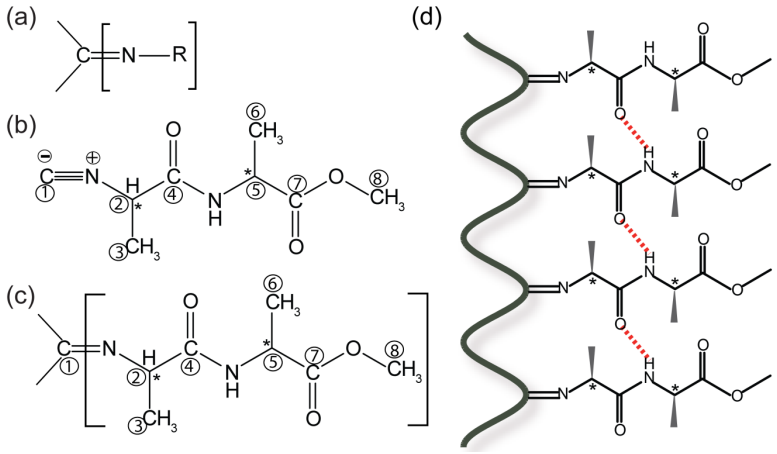

Figure 1.1 (a) Basic isocyanide polymer skeleton. (b) L-isocyaoalanyl-D-alanine methyl ester (L,D-IAA) monomer unit and (c) L-isocyanoalanyl-D-alanine methyl ester polymer (L,D-PIAA). The carbon positions are numbered in (b) and (c) for convenience in discussions. (d) Sketch of the L,D-PIAA showing the hydrogen bonds between 'n' and 'n+4' side chains. (left, outwards and into the plane of the drawing are omitted for clarity). The asterisks in (b) and (c) indicate chiral centers in the amino acids.

Polyisocyanodipeptides are shown to possess a persistence length of ~76 nm and hence form attractive scaffolds for the arrangement of electronically and optically interesting molecules and have been extensively studied over the last few years.[17-21] The perylenediimide moiety incorporated as side chain substituent to the backbone scaffold of the polyisocyanopeptide showed high exciton migration rates and charge densities.[22] UV/Vis absorption spectroscopy studies of porphyrin functionalized polyisocyanopeptides showed that the porphyrin stacks were excitationally coupled.[23] Carbazole functionalized polyisocyanopeptide grown on a silicon wafer were successfully incorporated into Light Emitting Diodes (LEDs).[24] Functionalized polymers can be exploited for applications in photovoltaic devices, LEDs, field effect transistors (FETs) and electrochromic devices etcetera. All these applications and further tuning, designing, and molding the properties of the materials requires precise knowledge of the molecular structure.

The structural conformation of polyisocyanides has been a subject of discussion for several decades and there have been various experimental and theoretical efforts to determine the structure and conformation of polyisocyanides.[9, 10, 25-28] The earliest

structural studies of polyisocyanides used Leybold molecular models of poly(α-phenylethyl isocyanide) indicating a tightly coiled helical structure for the polymer.[25] X-ray diffraction experiments were indicative of a conformation with one repeat unit per 1.0Å of the polymer chain length.[25] However, the X-ray diffraction analysis made assumptions regarding the packing of the polymers. An optical activity study of poly(α-phenylethyl isocyanide) showed tenfold increased specific rotation for the polymers as compared to that of the monomer units indicating a helical structure for the polymer.[29] Nolte et al. separated the racemic mixture of poly(*tert*-butyl isocyanide) into left and right handed enantiomers by column chromatography using a chiral support thus providing a strong experimental basis for the helical structure of the polyisocyanides.[10] In subsequent studies, Circular Dichroism (CD) spectroscopy and theoretical calculations of the CD spectrum of poly(*tert*-butyl isocyanide) enabled the determination of the screw sense of the polymer and in addition the polymer was estimated to have a 4_1 helical conformation based on theoretical calculations.[30] On the other hand, there were also numerous studies that raised questions regarding the rigorousness of the rigid 4_1 helical conformation for the polyisocyanides. Kollmar and Hoffman carried out molecular orbital calculations considering three main interactions in the polymer chain (see Figure 1.2).

1) Repulsion of the lone pair electrons of the isocyano nitrogen coming close to each other driving the structure away from the planar arrangement. 2) The 'π' electron conjugation of the neighboring C═N moieties increases the stability of a planar conformation. 3) Steric interactions of the side chain substituents (-R groups).

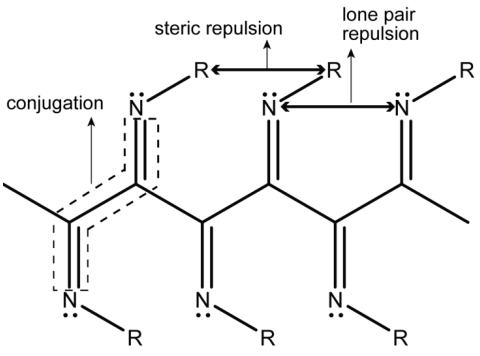

R= H, CH_3,$C(CH_3)_3$

Figure 1.2 General polyisocyanide skeleton backbone showing different interactions in the planar conformation (figure adapted from ref [31]).

The study showed qualitatively that N-lone pair repulsion near the backbone dominates and precludes a planar conformation and hence forces the backbone into a non-planar conformation. Thus the lone pair repulsion acts as an intrinsic factor causing the helical effect. The study also showed that the helical angle adopted by the polymers was influenced by the steric bulk of the substituent ─R groups.[28] For the bulky substituents such as the poly(*tert*-butyl isocyanide) they concluded that the helix angle approached that of a 4_1 helix. For less bulky substituents such as a CH_3 group the calculations predicted two possible structural minima of the helix with 95^o and 140^o helical angles. These calculations showed that the net contribution of the conjugation, lone pair repulsion and steric interactions determine the polymer conformation. The study was however limited to a few examples and did not take all possible factors into consideration. For example the rotation of the side chain ─R groups was fixed in all cases. A comparative study of the hydrodynamic properties of poly(α-phenylethyl isocyanide) and poly(β-phenylethyl isocyanide) led to the conclusion of a rigid rod like helical structure for the former polymer however a more flexible and undulating chain structure was proposed for the latter.[9] This structural characterization contradicts the observed lyotropic phase of poly(β-phenylethyl isocyanide).[26] Green et al. also expressed strong skepticism with regard to the rigid helical conformations of the polyisocyanides based on ^{13}C solution state NMR measurements and other analytical methods. For example, the CD spectrum of Poly(2,2-dimethyl-1,3-dioxolane-4-methyiso cyanide) was comparable to that of the poly(*tert*-butyl isocyanide) suggesting a helical conformation. However, the ^{13}C solution-state NMR spectra of the former polymer showed considerable dispersion in the chemical shifts suggesting a flexible coil like structure.[26] The poly(α-phenylethyl isocyanide) that was proposed to have a rigid helical structure with ~4_1 helical conformation also exhibited ^{13}C NMR chemical shift dispersion in the solution state.[26] The authors provided more examples that suggest against the straightforward acceptance of CD results to analyze the helical conformation of the polyisocyanides by mere comparison of the curve characteristics with that of the poly(*tert*-butyl isocyanide).[32] Clericuzio et al., proposed that the more favorable minimum conformation of the polyisocyanides was the 'non-helical syndio' conformation based on theoretical studies.[27] A schematic diagram of the syndio conformation and the helical conformation are shown in Figure 1.3. The syndio conformation can be considered as the dimers of the isocyanide monomers

covalently linked in a series. However in the calculations only small molecular units were considered and hence the results remain ambiguous for realistic situations.

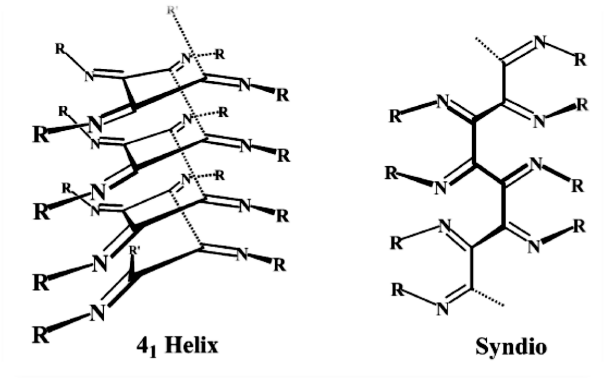

Figure 1.3 Schematic diagram of a Helix and a Syndio conformation of polyisocyanides. The figure is adapted from reference [33].

The structural study of the polyisocyanodipeptides using powder X-ray diffraction and the cast film method indicate the diameter of the polymers to be 15.9Å for L,L-PIAA and L,D-PIAA assuming a orthorhombic arrangement of the polymer rods.[34] Molecular modeling calculations showed that the syndio conformation is an unlikely structure for the polyisocyanodipeptides due to the large separation of the side chains in the polymer.[14, 34] However there are no direct experimental measurements performed to determine the backbone conformation. Thus the answer to the basic question of what is the exact conformation of the polyisocyanopeptides and in general the structure of the polyisocyanides remains unanswered. This formed the basic motivation of the thesis work. We use solid-state NMR methodology for the structural study of the hydrogen bond stabilized polyisocyanodipeptides.

1.1.1 Stereoisomers of polyisocyanodipeptides

The polyisocyanodipeptides have two chiral centers at the alpha carbon position of the amino acid residues. The chiral centers for the L-isocyanoalanyl-D-alanine methyl ester monomer units are indicated by asterisks in Figure 1.1b. The chiral centers lead to a preference for right or left handedness of the polymer helices formed. The alanine-alanine derived polyisocyanides lead to four stereoisomers based on the '*L*' and '*D*' conformation of the two alanines. These polymers are named here as L,L-PIAA, L,D-PIAA, D,L-PIAA and D,D-PIAA for convenience. Several techniques such as the CD spectroscopy, IR, X-

ray diffraction, AFM and NMR spectroscopy have been applied for the structural characterization of the polyisocyanodipeptides. These studies show that the stereoisomers exhibit several differences such as

1. In the presence of an acid, L,D-PIAA shows stronger CD signals and narrower bands in UV/vis spectrum than of L,L-PIAA.[34]
2. Molecular modeling studies indicate L,L-PIAA polymers are less stable compared to that of L,D-PIAA polymers due to unfavorable steric interactions in the former polymer.[14]
3. Viscometry and AFM studies of the polymers suggest that L,D-PIAA polymers attain significantly higher molecular weight compared to L,L-PIAA.[15]
4. Thermogravimetric Analysis (TGA) of the polymers shows that the L,D-PIAA polymer decomposes at a faster rate compared to the L,L-PIAA.[15]

From the differences described above, it is clear that the macroscopic physical properties of the polymers are altered with stereo specific differences of amino acid units in the side chains. Thus the structures of these polymers are probably influenced by the side chain combinations of the amino acids. The second aim of this thesis work is to try to understand the structural differences in the four stereoisomers of isocyanoalanyl-alanine derived polyisocyanodipeptides. We have used solid-state NMR spectroscopy to obtain structural information from the high resolution chemical shift and chemical shift anisotropy (CSA) tensor analysis of the four stereoisomers.

1.1.2 Carbazole functionalized polyisocyanides

Carbazole based materials are known for their favourable hole-transport and electroluminescent properties. Recently, Carbazole functionalized polyisocyanopeptides grown on a silicon wafer were successfully incorporated into Light Emitting Diodes (LEDs).[24] The diverse applications and performance efficiency of these materials crucially depend upon the conformation of the polymer that is formed. The carbazole moiety being a large aromatic group introduces aromatic σ-π/π-π weak interactions into the polymer structure. The structural changes that can take place in the presence of different interactions have yet to be understood. The third aim of this thesis work is to understand the structural organization under the influence of the multiple interactions in the carbazole polymers. The polymer is insoluble in many of the organic solvents. Thus

solid-state NMR is one of the few techniques that can provide information of the structural organization of the polymer.

1.1.3 Significance of solid-state NMR in structure characterization

The structural analysis of polyisocyanides was until now dominated by CD spectral analysis, X-ray diffraction, light scattering, liquid state NMR etc. Each of these techniques have contributed to the understanding of the structural organization of the polyisocyanides. However, they have certain limitations when it comes to the study of polymer structures in great detail. Circular Dichroism (CD) spectroscopy has been used to assign structural configuration of various polyisocyanides by directly comparing the CD curves of the other polyisocyanides to that obtained for the poly(*tert*-butylisocyanide).[35] Green et al., point out that the variation of CD band position of ~20 nm observed in various polyisocyanides published in literature could suggest a change in helix parameters of the polymers.[26, 35] As was mentioned earlier the authors have provided several other examples raising concerns over the direct structural prediction by the CD spectroscopic analysis.[26] In addition the CD spectra are strongly influenced by the optical activity of the side chain groups and can also be affected by solvent absorption.[32, 35] X-Ray diffraction is a well-established method to decipher molecular structure with atomic level accuracy in compounds with long-range order and hence is highly suitable for the study of crystalline compounds. In the case of polymers, powder-X-ray diffraction can give information regarding the size of the polymers but it still requires microcrystalline domains. In some cases the polymer material is completely amorphous and is not suitable for X-ray diffraction analysis. In general, the X-Ray methods are inefficient in predicting exact position of protons even in crystalline materials as the diffraction pattern is dominated by heavy atom diffraction. This is a serious compromise considering the fact that protons form an integral part of the ubiquitous and all-important hydrogen bonds. Liquid-state NMR offers in-depth studies on assemblies, but suffers from the fact that most local interactions critical to structure-function relationship in the native state, are strongly influenced by solvent interactions. Solid-state NMR (ssNMR) spectroscopy has become a powerful tool for the elucidation of the structure of compounds irrespective of the physical state (crystalline, glassy amorphous, gel, etc.) of the samples. Along with solution-state like isotropic interactions,

the presence of anisotropic interactions in the solid-state provides a greater versatility for structure and dynamics characterization. Anisotropic interactions such as chemical shift anisotropy (CSA), quadrupolar interaction and dipolar coupling interactions provide a means to access spatial orientation of molecular segments and distance measurements between nuclei facilitating structure characterization of polymers, biomolecules and various other materials.[36-40] ssNMR spectroscopy has ingeniously exploited the anisotropic nuclear spin interactions to obtain structural information such as torsion angles and distances.[37, 41-44] The relative orientation of different chemical moieties can be inferred by determining the relative orientation of anisotropic nuclear interactions such as dipole-dipole, dipole-CSA or CSA-CSA interactions. With fast magic angle spinning and multidimensional NMR spectroscopy, proton solid-state NMR is becoming more popular. In favourable cases proton NMR chemical shifts have been exploited to unambiguously establish hydrogen bonds [45-47] and also identify the weak σ- π/π–π interactions [46, 48, 49]. The advent of multidimensional NMR spectroscopy has opened up possibilities to extract information from the NMR spectrum that is usually not accessible in one dimensional NMR experiments [43, 50]. It is consequently used to determine molecular structures and estimate the time scale of dynamics in different molecular systems. In the solid state, molecular interactions such as hydrogen bonding and sometimes even the weakest of the interactions such as the aromatic σ- π/π–π interactions, are believed to define overall molecular arrangement and consequently the macroscopic properties of the material. A detailed insight into local information regarding structure, dynamics, and molecular interactions can be obtained using solid-state NMR in the native state of the compound unperturbed by external agents.

1.2 NMR Interactions

The NMR interactions of a nuclear spin system in an external magnetic field can be represented as

$$\mathcal{H} = \mathcal{H}_{ext} + \mathcal{H}_{int}$$

The external Hamiltonian $\mathcal{H}_{ext}$ results from the interaction of the spins with the external magnetic fields

$$\mathcal{H}_{ext} = \mathcal{H}_{RF} + \mathcal{H}_{z}$$

$\mathcal{H}_z$ is the Zeeman interaction. It is the interaction of the spins with the applied external field $\mathbf{B_o}$.

$\mathcal{H}_{RF}$ is the interaction of the spins with the applied radio frequency field. This is a time dependent interaction.

The internal Hamiltonian of a spin system consisting of two different type of nuclear spins I and S can be written as

$$\mathcal{H}_{int} = \mathcal{H}_\sigma + \mathcal{H}_D + \mathcal{H}_J + \mathcal{H}_Q$$

- $\mathcal{H}_\sigma$ is the chemical shielding Hamiltonian of spin I.
- $\mathcal{H}_D$ and $\mathcal{H}_J$ are the dipolar coupling and J-coupling interaction among the spins. The interaction between like spins is termed homonuclear and between that of unlike spins is termed as heteronuclear interaction.
- $\mathcal{H}_Q$ is the quadrupolar interaction of the I and the S spins if their spin quantum number is larger than 1/2.

The NMR interactions in the solid state are anisotropic in nature and hence are represented most conveniently in tensorial form. The Hamiltonians can be represented by second rank Cartesian tensors as

$$\mathcal{H} = \mathbf{I} \cdot \tilde{\mathbf{A}} \cdot \mathbf{S} = (I_x \quad I_y \quad I_z) \begin{pmatrix} A_{xx} & A_{xy} & A_{xz} \\ A_{yx} & A_{yy} & A_{yz} \\ A_{zx} & A_{zy} & A_{zz} \end{pmatrix} \begin{pmatrix} S_x \\ S_y \\ S_z \end{pmatrix}$$

where, **I** represents a spin vector and **S** is a spin vector or a field vector.

1.2.1 Zeeman Hamiltonian and RF Hamiltonian

Zeeman interaction or Zeeman Hamiltonian is the coupling of the spins to the static magnetic field $\mathbf{B_o}$.

$$\mathcal{H}_Z = \gamma_I \mathbf{I} \cdot \tilde{\mathbf{Z}} \cdot \mathbf{B_o}$$

Where $\mathbf{B_o} = (B_x \quad B_y \quad B_z)$ is the external magnetic field and $\tilde{\mathbf{Z}} = \gamma_I \tilde{\mathbf{1}}$

$$\mathcal{H}_Z = \gamma_I \cdot \boldsymbol{I} \cdot \tilde{\mathbf{1}} \cdot \mathbf{B_o}$$

$\tilde{\mathbf{1}}$ is the unit matrix which represents the coupling matrix between the spin I and the magnetic field $\mathbf{B_o}$. γ_I represents the gyromagnetic ratio of the nuclei. The Hamiltonian here is expressed in frequency units. The spin angular momentum operator $\hat{\boldsymbol{I}}_{\boldsymbol{z}}$ possesses the eigenvalues m = −I, (−I + 1), ...+I. A spin-½ nucleus thus gives rise to two energy

states corresponding to m=-1/2 and m=+1/2. The energy levels of a spin-½ nucleus in the absence and presence of an external magnetic field are shown in the Figure 1.4.

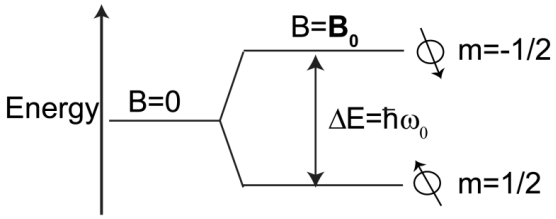

Figure 1.4 Zeeman splitting of energy levels of a spin-½ nucleus in the external magnetic field $\mathbf{B_o}$, where $\omega_o = \gamma B_o$.

The energy level splitting is known as the Zeeman splitting. The frequency difference between two energy levels is termed as the Larmor precession frequency and is denoted as ω_0.[51]

The Zeeman energy levels in Figure 1.4 are populated according to the Boltzmann distribution which is given by,

$$\rho_j^{eq} = \frac{\exp\left(\frac{-\hbar\omega_j}{k_B T}\right)}{\sum_k \exp\left(\frac{-\hbar\omega_k}{k_B T}\right)}$$

For a spin-1/2 system of nuclei the population difference between the two states is given by

$$\frac{N_{m=+1/2}}{N_{m=-1/2}} = \exp\left(\frac{\Delta E}{k_B T}\right)$$

At thermal equilibrium, the population of the spins in the lower energy state is always higher than the spins in the higher energy state. This difference in the population distribution gives rise to net magnetic moment (**M**) in the sample which is in the direction of the applied magnetic field.

1.2.2 Radio Frequency

The transitions between the Zeeman eigen energy levels of the spin states are achieved by the application of a time dependent $\mathbf{B_1}$ field which oscillates with frequency close to the difference in the energy levels.

The Hamiltonian due to the RF field is

$$\mathcal{H}_j^{RF} = \mathbf{I} \cdot \tilde{\mathbf{Z}} \cdot \mathbf{B_1}$$

$\tilde{\mathbf{Z}} = \gamma_I \tilde{\mathbf{1}}$; $\tilde{\mathbf{1}}$ is the unit matrix.

$$\mathcal{H}_j^{RF} = -\frac{1}{2}\gamma_j \mathrm{B}_1 \left[\cos\left(\omega_{ref} t + \varphi\right) \hat{I}_{jx} + \sin\left(\omega_{ref} t + \varphi\right)\right] \hat{I}_{jy}$$

Where φ is the phase of the RF field and ω_{ref} is the frequency of the irradiation field.

1.2.3 Shielding Hamiltonian

Nuclear spins are surrounded by electrons. The magnetic field experienced by the spin I is altered by the surrounding electron clouds (see Figure 1.5).

In a semi-classical picture this can be described in two parts.

One is called the diamagnetic chemical shielding which can be described as a two-step process.

1. The external magnetic field $\boldsymbol{B_o}$ induces an electronic current in the bonds surrounding the nucleus.

2. The circulating electrons in turn generate a magnetic field $\boldsymbol{B_{loc}}$ which subtracts from or adds to $\boldsymbol{B_o}$ (shields or "deshields").

The paramagnetic effect involves excited states of the molecules induced by the high magnetic field. Especially when there are low lying LUMO's the paramagnetic term can give very significant shifts to lower field.

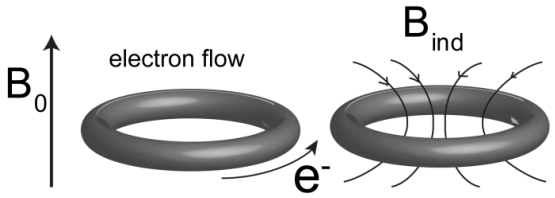

Figure 1.5 The diamagnetic currents of the electrons and the induced diamagnetic field.

Due to the shielding interaction the nuclear spins in different chemical environments experience a different net magnetic field $\boldsymbol{B_{loc}}$ which is given by the sum of the external magnetic field and the induced fields. The direction and magnitude of the induced fields vary depending on the molecular geometry and orientation. Thus nuclei in different chemical environments precess with different frequencies.

$$\boldsymbol{B_{loc} = B_o + B_{ind}}$$

The chemical shielding interaction $\mathcal{H}_\sigma$ is given by

$$\mathcal{H}_\sigma = \boldsymbol{I} \cdot \tilde{\boldsymbol{\sigma}} \cdot \boldsymbol{B_o}$$

The shielding tensor $\tilde{\boldsymbol{\sigma}}$ can be expressed as

$$\tilde{\boldsymbol{\sigma}} = \begin{pmatrix} \sigma_{xx} & \sigma_{xy} & \sigma_{xz} \\ \sigma_{yx} & \sigma_{yy} & \sigma_{yz} \\ \sigma_{zx} & \sigma_{zy} & \sigma_{zz} \end{pmatrix}$$

Principal Axis System

The chemical shift tensor is generally expressed in a coordinate frame of reference in which all the off diagonal tensor elements vanish. i.e.

$$\tilde{\boldsymbol{\sigma}}_{\boldsymbol{PAS}} = \begin{pmatrix} \sigma_{XX} & 0 & 0 \\ 0 & \sigma_{YY} & 0 \\ 0 & 0 & \sigma_{ZZ} \end{pmatrix}$$

This coordinate frame of reference is called as the Principal Axis System (PAS). The chemical shielding can be separated into two parts

The isotropic part:

$$\mathcal{H}_{CS,iso} = \sigma_{iso} \gamma B_o \hat{I}_z$$

And the anisotropic part:

$$\mathcal{H}_{CS,aniso} = \left(\frac{1}{2}\Delta\sigma[(3cos^2\theta - 1) + \eta_{cs} sin^2\theta cos(2\phi)]\right) \hat{I}_z$$

Where, $\sigma_{iso} = \frac{1}{3}(\sigma_{XX} + \sigma_{YY} + \sigma_{ZZ})$ is the isotropic shift value, $\Delta\sigma = \sigma_{ZZ} - \sigma_{iso}$ is the chemical shift anisotropy and $\eta = \frac{\sigma_{YY} - \sigma_{XX}}{\Delta\sigma}$ is the asymmetry of the chemical shift. θ, ϕ are the polar angles describing the orientation of the $\boldsymbol{B_o}$ field in the Principal Axis System(PAS) of the chemical shift tensor.

1.2.4 Powder Spectrum

The NMR frequencies of a powder sample with anisotropic interactions such as the chemical shift anisotropy depend on the orientation of the molecular segment in the external magnetic field. In a single crystal all molecules orient in a particular direction and hence a given nucleus has a single chemical shift value in a particular direction giving rise to a single line in the NMR spectrum. However, in general most samples exist in the form of powders in which molecules are oriented in all possible directions. This

gives rise to a continuous distribution of frequencies in the NMR spectrum of a nucleus. This continuous distribution of frequencies creates a spectral line shape that is characteristic of the chemical shift anisotropy parameters of the particular nucleus and is termed as the powder spectrum in solid-state NMR. For example, the ring currents induced by the electrons in the '^{13}C═O'(carbonyl carbon) moiety depend on the orientation angle 'θ' of the molecular segment consisting of the sp^2 plane of the carbon, causing a distribution in the chemical shift of the carbon in different molecular segments (Figure 1.6).

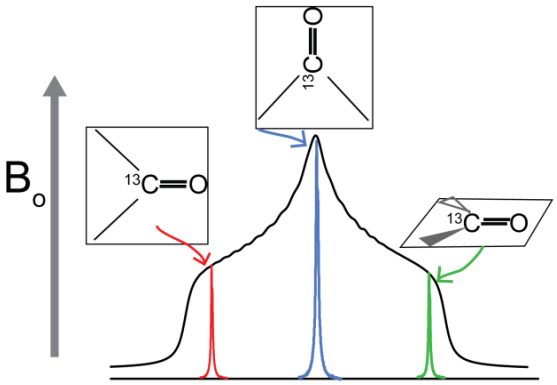

Figure 1.6 The powder spectrum of carbonyl carbon ^{13}C=O illustrating the chemical shift position of carbons in molecular fragments with different orientations in the external field.

The line shape of the powder spectrum depends on the asymmetry and the anisotropy parameters defined above. Figure 1.7 illustrates the CSA powder line shapes for different values of asymmetry parameter. The principal components of the CSA tensor can be measured directly from the singularities in the powder spectrum.

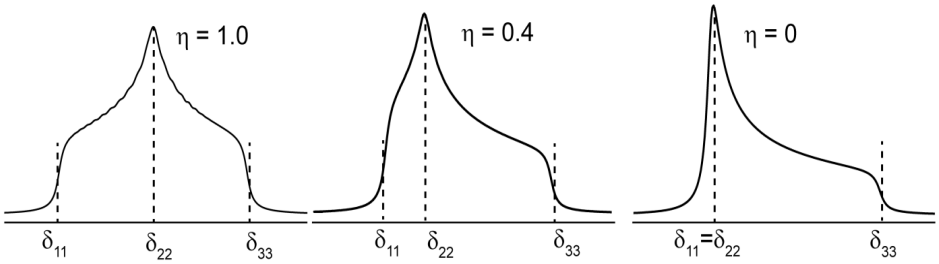

Figure 1.7 The powder line shape of a spin-1/2 nucleus for various asymmetry values. (see below for the description of δ_{11}, δ_{22} and δ_{33} and η)

Carbons that are sp^3 hybridized have symmetric electron distribution around the nucleus and hence have small anisotropies of ~15-30 ppm whereas sp^2 and sp hybridized carbons have asymmetric distribution of the electron clouds and hence have larger anisotropies. Typically carbonyl carbons have anisotropies of ~70-100 ppm. Chemical shift tensors are usually represented as ellipsoids with the principal axis of the ellipsoid coinciding with the principal components of the CSA tensor.

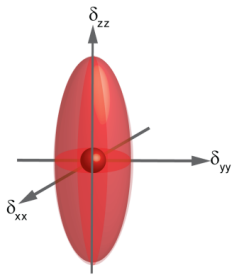

Figure 1.8 CSA tensor ellipsoid. The principal components of the tensor coincide with the principal axis of the ellipsoid.

In routine use the NMR frequencies are reported as chemical shift frequencies (υ) defined by

$$\upsilon = \frac{\gamma}{2\pi} B_0(1-\sigma)$$

Where σ is the shielding parameter. The chemical shifts thus have opposite sign as that of the shielding parameter.

The chemical shift frequency is expressed as a unit less field independent parameter using the following relation [52].

$$\delta_{sample} = \left(\frac{\upsilon_{sample} - \upsilon_{reference}}{\upsilon_{reference}}\right) \times 10^6$$

The chemical shielding tensor expressed in its principal axis system (PAS) is diagonal. And the principal components $\delta_{xx}^{PAS}, \delta_{yy}^{PAS}, \delta_{zz}^{PAS}$ form the elements of the diagonal tensor. The principal components are defined accordingly as

$$\left|\delta_{zz}^{PAS} - \delta_{iso}^{j}\right| \geq \left|\delta_{xx}^{PAS} - \delta_{iso}^{j}\right| \geq \left|\delta_{yy}^{PAS} - \delta_{iso}^{j}\right|$$

defining the anisotropy using the shift tensor

$$\zeta_\delta = \delta_{zz}^{PAS} - \delta_{iso}^{j}$$

$$\eta_\delta = \frac{\delta_{yy}^{PAS} - \delta_{xx}^{PAS}}{\zeta_\delta}$$

The components of the chemical shift tensor δ with the numerical subscripts where the three principal tensor components are labeled as $\delta_{11} \geq \delta_{22} \geq \delta_{33}$. The δ_{33} component is the most shielded component and $\delta_{11}$is the least shielded component.

1.2.5 Dipolar coupling Hamiltonian

The dipolar coupling is the through space interaction between the magnetic moments of two nuclear spins. It is also called the direct coupling interaction. The local field of one spin influences the net magnetic field felt by the other spin.

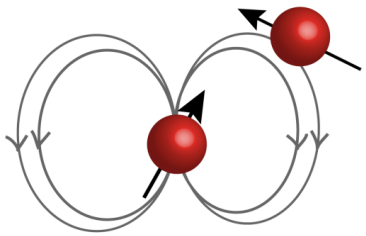

Figure 1.9 Nuclear spin I_1 in the local magnetic field created by the neighboring spin I_2.

The Hamiltonian of the dipolar coupling interaction is given by

$$\mathcal{H}_D = \mathbf{I_1} \cdot \tilde{\mathbf{D}}_{\mathbf{12}} \cdot \mathbf{I_2}$$

Here $\tilde{\mathbf{D}}_{\mathbf{12}}$ here represents the dipolar tensor. In the principal axis system the dipolar tensor is axially symmetric and trace of the matrix is zero (Trace of the matrix $\tilde{\mathbf{D}}_{\mathbf{12}}$ is zero, i.e., there is no isotropic component).

$$\tilde{\boldsymbol{D}}_{\boldsymbol{PAS}} = \begin{pmatrix} -\frac{d}{2} & 0 & 0 \\ 0 & -\frac{d}{2} & 0 \\ 0 & 0 & d \end{pmatrix}$$

The dipolar coupling interaction can be categorized into two types. When the two interacting spins are of the same spin species(carbon-carbon, proton-proton etc..) then the

interaction is called the homonuclear dipolar coupling and if the interacting spins are of different spin types(carbon-nitrogen, proton-carbon…etc) then the interaction is called the heteronuclear dipolar coupling. The dipolar interaction is several orders of magnitude smaller than the $\mathbf{B_0}$ field, so the secular approximation (truncation) applies to the corresponding Hamiltonian. The secular (truncated) form of the dipolar Hamiltonian for a pair of like-spins is

$$\mathcal{H}_D^{II} = \frac{d}{2}(3cos^2\theta - 1)(3I_{1z}I_{2z} - \boldsymbol{I_1} \cdot \boldsymbol{I_2})$$

and the secular (truncated) form of the dipolar Hamiltonian for a pair of unlike-spins is

$$\mathcal{H}_D^{IS} = \frac{d}{2}(3cos^2\theta - 1)(2I_{1z}S_{2z})$$

Where, in the two above equations, d is the dipolar coupling constant, θ describes the orientation of the vector joining the two spins w.r.t to the $\mathbf{B_0}$ field and

$$d = -\frac{\mu_0}{4\pi}\frac{\gamma_1\gamma_2}{r_{12}^3}\hbar$$

γ_1, γ_2 are the magnetogyric ratios of the two spins in rad s^{-1} , r_{12} is the distance between the two nuclear spins.

Pake Doublet

For spin-1/2 nuclei the spin magnetic moments are aligned either parallel or anti-parallel to the $\mathbf{B_0}$ field hence they either increase or decrease the local field at the neighboring spin splitting the line into a doublet. The frequency difference between the doublets is

$$\nu = \frac{3d}{2}(3cos^2\theta - 1) \text{ (Hz)} \quad \rightarrow \text{considering homonuclear spins}$$

The direct dipole-dipole coupling provides information about the distance between the two interacting nuclei. In a single crystal the dipolar coupling between two spins gives rise to doublet whose separation depends on the angle of orientation θ with respect to the external magnetic field. In a powdered sample all possible orientations of the nuclear spins are possible which results in a characteristic doublet powder line shape called as the pake doublet. The splitting between the two maxima in the pake pattern is the dipolar coupling constant and can be used to measure the distance between the two coupled nuclei (see Figure 1.10).

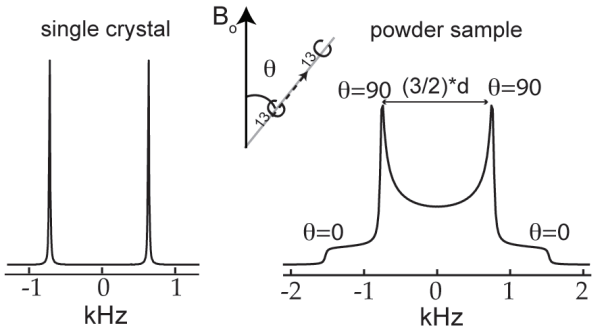

Figure 1.10 Dipolar coupling pattern of two like nuclear spins in a single crystal and powder sample.

Homogeneous broadening

The secular homonuclear dipolar coupling Hamiltonian can be expressed in two parts

$$\mathcal{H}_D^{II} = \frac{d}{2}(A + B)$$

Where,

$$A = (3cos^2\theta - 1)(\hat{I}_{1z}\hat{I}_{2z})$$

$$B = -\frac{1}{4}(3cos^2\theta - 1)(\hat{I}_{1+}\hat{I}_{1-} + \hat{I}_{1-}\hat{I}_{1+})$$

The term A is inhomogeneous and causes first order changes in the energy level splittings. The term B contains the $\hat{I}_{1+}\hat{I}_{1-} + \hat{I}_{1-}\hat{I}_{1+}$operator is homogeneous term which mixes the degenerate Zeeman states. In a solid-state powder sample each nuclear spin is coupled to every other nuclear spin in the vicinity. This causes severe broadening of the NMR spectrum. The effects of A and B in an ensemble of interacting spins are better understood with the help of an energy level diagram as in Figure 1.11.

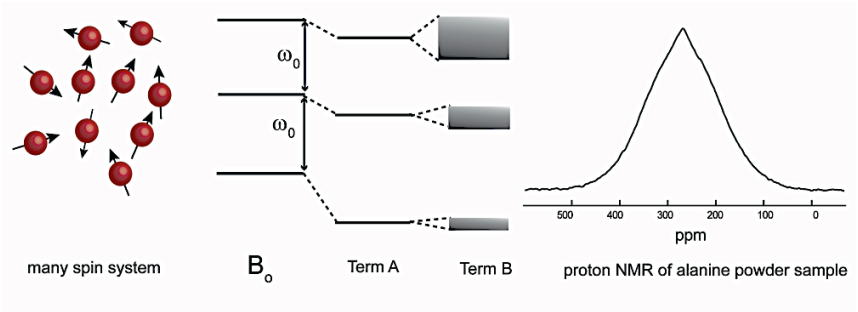

Figure 1.11 Effect of homogenous broadening in homonuclear multi spin system

The homogeneous broadening is the most commonly faced problem in solid state NMR particularly for the proton nuclei which are abundant and have a high gyromagnetic ratio. The coupling between proton nuclei is thus very strong and several spins are spatially close to each other causing homogenous line broadening as shown in Figure 1.11. Recording narrow line spectra in solid-state NMR has been made possible using MAS and Fast-MAS methods, which will be discussed below.

1.3 Magic Angle Spinning

In solid-state powder samples many crystallites are oriented in random directions. The nuclear spin interactions such as the chemical shielding, dipolar coupling etcetera depend on the orientation of the molecular segment in the external magnetic field. These anisotropic NMR interactions are a boon as well as a bane depending on the subject under study. The anisotropic interactions are a direct measure of chemical environment around a nucleus and they also possess distance information. However, when several inequivalent nuclei are present in a system, which is often the case, the powder patterns from each of the nuclei may overlap. This makes it difficult to obtain information about a particular nucleus or for all nuclei under interest. This problem does not arise in liquid state NMR since the rate of change of molecular orientation is fast in liquids compared to the magnitude of the anisotropic interactions. Thus the anisotropic spin interactions are averaged in the liquid state. The spin interactions can be manipulated by rotation of the sample about an axis making an angle θ_r with the external magnetic field $\mathbf{B_o}$. If the rotation axis is inclined at the "magic angle" $\cos^{-1}\sqrt{\frac{1}{3}} \approx 54.74^o$ second rank tensor interactions can be averaged out.[53, 54] This technique is called Magic Angle Spinning (MAS) and is shown schematically in Figure 1.12. When the spinning speed (ω_r) is smaller than that of the interaction magnitude, the anisotropic powder line shape is split into spinning sidebands which are separated at $n*\omega_r$ from that of the isotropic shift position. Anisotropic information can be extracted with accuracy from the spinning

sidebands. The effect of magic angle spinning on the powder line shape of ^{13}C NMR of glycine is shown in Figure 1.13.

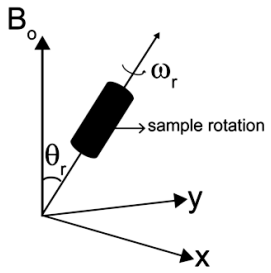

Figure 1.12 Schematic representation of the rotation of the NMR sample about an axis tilted at an angle θ to the external magnetic field $\mathbf{B_o}$.

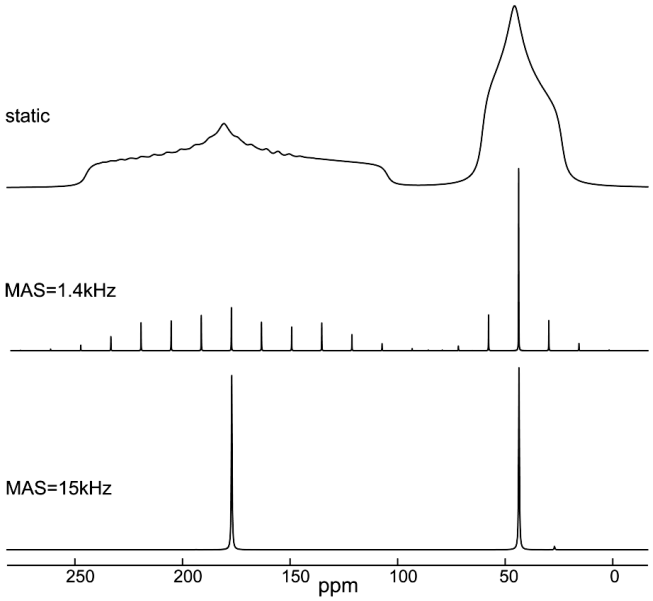

Figure 1.13 Simulated static and MAS spectra of glycine. At high spinning speeds the anisotropic interactions are averaged completely leaving only the isotropic line.

In general proton-proton dipolar couplings and proton-carbon heteronuclear dipolar are stronger than 20 kHz and require very fast-MAS to average the interactions. Improvements in MAS techniques have made it possible to spin the samples at rates ≥ 70 kHz leading to high resolution ^{1}H NMR spectroscopy.[55]

1.4 Scope of this thesis

Chapter 2. The backbone conformation of the L-alanyl-D-alanine polyisocyanide is determined using advanced solid-state NMR techniques. 2D NMR experiments such as double quantum-single quantum correlation spectroscopy (DOQSY) are used to correlate the chemical shift anisotropy tensors of the backbone carbons that are directly bonded to each other thus determining the helical angle of the polyisocyanide backbone. 2D-separated local field spectroscopy (2D-SLF) is used to obtain orientation angles of the CSA tensor in the molecular frame that is essential in addition to the DOQSY data to build a complete polymer model. Molecular modeling calculations are used to refine the structure obtained from the experimental data.

Chapter 3. In the measurement of double quantum single quantum spectrum using a 10% ^{13}C-^{15}N enriched L,D-PIAA sample we realized that the sensitivity of the experiment was very low leading to long experimental time and imposed demands on the sample quantity and instrument time. In general in most cases, solid-state NMR suffers from low sensitivity when the experiments involve scarce, low gamma nuclei such as that of ^{13}C, ^{15}N, ^{29}Si. This normally leads to long instrument time. There have been several sensitivity enhancement techniques in solid-state NMR such as the Magic Angle Spinning, CPMG-acquisition etc. For the case of static experiments such as DOQSY which involves detection of dipolar coupled homonuclear spin pairs the existing sensitivity enhancement by CPMG acquisition is not applicable due to the presence of dipolar coupling interaction. We modify the CPMG pulse sequence so as to achieve sensitivity enhancement for dipolar coupled spin pairs.

Chapter 4 The isotropic chemical shifts and chemical shift anisotropy of the four stereoisomers of PIAA i.e. L,D-PIAA, D,L-PIAA, L,L-PIAA and D,D-PIAA and the monomers L,D-IAA and L,L-IAA and D,L-IAA are measured and compared with each other. The change in the chemical shifts and anisotropy tensors are analyzed to obtain information regarding structural regularity in the polymers.

Chapter 5. Carbazole functionalized polyisocyanopeptide and the corresponding monomer are studied using solid-state NMR. Chemical shift assignments are made for the monomer and the polymer. Weak and strong hydrogen bonding interactions are

characterized in the carbazole monomer crystal lattice. This study provides some ideas of the structural arrangement of the functional moieties in the polymer. In addition we have explored in detail the weak interactions in the monomer crystal lattice. Useful chemical shift information of the protons and carbons involved in the weak interactions is provided.

1.5 References

[1] J.M. Lehn, Toward self-organization and complex matter, Science, 295 (2002) 2400-2403.

[2] G.M. Whitesides, J.P. Mathias, C.T. Seto, Molecular Self-Assembly and Nanochemistry - a Chemical Strategy for the Synthesis of Nanostructures, Science, 254 (1991) 1312-1319.

[3] G. Mcdermott, S.M. Prince, A.A. Freer, A.M. Hawthornthwaite-lawless, M.Z. Papiz, R.J. Cogdell, N.W. Isaacs, Crystal-Structure of an Integral Membrane Light-Harvesting Complex from Photosynthetic Bacteria, Nature, 374 (1995) 517-521.

[4] F.J.M. Hoeben, P. Jonkheijm, E.W. Meijer, A.P.H.J. Schenning, About Supramolecular Assemblies of π-Conjugated Systems, Chemical Reviews, 105 (2005) 1491-1546.

[5] J.A.A.W. Elemans, R. Van Hameren, R.J.M. Nolte, A.E. Rowan, Molecular materials by self-assembly of porphyrins, phthalocyanines, and perylenes, Advanced Materials, 18 (2006) 1251-1266.

[6] H.Z. Tang, Y.J. Lu, G.L. Tian, M.D. Capracotta, B.M. Novak, Stable helical polyguanidines: Poly{N-(1-anthryl)-N '-[(R)- and/or (S)-3,7-dimethyloctyl]guanidines}, J Am Chem Soc, 126 (2004) 3722-3723.

[7] H.-Z. Tang, B.M. Novak, J. He, P.L. Polavarapu, A Thermal and Solvocontrollable Cylindrical Nanoshutter Based on a Single Screw-Sense Helical Polyguanidine, Angewandte Chemie International Edition, 44 (2005) 7298-7301.

[8] J. Budhathoki-Uprety, B.M. Novak, Synthesis of Alkyne-Functionalized Helical Polycarbodiimides and their Ligation to Small Molecules using 'Click' and Sonogashira Reactions, Macromolecules, 44 (2011) 5947-5954.

[9] F. Millich, Rigid rods and the characterization of polyisocyanides, in: Polymerization Reactions, Springer Berlin / Heidelberg, 1975, pp. 117-141.

[10] R.J.M. Nolte, V. beijnen.A.J.M, W. Drenth, Chirality in Polyisocyanides, J Am Chem Soc, 96 (1974) 5932-5933.

[11] R.J.M. Nolte, Vanbeijn.Aj, W. Drenth, Chirality in Polyisocyanides, J Am Chem Soc, 96 (1974) 5932-5933.

[12] W. Drenth, R.J.M. Nolte, Poly(iminomethylenes): Rigid rod helical polymers, Accounts of Chemical Research, 12 (1979) 30-35.

[13] J.M. Van Der Eijk, R.J.M. Nolte, V.E.M. Richters, W. Drenth, Polymeric model system for protein-bilirubin interaction, Biopolymers, 19 (1980) 445-448.

[14] J.J.L.M. Cornelissen, J.J.J.M. Donners, R. de Gelder, W.S. Graswinckel, G.A. Metselaar, A.E. Rowan, N.A.J.M. Sommerdijk, R.J.M. Nolte, β-Helical Polymers from Isocyanopeptides, Science, 293 (2001) 676-680.

[15] J.J.L.M. Cornelissen, W.S. Graswinckel, P.J.H.M. Adams, G.H. Nachtegaal, A.P.M. Kentgens, N.A.J.M. Sommerdijk, R.J.M. Nolte, Synthesis and characterization of polyisocyanides derived from alanine and glycine dipeptides, Journal of Polymer Science Part A: Polymer Chemistry, 39 (2001) 4255-4264.

[16] C.M. Gowda, E.R.H. van Eck, A.M. van Buul, E. Schwartz, G.W.P. van Pruissen, J.J.L.M. Cornelissen, A.E. Rowan, R.J.M. Nolte, A.P.M. Kentgens, Direct Backbone Structure Determination of Polyisocyanodipeptide Using Solid-State Nuclear Magnetic Resonance, Macromolecules, 45 (2012) 2209-2218.

[17] E. Schwartz, S.L. Gac, J.J.L.M. Cornelissen, R.J.M. Nolte, A.E. Rowan, Macromolecular multi-chromophoric scaffolding, Chemical Society Reviews, 39 (2010) 1576-1599.

[18] V. Palermo, E. Schwartz, C.E. Finlayson, A. Liscio, M.B.J. Otten, S. Trapani, K. Mullen, D. Beljonne, R.H. Friend, R.J.M. Nolte, A.E. Rowan, P. Samorì, Macromolecular Scaffolding: The Relationship Between Nanoscale Architecture and Function in Multichromophoric Arrays for Organic Electronics, Advanced Materials, 22 (2010) E81-E88.

[19] Z.Q. Wu, K. Nagai, M. Banno, K. Okoshi, K. Onitsuka, E. Yashima, Enantiomer-Selective and Helix-Sense-Selective Living Block Copolymerization of Isocyanide Enantiomers Initiated by Single-Handed Helical Poly(phenyl isocyanide)s, J Am Chem Soc, 131 (2009) 6708-6718.

[20] Y. Hase, K. Nagai, H. Iida, K. Maeda, N. Ochi, K. Sawabe, K. Sakajiri, K. Okoshi, E. Yashima, Mechanism of Helix Induction in Poly(4-carboxyphenyl isocyanide) with Chiral Amines and Memory of the Macromolecular Helicity and Its Helical Structures, J Am Chem Soc, 131 (2009) 10719-10732.

[21] P. Samorí, C. Ecker, I. Gössl, P.A.J. De Witte, J.J.L.M. Cornelissen, G.A. Metselaar, M.B.J. Otten, A.E. Rowan, R.J.M. Nolte, J.P. Rabe, High shape persistence in single polymer chains rigidified with lateral hydrogen bonded networks, Macromolecules, 35 (2002) 5290-5294.

[22] E. Schwartz, V. Palermo, C.E. Finlayson, Y.-S. Huang, M.B.J. Otten, A. Liscio, S. Trapani, I. González-Valls, P. Brocorens, J.J.L.M. Cornelissen, K. Peneva, K. Müllen, F.C. Spano, A. Yartsev, S. Westenhoff, R.H. Friend, D. Beljonne, R.J.M. Nolte, P. Samorì, A.E. Rowan, "Helter-Skelter-Like" Perylene Polyisocyanopeptides, Chemistry – A European Journal, 15 (2009) 2536-2547.

[23] P.A.J. de Witte, M. Castriciano, J.J.L.M. Cornelissen, L. Monsù Scolaro, R.J.M. Nolte, A.E. Rowan, Helical Polymer-Anchored Porphyrin Nanorods, Chemistry – A European Journal, 9 (2003) 1775-1781.

[24] E. Schwartz, et.al., Synthesis, Characterization, and Surface Initiated Polymerization of Carbazole Functionalized Isocyanides, Chemistry of Materials, 22 (2010) 2597-2607.

[25] F. Millich, R.G. Sinclair, Polyisonitriles. I. Original structure and possible rearrangement of poly(α-phenylethylisonitrile), Journal of Polymer Science Part C: Polymer Symposia, 22 (1968) 33-43.

[26] M.M. Green, R.A. Gross, F.C. Schilling, K. Zero, C. Crosby, Macromolecular stereochemistry: effect of pendant group structure on the conformational properties of polyisocyanides, Macromolecules, 21 (1988) 1839-1846.

[27] M. Clericuzio, G. Alagona, C. Ghio, P. Salvadori, Theoretical Investigations on the Structure of Poly(iminomethylenes) with Aliphatic Side Chains. Conformational Studies and Comparison with Experimental Spectroscopic Data, J Am Chem Soc, 119 (1997) 1059-1071.

[28] C. Kollmar, R. Hoffmann, Polyisocyanides: electronic or steric reasons for their presumed helical structure?, J Am Chem Soc, 112 (1990) 8230-8238.

[29] F. Millich, G.K. Baker, Polyisonitriles. III. Synthesis and Racemization of Optically Active Poly(α-phenylethylisonitrile), Macromolecules, 2 (1969) 122-128.

[30] A.J.M. Van Beijnen, R.J.M. Nolte, W. Drenth, A.M.F. Hezemans, Screw sense of polyisocyanides, Tetrahedron, 32 (1976) 2017-2019.

[31] G.A. Metselaar, Polymerisation of Isocyanopeptides in, 2006.

[32] A.J.M. Van Beijnen, R.J.M. Nolte, A.J. Naaktgeboren, J.W. Zwikker, W. Drenth, A.M.F. Hezemans, Helical configuration of poly(iminomethylenes). Synthesis and CD spectra of polymers derived from optically active isocyanides, Macromolecules, 16 (1983) 1679-1689.

[33] E. Gomar-Nadal, L. Mugica, J. Vidal-Gancedo, J. Casado, J.T.L. Navarrete, J. Veciana, C. Rovira, D.B. Amabilino, Synthesis and doping of a multifunctional tetrathiafulvalene-substituted poly (isocyanide), Macromolecules, 40 (2007) 7521-7531.

[34] J.J.L.M. Cornelissen, W.S. Graswinckel, A.E. Rowan, N.A.J.M. Sommerdijk, R.J.M. Nolte, Conformational analysis of dipeptide-derived polyisocyanides, Journal of Polymer Science Part A: Polymer Chemistry, 41 (2003) 1725-1736.

[35] A.J.M. van Beijnen, R.J.M. Nolte, W. Drenth, A.M.F. Hezemans, P.J.F.M. van de Coolwijk, Helical Configuration of Poly(iminomethylenes). Screw Sense of Polymers Derived from Optically Active Alkyl Isocyanides, Macromolecules, 13 (1980) 1386-1391.

[36] I. Schnell, A. Watts, H.W. Spiess, Double-quantum double-quantum MAS exchange NMR spectroscopy: Dipolar-coupled spin pairs as probes for slow molecular dynamics, Journal of Magnetic Resonance, 149 (2001) 90-102.

[37] K. Schmidt-Rohr, A Double-Quantum Solid-State NMR Technique for Determining Torsion Angles in Polymers, Macromolecules, 29 (1996) 3975-3981.

[38] H.W.S. Klaus Schmidt-Rohr, Multidimensional Solid-State NMR and Polymers, 1996.

[39] J. Goetz, Orientational Information in Solids from REDOR Sidebands, Journal of Magnetic Resonance, 129 (1997) 222-223.

[40] S.L. Grage, A. Watts, Applications of REDOR for Distance Measurements in Biological Solids, in: G.A. Webb (Ed.) Annual Reports on NMR Spectroscopy, Academic Press, 2006, pp. 191-228.

[41] L. Odgaard, M. Bak, H.J. Jakobsen, N.C. Nielsen, 13C Chemical Shift and 13C-14N Dipolar Coupling Tensors Determined by 13C Rotary Resonance Solid-State NMR, Journal of Magnetic Resonance, 148 (2001) 298-308.

[42] J.D. van Beek, B.H. Meier, A DOQSY approach for the elucidation of torsion angle distributions in biopolymers: Application to silk, Journal of Magnetic Resonance, 178 (2006) 106-120.

[43] K. Schmidt-Rohr, H.W. Spiess, Multidimensional solid-state NMR and polymers, Academic Press, London, 1994.

[44] J.D. van Beek, L. Beaulieu, H. Schafer, M. Demura, T. Asakura, B.H. Meier, Solid-state NMR determination of the secondary structure of Samia cynthia ricini silk, Nature, 405 (2000) 1077-1079.

[45] A. Bohle, G. Brunklaus, M.R. Hansen, T.W. Schleuss, A.F.M. Kilbinger, J. Seltmann, H.W. Spiess, Hydrogen-Bonded Aggregates of Oligoaramide−Poly(ethylene glycol) Block Copolymers, Macromolecules, 43 (2010) 4978-4985.

[46] S.P. Brown, I. Schnell, J.D. Brand, K. Mullen, H.W. Spiess, The competing effects of [small pi]-[small pi] packing and hydrogen bonding in a hexabenzocoronene carboxylic acid derivative: A 1H solid-state MAS NMR investigation, Physical Chemistry Chemical Physics, 2 (2000) 1735-1745.

[47] J.R. Yates, T.N. Pham, C.J. Pickard, F. Mauri, A.M. Amado, A.M. Gil, S.P. Brown, An Investigation of Weak CH···O Hydrogen Bonds in Maltose Anomers by a Combination of Calculation and Experimental Solid-State NMR Spectroscopy, J Am Chem Soc, 127 (2005) 10216-10220.

[48] P. Sozzani, A. Comotti, S. Bracco, R. Simonutti, Cooperation of multiple CH center dot center dot center dot pi interactions to stabilize polymers in aromatic nanochannels as indicated by 2D solid state NMR, Chemical Communications, (2004) 768-769.

[49] D. Wasserfallen, I. Fischbach, N. Chebotareva, M. Kastler, W. Pisula, F. Jäckel, M.D. Watson, I. Schnell, J.P. Rabe, H.W. Spiess, K. Müllen, Influence of Hydrogen Bonds on the Supramolecular Order of Hexa-<I>peri</I>-hexabenzocoronenes, Advanced Functional Materials, 15 (2005) 1585-1594.

[50] S.P. Brown, Recent Advances in Solid-State MAS NMR Methodology for Probing Structure and Dynamics in Polymeric and Supramolecular Systems, Macromolecular Rapid Communications, 30 (2009) 688-716.

[51] M.H. Levitt, Spin dynamics : basics of nuclear magnetic resonance, John Wiley & Sons, Chichester ; New York, 2001.

[52] R.K. Harris, E.D. Becker, S.M. Cabral de Menezes, R. Goodfellow, P. Granger, NMR Nomenclature: Nuclear Spin Properties and Conventions for Chemical Shifts: IUPAC Recommendations 2001, Solid State Nuclear Magnetic Resonance, 22 (2002) 458-483.

[53] I.J. Lowe, Free induction decays of rotating solids, Physical Review Letters, 2 (1959) 285-287.

[54] E.R. Andrew, A. Bradbury, R.G. Eades, Removal of dipolar broadening of nuclear magnetic resonance spectra of solids by specimen rotation, Nature, 183 (1959) 1802-1803.

[55] A. Samoson, T. Tuherm, Z. Gan, High-Field High-Speed MAS Resolution Enhancement in 1H NMR Spectroscopy of Solids, Solid State Nuclear Magnetic Resonance, 20 (2001) 130-136.

Chapter 2

Direct backbone structure determination of polyisocyanodipeptide using solid-state NMR

Chandrakala M. Gowda, Ernst R. H. van Eck, Arend M. van Buul, Erik Schwartz, Gijsbrecht W.P. van Pruissen, Jeroen J. L. M. Cornelissen, Alan E. Rowan, Roeland Nolte and Arno P. M. Kentgens, *Macromolecules 2012, 45, 2209−2218*

2.1 Introduction

Polyisocyanodipeptides with their stable and rigid architecture have proven to be useful as a supporting framework for the functional groups such as carbazoles, porphyrins, perylenes, etcetera, (see Figure 2.1)[1-4] The efficiency and applicability of a functional material is determined to a large extent by the structural conformation of the polymer. The backbone conformation of polyisocyanides has been a subject of discussion for several decades and there have been several experimental and theoretical efforts to determine the structure and conformation of polyisocyanides. However due to lack of strong and confirmative experimental evidence there have been varying opinions and mixed results obtained for the structure of the polyisocyanides (For details see introduction chapter of the thesis).[5-12] Cornelissen et al. synthesized polyisocyanides with peptide sidechains, for example poly(L-isocyanoalanyl-D-alanine methyl ester (L,D-PIAA) (Figure 2.1b) and poly(L-isocyanoalanyl-L-alanine methyl ester) (L,L-PIAA)), with an aim to stabilize the backbone of the polyisocyanides by means of hydrogen bonds.[13] The presence of strong N─H----O═C hydrogen bonding interactions between the amide moieties of the side chains was confirmed by solid-state ^{1}H NMR and Infra-Red (IR) studies.[13, 14] Molecular modeling calculations were indicative of a 4_1 helical

conformation; however there is no direct experimental proof to confirm the structure.[13, 15] The aim of this chapter is to experimentally determine the backbone conformation of the polyisocyanodipeptide (L,D-PIAA) using solid-state NMR techniques.

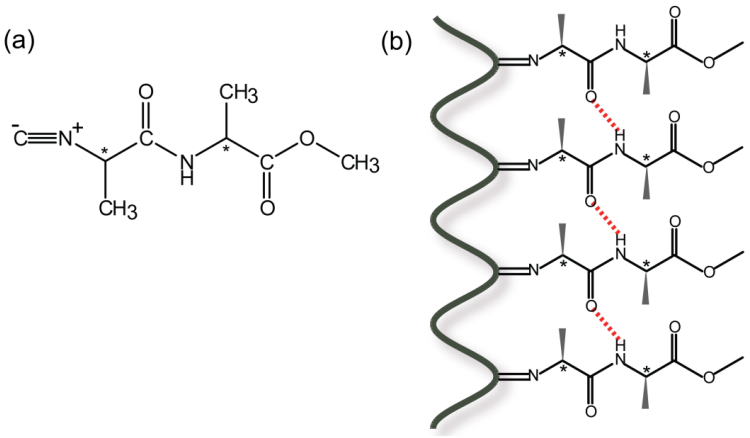

Figure 2.1 (a) Molecular skeleton of the L-isocyanoalanyl-D-alanine methyl ester monomer. (b) Sketch of the polymer L-isocyanoalanyl-D-alanine methyl ester (L,D-PIAA) with the proposed hydrogen bonding array between sidechains n and (n+4). The asterisks indicate the chiral centers. (The side chains to the left, outwards and into the plane of the drawing are omitted for clarity).

Determining the structural parameters such as the torsion angles and orientation of molecular segments in unoriented materials such as the polymers and proteins or inorganic materials is challenging. Solid-state NMR has proven to be a versatile and promising technique for the elucidation of structures in various material forms. Structural studies by solid-state NMR has been done in several ways: (1), Obtaining distance between the nuclei using dipolar coupling interactions in MAS experiments.[16, 17] (2) Using anisotropic measurements of dipole-dipole couplings, anisotropic chemical shifts, and nuclear quadrupolar couplings in spinning and static experiments to obtain relative orientation angles of the tensors.[18-28] (3) Using isotropic chemical shifts [29, 30] to elucidate useful structure information. Here, to determine the backbone conformation angle of the polyisocyanodipeptide L,D-PIAA, we use the method in which two ^{13}C CSA tensors of neighboring molecular segments are correlated to each other thus obtaining the relative orientation of the molecular segments. Torsion angle determination using correlation of CSA tensors using the DQ-SQ experiment (DOQSY) was first

demonstrated in simple peptide segments and polyethylene.[28] A variation of the experiment was used for the determination of secondary structure of the protein *Samia cynthia ricini* silk.[31] Tycko et al. used the MAS 2D-exchange experiments to obtain relative CSA tensor orientation angles in small peptides.[27]

The polymer backbone structure can be fully determined from the relative orientation of the two neighboring ^{13}C CSA tensors given that the orientation of the ^{13}C CSA tensor is known in the molecular frame. Relative orientation of two neighboring ^{13}C CSA tensors is obtained using DOQSY experiment. The orientation of the ^{13}C CSA tensor in the molecular frame is obtained by CSA-dipolar correlation experiments such as the 2D-Separated Local Field (2D-SLF) experiments.[32, 33] SIMPSON simulations were performed to extract the orientation angles from the experimental DOQSY and 2D-SLF spectra.[34] The structural constraints obtained from the DOQSY and 2D-SLF data are used to build the L,D-PIAA model. The polymer model was subsequently subjected to Molecular Dynamics simulations in order to obtain the energy minimized structure.

2.2 Material and Method

Samples: The unlabeled L,D-PIAA sample was used to record 1D carbon NMR spectra. For the 2D NMR experiments the L,D-PIAA sample was enriched with ^{13}C and ^{15}N at the backbone imine carbon and nitrogen to get a 10% ^{13}C═^{15}N spin pair enrichment in the polymer. To this end a L,D -IAA monomer, in which the isocyano group was ^{13}C and ^{15}N enriched, was synthesized. This monomer was subsequently copolymerized with an unlabeled L,D -IAA monomer using a feed ratio of 1:9 (^{13}C-^{15}N- L,D -IAA: L,D -IAA, respectively) to obtain the 10% ^{13}C═^{15}N spin pair enriched L,D-PIAA sample as previously discussed.[14]

NMR:

1D experiments: 1D ^{13}C NMR spectra were recorded using Cross Polarization Magic Angle Spinning (CPMAS) experiments on a Varian 600MHz infinity spectrometer using a 4mm triple resonance MAS probe. The proton 90^{o} pulse length was 5μs and the proton RF field for spinlock during cross polarization (CP) was set to 50 kHz. Protons were decoupled in the direct dimension using the Continuous Modulation (CM) decoupling scheme[35] at an RF field strength of 76 kHz. The spinning speed was set to 4500Hz or

6000Hz. The spectra are referenced using the CH_2 carbon peak of adamantane at 38.48ppm as an external reference.

2D experiments: All 2D experiments were recorded in static mode on a Varian 400MHz infinity spectrometer using a 4mm triple resonance MAS probe and 10% $^{13}C{=}^{15}N$ spin pair enriched L,D-PIAA sample.

The ^{13}C-^{15}N 2D-SLF spectrum (Figure 2.4a) was recorded using the pulse sequence shown in Figure 2.2a. As a first step, the proton (^1H) magnetization is transferred to nitrogen (^{15}N) using a 35 kHz spinlock RF field on ^1H and ^{15}N nuclei each for a duration of 2.4ms. In the second step, the magnetization from nitrogen (^{15}N) to the carbons (^{13}C) is transferred using a 35 kHz spinlock RF field for both ^{15}N and ^{13}C for 2.5ms. The $^{13}C{=}^{15}N$ dipolar coupling evolution was recorded in steps of 55.55μs (t_1). A total of 21 t_1 increment points accumulating 2500 scans each were recorded in the indirect dimension. A ^{13}C spin echo of duration $2*\tau$ with τ=1200μs is created. The total echo time depends on the spin-spin relaxation time (T_2) of the ^{13}C nuclei. The ^{13}C chemical shift evolution during time τ is refocused using a 180^o pulse on the carbons (^{13}C) at the center of the echo time $2*\tau$. The refocusing of $^{13}C{=}^{15}N$ heteronuclear dipolar coupling is perturbed by an additional 180^o pulse at time t_1 on nitrogen (^{15}N). The dipolar coupling is evolved by shifting the position of the 180^o pulse on the nitrogen channel with small time increments t_1. Efficient ^{15}N decoupling in the direct dimension was achieved using the broad-band WALTZ-16 decoupling scheme employing 16.6μs pulse length.[36] Quadrature detection in the indirect dimension is not necessary as it only consists of a symmetric dipolar coupling evolution.

The DOQSY spectrum was recorded using the pulse sequence shown in Figure 2.2b.[28] ^1H-^{13}C Cross polarization was done using 45 kHz spinlock field strength on ^1H and ^{13}C for a duration of 1.5ms. The ^1H and ^{13}C 90^o pulses were 3.2μs and 3.3μs respectively. Protons were decoupled using an RF field strength of 70 kHz using the Two Pulse Phase Modulated (TPPM)[37] decoupling scheme during the excitation, evolution and acquisition time. The double-quantum (DQ) excitation time was optimized to select maximum signal from directly bonded $^{13}C{-}^{13}C$ spin pairs as calculated by the SIMPSON simulation program.[34] The double quantum excitation profile showed the maximum signal for single bond separated spin pair at $2*\tau$=200μs. However, two bond separated

^{13}C—^{12}C—^{13}C spin pairs occur as often as directly bonded ^{13}C—^{13}C spin pairs potentially obscuring the spectrum. Hence a DQ excitation time of $2*\tau$=160μs was chosen for DQ excitation which kept the ratios of intensities from single bond to two bond separated spin pairs to 8:1 while the DQ excitation time $2*\tau$=200μs would result in a ratio of 5:1. The total DQ reconversion time was set equal to that of the DQ excitation time. Quadrature detection in the ω_1 dimension was achieved using the time proportional phase increment (TPPI) method.[38] The indirect dimension consisted of 42 t_1 increments and was acquired in a total of 6 days of time. A detailed discussion and theoretical treatment of the sequence is given in ref [39] and ref [28].

Simulation, Model building and Energy minimization: ^{13}C CSA spinning sideband analyses were performed using Herzfeld and Berger Analysis (HBA) software package (HBA 1.6.12 K. Eichele, R. E. Wasylishen Dalhousie University & Universit¨at T¨ubingen, 2010). NMR simulations were performed using the SIMPSON simulation program.[34] The simulations for extraction of the orientation angles were set up to closely mimic the experimental conditions. The 2D-SLF simulations were performed by varying the dipolar orientation angles in the principal axis frame of the ^{13}C CSA tensor ($\beta_{\mathrm{D}}^{\mathrm{C1N1}}$, $\gamma_{D}^{\mathrm{C1N1}}$) over a grid of 0^o to 90^o in steps of 5^o each. For the simulation of the DOQSY spectra, in view of reducing the computational time initially a broad grid simulation of the spectra was run with $\alpha_{\mathrm{CSA}}^{\mathrm{C1C2}}$and $\gamma_{\mathrm{CSA}}^{\mathrm{C1C2}}$ varying from 0^o to 360^o in steps of 30^o each and $\beta_{\mathrm{CSA}}^{\mathrm{C1C2}}$ varying from 0^o to 90^o in steps of 10^o. In the region of the probable minima obtained in the broad grid of simulations, a fine grid of simulation was further set up with $\alpha_{CSA}^{\mathrm{C1C2}}$and $\gamma_{\mathrm{CSA}}^{\mathrm{C1C2}}$ varying in steps of 10^o each and $\beta_{\mathrm{CSA}}^{\mathrm{C1C2}}$ varying in steps of 5^o in the vicinity of the minima only. The simulated 2D-SLF and DOQSY spectra were processed identically to the experimental spectrum using the matNMR processing toolbox in Matlab.[41] The polymer model was built in a Matlab program using the orientation angles obtained from the analysis of the DOQSY and the 2D-SLF spectrum and was subsequently energy minimized using the Accelrys Materials Studio program.[41]

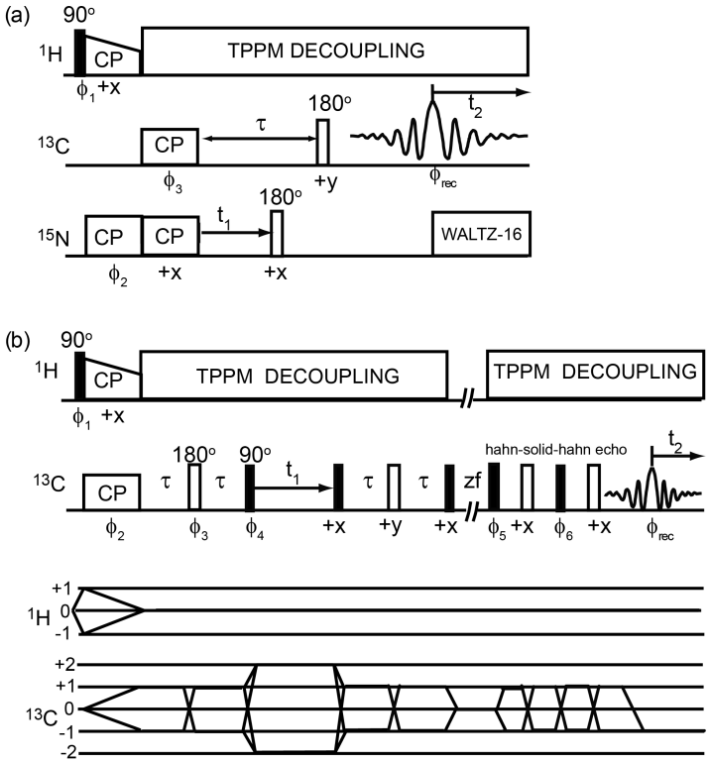

Figure 2.2. (a) The ^{13}C-^{15}N 2D-SLF pulse sequence with double CP transfer steps to select ^{13}C magnetization from carbons that are directly bonded to ^{15}N nuclei. Phase cycle ϕ_1=1,3; ϕ_2=0,0,2,2; ϕ_3=(0,0,0,0,2,2,2,2); ϕ_{rec}=(3,1,1,3,1,3,3,1);

(b) DOQSY pulse sequence and the coherence transfer pathway. 2τ represents the double quantum excitation and reconversion time while t_1 is the indirect dimension evolution time. The z-filter (zf) time was set to 1ms during which unwanted coherences are dephased due to the heteronuclear dipolar coupling to protons.[39] The Hahn-solid-Hahn echo is applied to avoid baseline distortions.[28] The pulse phases ϕ_2, ϕ_3 and ϕ_4 are cycled in four steps to select double quantum coherences. ϕ_1=1,3; ϕ_2=(1,1,2,2,3,3,0,0); ϕ_3=(0,0,1,1,2,2,3,3, 1,1,2,2,3,3,0,0, 2,2,3,3,0,0,1,1, 3,3,0,0,1,1,2,2); ϕ_4=(0,0,1,1,2,2,3,3); ϕ_5=(2_{32},3_{32},0_{32},1_{32}); ϕ_6=(1_{32},2_{32},3_{32},0_{32}, 3_{32},0_{32},1_{32},2_{32}); ϕ_{rec}=((0,2,2,0,0,2,2,0,2,0,0,2,2,0,0,2)$_2$ (1,3,3,1,1,3,3,1,3,1,1,3,3,1,1,3)$_2$ (2,0,0,2,2,0,0,2,0,2,2,0,0,2,2,0)$_2$ (3,1,1,3,3,1,1,3,1,3,3,1,1,3,3,1)$_2$).

2.3 Results and Discussions

2.3.1 ^{13}C Chemical shift anisotropy tensor

The 1D ^{13}C CPMAS spectrum L,D-PIAA shown in Figure 2.3. [14] The isocyano carbon that forms the backbone of the polymer chain has an isotropic chemical shift value of 160.9 ppm and the chemical shift anisotropy tensor of the carbon is ~96 ppm. The sample spinning at magic angle creates spinning sidebands on either side of the isotropic shift and is indicated by asterisk marks. The CSA tensor information can be obtained using the Herzfeld and Berger Analysis spinning sideband analysis (HBA).[43] The area of each spinning sidebands are used for the HBA analysis. In the presence of additional anisotropic interactions such as the dipolar coupling, quadrupolar coupling etc. the spinning sideband intensities are a net effect of the CSA, dipolar coupling interaction and the residual dipolar coupling as a result of the quadrupolar coupling interaction.[44] In the natural abundant polymer sample the ^{13}C imine carbon is bonded to NMR active ^{14}N quadrupolar nuclei by means of a double bond. For a $^{13}C{=}^{14}N$ group the typical dipolar coupling is of the order of 1100 Hz. At a magic-angle spinning frequency of 4500 Hz, which is ~4 times larger than the dipolar coupling interaction, the $^{13}C{=}^{14}N$ heteronuclear dipolar coupling is averaged to a large extent. The cross terms between the dipolar and quadrupolar interactions at high field strengths (here 14.1 T) are generally negligible.[18] Hence in this case the CSA interaction is dominant and the principal components (δ_{11}, δ_{22}, δ_{33}) of the ^{13}C CSA tensor can be determined by the Herzfeld and Berger spinning sideband analysis.[43] Since the spinning sidebands are well separated, the sideband integrals provide a highly reliable CSA tensor analysis. The principal CSA tensor components of the backbone ^{13}C were determined to be δ_{11}=254 ppm, δ_{22}=145 ppm and δ_{33}=83 ppm. The tensor values obtained at multiple spinning speeds (4500 Hz and 6000 Hz) were reproducible to within an accuracy of ±2 ppm. The chemical shift anisotropy reflects the electronic environment around the nucleus. Thus the relative orientation of the molecular segments in the polymer chain is determined by measuring the relative orientation of the tensor components of the two neighboring carbon nuclei along the polymer backbone. The exact structure determination further requires fixing the orientation of the ^{13}C CSA tensor components in the molecular frame. We use the 2D-DOQSY and 2D-SLF solid-state NMR experiments to obtain this information.

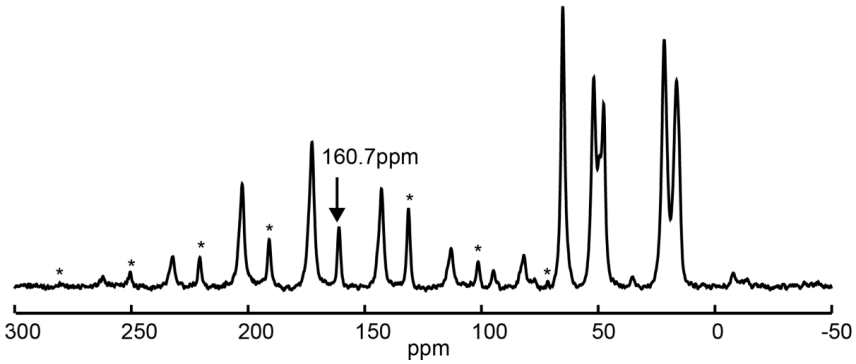

Figure 2.3. ^{13}C CPMAS spectrum of natural abundance L,D-PIAA. The peak at 160.7 ppm corresponds to the backbone carbon. The spinning sidebands are indicated by asterisks.

2.3.2 Relative ^{13}C CSA and ^{13}C-^{15}N dipolar tensor orientation

The dipolar interaction acts along the line connecting the two interacting nuclei. For a directly bonded spin pair such as the C=N in the polyisocyanides, the correlation of the ^{13}C CSA tensor to the dipolar coupling interaction provides information about the absolute orientation of the CSA tensor in the molecular frame. 2D-Separated Local Field (2D-SLF) experiments are used to obtain CSA-dipolar orientation information in static case.[22, 32, 33] Other experiments such as Rotational Echo Double Resonance (REDOR) sideband de-phasing and rotary resonance experiment proved to be very useful for samples with multiple spin sites and for natural abundant spin systems where MAS is essential to resolve the peaks and to increase sensitivity.[18, 25] However, we resorted to the 2D-SLF experiment to obtain the orientation of the ^{13}C-^{15}N dipolar vector in the principal frame of the ^{13}C CSA tensor using a 10% ^{13}C═^{15}N spin pair enriched L,D-PIAA. The two-dimensional spread of the resonance frequencies in the 2D-SLF spectrum allows a reliable spectral analysis. In addition, it does not suffer from extreme sensitivity to RF inhomogeneity as in a rotary resonance experiment.[18] The non-modulated natural abundant ^{13}C signals would appear in the form of a central ridge of the SLF spectrum in the indirect dimension whilst the ^{13}C coupled to ^{15}N will spread in the form of ridge pattern in the 2D spectra characteristic to the relative CSA-DD orientation angles. A double CP is used to create ^{13}C magnetization on the backbone carbon that is directly bonded to the imino nitrogen (^{13}C═^{15}N). The magnetization is first transferred from

protons (^{1}H) to ^{15}N and subsequently transferred from ^{15}N to the directly bonded ^{13}C. The experimental 2D-SLF spectrum, free of such a central ridge, is shown in Figure 2.4a. Figure 2.4b shows the simulated spectrum that best matches the experimental spectrum. The details of the simulations and the fitting are discussed below. In the 2D-SLF spectrum the frequencies in the direct dimension are a function of the ^{13}C CSA tensor and the frequencies in the indirect dimension are a function of ^{13}C═^{15}N dipolar coupling. The 2D spectral features showing specific patterns of ridges are a function of the relative orientation angles of the CSA and dipolar interaction tensors.

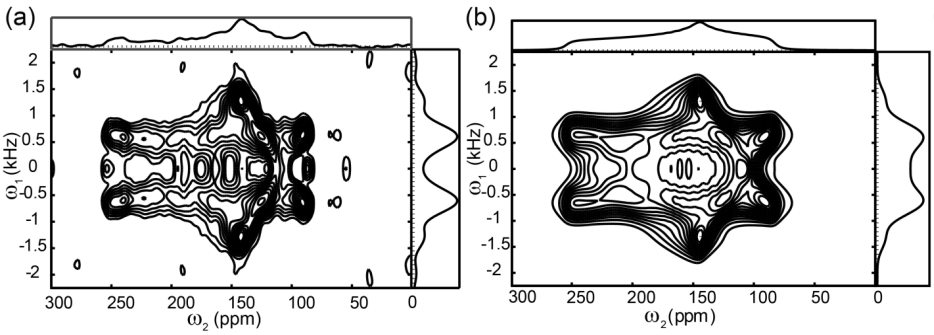

Figure 2.4 (a) Experimental 2D-SLF spectrum of 10% ^{13}C-^{15}N spin pair enriched L,D-PIAA. The sum projection of the spectrum in the direct dimension represents the powder spectrum resulting from the CSA and the sum projection of the spectrum in the indirect dimension gives rise to the heteronuclear dipolar coupling pake doublet pattern. (b) The best fit simulation of the 2D-SLF experiment for a relative orientation of the dipolar C1-N1 vector given by the Euler angles β_{D}^{C1N1} =80^{o} and γ_{D}^{C1N1}= 90^{o}. (c) The ^{13}C═^{15}N dipolar vector in the principal axis frame of the ^{13}C CSA tensor of the imine carbon. The labels C1 and N1 are used in the discussions below for convenience.

SIMPSON simulations were performed to extract the magnitude of the ^{13}C═^{15}N dipolar coupling and the relative orientation angles of the dipolar coupling tensor in the principal axis frame of the ^{13}C CSA tensor. First, we extract the magnitude of the dipolar coupling using the sum projection of 2D-SLF spectra in the indirect dimension (ω_1) which represents the Pake doublet pattern of the ^{13}C═^{15}N dipolar coupling. 1D SIMPSON simulations with varying magnitudes of dipolar coupling were performed to generate ^{13}C═^{15}N Pake patterns (Figure 2.5).

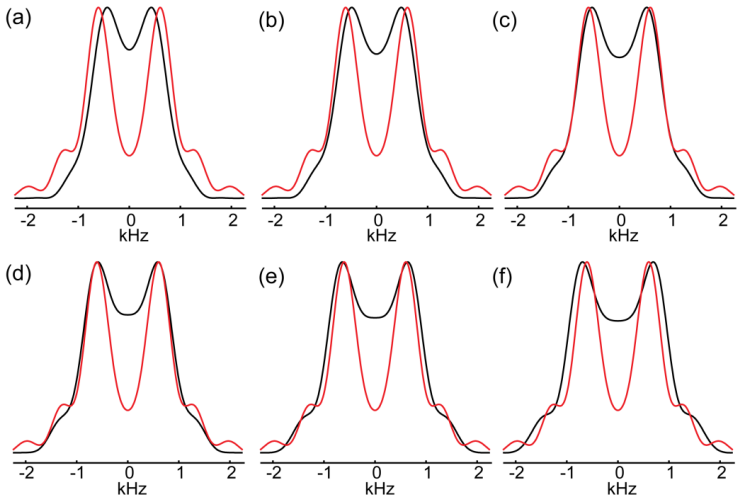

Figure 2.5 Simulated Pake doublet powder patterns (black) of the $^{13}C{=}^{15}N$ heteronuclear dipolar coupling with the dipolar coupling magnitude varied as (a)1200 Hz, (b)1300 Hz, (c)1400 Hz, (d)1500 Hz, (e)1600 Hz, (f)1700 Hz. Experimental spectrum is shown in red.

The best matching for the dipolar coupling magnitude was obtained for a $^{13}C{=}^{15}N$ dipolar coupling of 1495±50 Hz which corresponds to a $^{13}C{=}^{15}N$ bond length of 1.27 Å ± 0.02 Å. Secondly, to extract the relative CSA-dipolar orientation angles the dipolar coupling magnitude determined above is used. In the SIMPSON spin system the principal axis frame of the ^{13}C CSA tensor is considered as the reference frame i.e. the Euler angles relating the principal axis frame and the laboratory frame are given by (α_{CSA}^{C1}, β_{CSA}^{C1}, γ_{CSA}^{C1}) = (0, 0, 0). The dipolar tensor is related to this reference frame by the Euler angles ($\alpha_{\mathrm{D}}^{\mathrm{C1N1}}$, $\beta_{\mathrm{D}}^{\mathrm{C1N1}}$, $\gamma_{\mathrm{D}}^{\mathrm{C1N1}}$). The dipolar coupling is a uniaxial tensor and is invariant to rotation around the $^{13}C{=}^{15}N$ bond. The simulations thus determine two of the Euler angles that relate the unique axis of the dipolar coupling tensor in the principal axis frame of the ^{13}C CSA tensor described by β_D^{C1N1} and $\gamma_{\mathrm{D}}^{\mathrm{C1N1}}$. A plot of simulated spectra for varying β_D^{C1N1} and $\gamma_{\mathrm{D}}^{\mathrm{C1N1}}$ is shown in Figure 2.6.

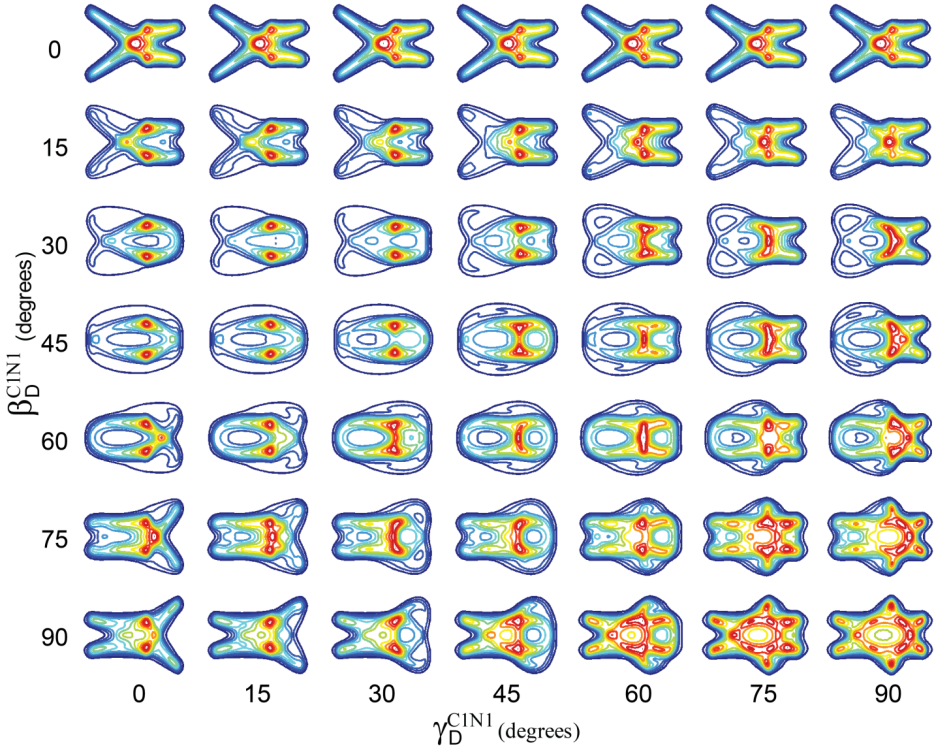

Figure 2.6: Series of plots of the ^{13}C-^{15}N 2D-SLF simulations performed with SIMPSON varying the β_D^{C1N1} and γ_D^{C1N1} angles orienting the dipolar CN vector with respect to the C1 CSA principal axis frame from 0° to 90°.

It can be seen that when the β_D^{C1N1} rotation angle is zero the spectra are insensitive to a change in γ_D^{C1N1} angle. As the β_D^{C1N1} angle approaches 90° the spectral patterns become highly sensitive to variations in γ_D^{C1N1} angle. The D2h symmetry of the dipolar coupling interaction leads to the symmetry equivalence of the angles (θ, ϕ); $(\theta, 180-\phi)$; $(\theta, 180+\phi)$; $(\theta, -\phi)$; $(180-\theta, \phi)$; $(180-\theta, 180-\phi)$; $(180-\theta, 180+\phi)$; $(180-\theta, -\phi)$.[45, 46] Chi-square plot of the complete grid simulations of the SLF spectrum with $(\beta_D^{C1N1}, \gamma_D^{C1N1})$ varying from (0°, 0°) to (180°, 360°) is shown in Figure 2.7.

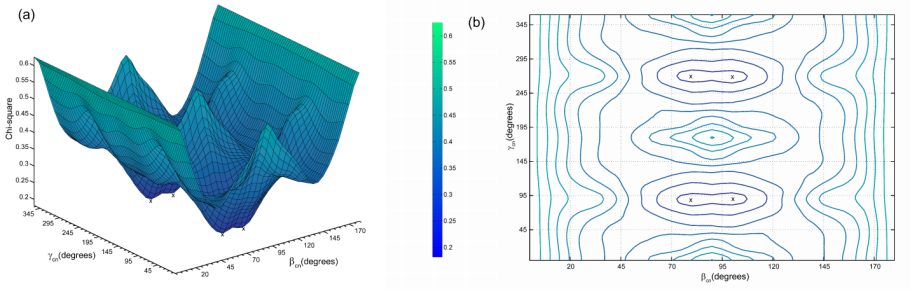

Figure 2.7 (a) The chi square plots of the minima, with $(\beta_D^{C1N1}, \gamma_D^{C1N1})$ varying from (0°, 0°) to (180°, 360°), shows the D2h symmetry of the dipolar coupling interaction. (b) Top view of the chi square plot with 'x' marks indicating the minima.

The best matching simulation is obtained for $(\beta_D^{C1N1}, \gamma_D^{C1N1})$ = (80°, 90°) and is shown in Figure 2.4b. In the case of uniaxial tensors the Euler angles β_D^{C1N1} and γ_D^{C1N1} become equivalent to the polar angles (θ, ϕ) of a spherical coordinate system and hence the dipolar coupling vector can be represented as shown in Figure 2.8.[45, 46] The simulations provide a very good match to the experimental spectrum despite the fact that the simulations were performed assuming single pulse excitation, whereas the experimental spectrum was obtained using $^{13}C{=}^{15}N$ cross polarization experiment. In the present case the angle γ_D^{C1N1}= 90° restricts the symmetry related angle combinations to a total of four being (80°, 90°); (80°, 270°); (100°, 90°); (100°, 270°) that would all result in the same 2D-SLF spectrum.

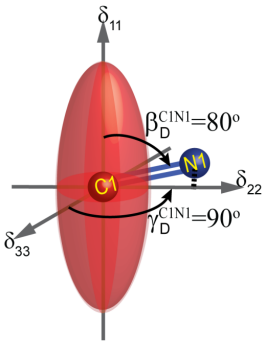

Figure 2.8 Orientation of the C═N bond in the CSA tensor frame obtained from the SLF data.

2.3.3 Relative ^{13}C CSA tensor orientations

The relative orientation angles β_D^{C1N1}, γ_D^{C1N1} of the $^{13}C—^{13}C$ dipolar tensor in the ^{13}C CSA tensor frame partially fixes the ^{13}C CSA tensor in the molecular frame. The unknown angle, α_D^{C1N1}, which is the rotation around the $^{13}C═^{15}N$ bond will be determined using the geometry information as explained later. In the next step we wish to determine the relative orientation angles between the CSA tensors of two neighboring carbons in the polymer backbone. This information combined with that of the orientation of the ^{13}C CSA tensor in the molecular frame can be used to determine the complete backbone conformation. Several experiments have been described in the literature to extract relative orientation angles of neighboring carbon CSA tensors. For static samples Double Quantum Single-Quantum Spectroscopy (DOQSY) and its variants have been used to determine torsion angles in polymers and biopolymers such as Samia cynthia ricini silk.[28, 31, 47] Tycko et al. used the rotor synchronized 2D exchange spectroscopy under MAS to extract relative tensor orientations in peptide samples.[27] Experiments have also been designed to obtain torsion angles using dipolar interaction tensors such as the NCCN-2Q-HLF.[24] We have made use of the DOQSY pulse sequence shown in Figure 2.2b.[28] This sequence has the advantage that for strongly coupled spins a short DQ excitation time of the order of 160μs to 240μs can be employed to excite DQ coherences. Sequences involving a large number of pulses are not practical for strongly coupled spins as the minimum DQ excitation time is limited by the number of pulses and pulse lengths to be used.[47] The sample used here, 10% $^{13}C═^{15}N$ spin pair enriched L,D-PIAA contains 1% directly bonded $^{13}C—^{13}C$ spin pairs. A potential contribution to the double quantum spectra can arise from 1% two bond separated $^{13}C—^{12}C—^{13}C$ spin pairs. The dipolar coupling is inversely proportional to the cube of the distance hence the directly bonded spins are strongly coupled with a magnitude of ~2200 Hz for a $^{13}C—^{13}C$ spin pair whilst the two-bond separated $^{13}C—^{12}C—^{13}C$ carbon spin pairs have a dipolar coupling of magnitude ~500 Hz. The DQ excitation profile of the directly bonded and two bond separated carbon spin pairs is shown in

Figure 2.9.

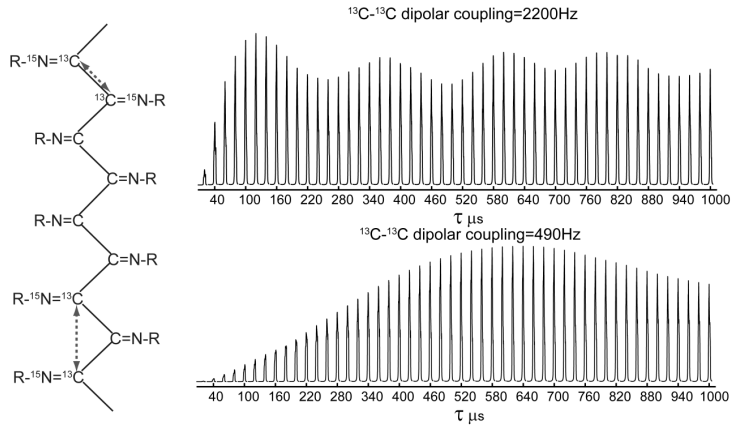

Figure 2.9 Simulated DQ excitation profile of the powder spectrum of the directly bonded and two bond separated ^{13}C spin pairs.

The experimental DOQSY spectrum is shown in Figure 2.10a. The frequency in the direct dimension is determined by the ^{13}C CSA and ^{13}C-^{13}C dipolar coupling while the frequency in the indirect dimension is a function of the sum of the ^{13}C CSA tensors.[28] The DQ excitation efficiency is a function of ^{13}C—^{13}C dipolar coupling strength and hence the powder line shape of a DQ filtered carbon spectrum is a function of ^{13}C—^{13}C dipolar vector orientation. To obtain uniform DQ excitation over the full powder pattern, DOQSY spectra have to be recorded at varying excitation times (2*τ) and added together as described in reference [28]. However, in the present case we refrain from doing this and preferred to use a single DQ excitation time due to the concern of increased signal contributions from two-bond separated (^{13}C—^{12}C—^{13}C) spin pairs in the spectrum. The effects of ^{13}C—^{13}C dipolar coupling on the spectrum have been taken into account in the simulations. However, this requires the information of the orientation of the ^{13}C—^{13}C dipolar coupling vector in the ^{13}C CSA which will be discussed later in the chapter below.

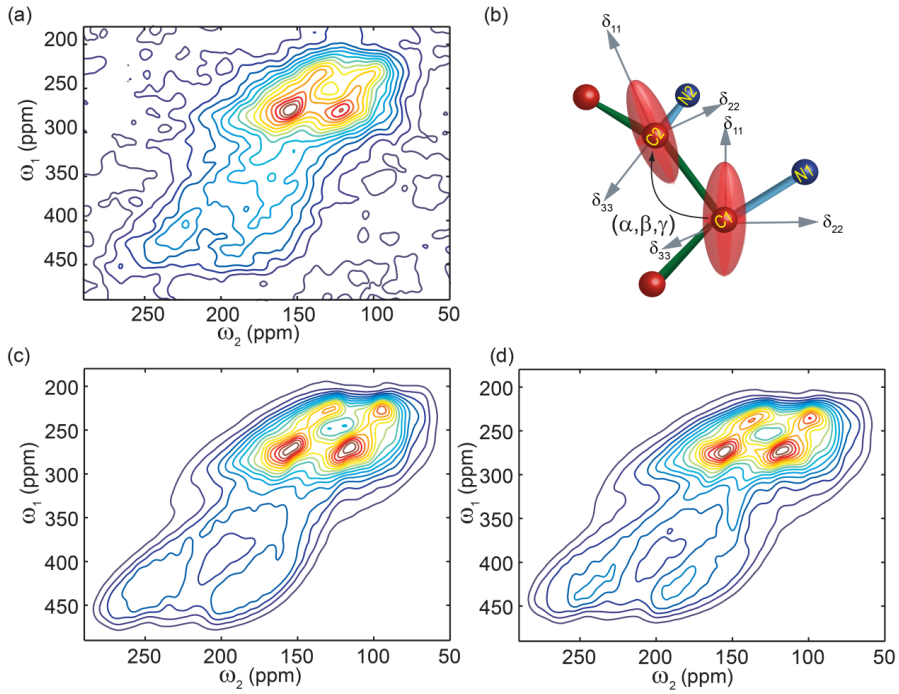

Figure 2.10. (a) Experimental 2D DOQSY spectrum of 10% $^{13}C{=}^{15}N$ spin pair labeled (L,D-PIAA) polymer using a DQ excitation and reconversion time of 160μs. (b) Relative orientation of principal CSA tensor frames of ^{13}C-^{13}C carbon spin pairs along the polymer backbone. The CSA tensors are shown as ellipsoids around the respective carbons. The labels are used for convenience in discussions below. (c) and (d) Best matching simulations of the DOQSY spectrum indicating the Euler angles $(\alpha, \beta, \gamma)_{CSA}^{C1C2}$ of c) (250°, 45°, 30°) and d) (240°, 50°, 30°) respectively. This can be translated to a relative rotation of the CSA frame about a specific rotation axis (see Table 2-1) of 90° or 100° for (c) and (d) respectively.

The relative orientations of the ^{13}C CSA tensors were extracted by the least square fitting of the experimental spectra with the SIMPSON simulations. All non-negligible interactions that influence the spectrum were considered in the simulations. This requires the knowledge of both the magnitude and the orientation angles of the interaction in a given reference frame. The current spin system depicted in Figure 2.10b consists of a $^{13}C{=}^{13}C$ spin pair with each carbon atom dipolar coupled to a ^{15}N atom, with the ellipsoids representing the CSA tensor of the carbons. Associated with this spin system one can identify three dominant interactions that will influence the DOQSY spectrum. Firstly, the chemical shift anisotropy of the carbons C1 and C2. Secondly, the

heteronuclear $^{13}C{=}^{15}N$ dipolar coupling of the two carbon nitrogen spin pairs and thirdly, we have the homonuclear $^{13}C{-}^{13}C$ dipolar coupling. In the simulations the principal axis frame of the C1 carbon CSA tensor was fixed as the reference frame.[34, 48] The magnitude and relative orientation of the $^{13}C1{=}^{15}N1$ in the ^{13}C CSA reference frame is determined from the SLF data. To simulate the effect of $^{13}C2{=}^{15}N2$ dipolar coupling on the DOQSY spectrum the relative orientation of $^{13}C2{=}^{15}N2$ dipolar tensor in the reference frame has to be determined. This is obtained by multiplying the rotation matrices $R_D^{C2N2} = R_{CSA}^{C1C2} * R_D^{C1N1}$ where, the rotation matrix R_{CSA}^{C1C2} refers to the coordinate transformation relating the C2 carbon CSA tensor to the reference frame. R_D^{C1N1} is the rotation matrix relating the C1N1 dipolar vector to the reference frame. The Euler angles from the resultant matrix R_D^{C2N2} are the Euler transformation angles orienting the C2-N2 dipolar tensor in the reference frame.[49]

The orientation of the $^{13}C1{-}^{13}C2$ dipolar coupling vector in the reference frame was obtained by combined consideration of the SLF result, the standard geometry of sp^2 hybridized atoms and the general orientation of δ_{33} tensor component with respect to the sp^2 plane. The backbone carbon atom of the imine (C1=N1) group is sp^2 hybridized hence all the atoms directly bonded to C1 lie in a plane with bond angles of ~120°. Experiments and abinitio quantum mechanical calculations on several compounds with sp^2 hybridized carbon atoms indicate that the most shielded component (δ_{33}), of the sp^2 hybridized carbon is perpendicular to the sp^2 plane of the atoms.[50-53] Assuming a similar orientation of the tensors in the present case and using the orientation of the C1=N1 bond from the 2D-SLF data analysis, the arrangement of the atoms bonded to the imine carbon is as shown in Figure 2.11. The dipolar orientation angles (β_D^{C1C2} , γ_D^{C1C2}) of the $^{13}C1{-}^{13}C2$ dipolar vector in the principal axis frame of the C1 CSA tensor can thus be obtained. There is an equal probability of either one of the two neighboring carbon atoms being labeled. The two set of Euler angles corresponding to the two possible neighbors of C1 are (β_D^{C1C2} , γ_D^{C1C2}) = (160°, 270°) and (β_D^{C1C2} , γ_D^{C1C2}) = (40°, 270°). The Euler angles (β_D^{C1C2} , γ_D^{C1C2}) define the polar and the azimuthal angle of the $^{13}C1{-}^{13}C2$ vectors in the principal axis frame of C1 CSA tensor. The ^{13}C-^{13}C dipolar coupling has been assigned a value of 2200Hz considering a typical $^{13}C{-}^{13}C$ single bond length of 1.5Å.

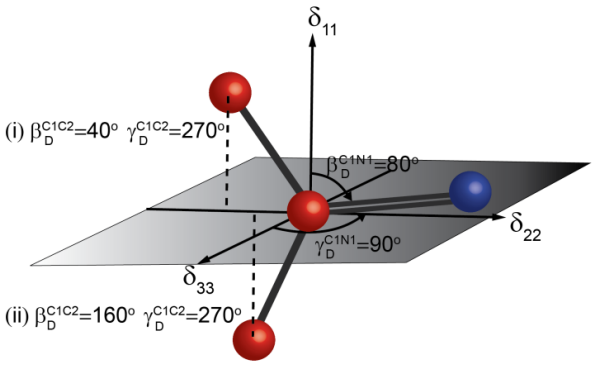

Figure 2.11 The angles (β_D^{C1C2} , γ_D^{C1C2}) and (β_D^{C1N1} , γ_D^{C1N1}) define the orientation of the ^{13}C—^{13}C dipolar vector and ^{13}C═^{15}N bond in the ^{13}C CSA frame of the central imine carbon. The dashed lines are the projections of the two C1C2 vector onto the plane defined by δ_{33} and δ_{22}.

Simulations were done using the angles β_D^{C1C2} = 160°, γ_D^{C1C2} = 270° for the orientation of the ^{13}C1—^{13}C2 dipolar tensor in the PAS of the ^{13}C CSA tensor of C1. Initially a broad grid simulation of the spectra was run with $\alpha_{\mathrm{CSA}}^{\mathrm{C1C2}}$ and $\gamma_{\mathrm{CSA}}^{\mathrm{C1C2}}$ varying from 0° to 360° in steps of 30° each and $\beta_{\mathrm{CSA}}^{\mathrm{C1C2}}$ varying from 0° to 90° in steps of 20° (the corresponding 180-$\beta_{\mathrm{CSA}}^{\mathrm{C1C2}}$ simulations are symmetry equivalent and hence the simulations for $\beta_{\mathrm{CSA}}^{\mathrm{C1C2}}$> 90° are not run). The least square fitting of the experimental spectrum showed minima near $\beta_{\mathrm{CSA}}^{\mathrm{C1C2}}$ ranging from 40° to 50° degrees. In the second step, a fine grid of simulations was set up with $\beta_{\mathrm{CSA}}^{\mathrm{C1C2}}$ fixed at 30°, 40°, 45°, 50°, and 55° with $\alpha_{CSA}^{\mathrm{C1C2}}$ and $\gamma_{\mathrm{CSA}}^{\mathrm{C1C2}}$ in steps of 20° each near the minima values obtained in the broad grid simulations. These fine grid simulations indicated minima at $\beta_{\mathrm{CSA}}^{\mathrm{C1C2}}$ values of 40°, 45° and 50°. The spectra at β=40° were examined and excluded as false minima as the simulated spectral patterns visibly did not match the experimental spectrum very well. CSA symmetry considerations theoretically yield 16 DOQSY spectra that are equivalent.[22] The presence of the ^{13}C—^{13}C dipolar interaction reduces the number of symmetry related angle combinations to eight, which are $[\alpha, \beta, \gamma\ ]$, $[180-\alpha, \beta, 180-\gamma]$, $[180+\alpha, \beta, \gamma]$, $[-\alpha, \beta, 180-\gamma]$, $[\ -\alpha, 180-\beta, 180+\gamma\ ]$, $[\ 180-\alpha, 180-\beta, 180+\gamma\ ]$, $[\ 180+\alpha, 180-\beta, -\gamma\ ]$, $[180+\alpha, 180-\beta, 180-\gamma]$. The two simulated spectra that best match the experimental spectrum are shown in Figure 2.10 c and d. The angles [250° 45° 30° 90°] and [240° 50° 30° 100°] corresponding to the minima are represented in the order $[\alpha, \beta, \gamma, \theta]$ where θ

describes the rotation about an axis [nx ny nz] in the reference frame. This axis and rotation angle θ are obtained by an axis-angle transformation where the Euler rotations over the angles $(\alpha, \beta, \gamma)_{CSA}^{C1C2}$ are mimicked by a rotation θ about a unique axis [n_x n_y n_z] having the same net effect. [49] This is a convenient representation as the orientation of the ^{13}C CSA tensor of a neighboring carbon in the polymer backbone can be obtained by a rotation around the polymer chain axis over an angle depending on the pitch of the (helical) chain. Table 2-1 lists the symmetry related sets of Euler angles which produce spectra identical to the simulated spectra shown in Figure 2.10c and d together with the corresponding rotation axis [n_x n_y n_z] and angle θ. As can be seen the symmetry related Euler angles produce rotation angles (θ) of different magnitudes such as 100^o, 90^o, 138^o, 107^o, 167^o etc. The true minima were identified by building a model of the L,D-PIAA backbone using the structural constrainsts obtained from 2D-SLF and DOQSY data as is described in the next section.

Table 2-1 Set of 8 symmetry related Euler angle combinations for the relative orientation of principal axis system of the CSA of neighboring carbons in the polymer backbone yielding equivalent DOQSY spectra as the minima identified in Figure 2.10. Alternatively, the Euler rotations can be mimicked by a rotation θ about a unique axis [n_x n_y n_z] having the same overall effect. All angles are in degrees.

α_{CSA}^{C1C2}	β_{CSA}^{C1C2}	γ_{CSA}^{C1C2}	θ	[n_x n_y n_z]		α_{CSA}^{C1C2}	β_{CSA}^{C1C2}	γ_{CSA}^{C1C2}	θ	[n_x n_y n_z]
240	50	30	100	[0.53 0.14 -0.83]		110	135	210	138	[-0.75 -0.63 -0.14]
120	130	210	132	[-0.70 -0.70 -0.11]		250	45	30	90	[0.50 0.18 -0.84]
60	130	330	132	[-0.70 0.70 0.11]		70	135	330	138	[-0.75 0.63 0.14]
300	50	150	100	[0.53 -0.14 0.83]		290	45	150	90	[0.50 -0.18 0.84]
300	130	210	167	[0.64 -0.64 0.41]		70	45	30	107	[-0.16 0.44 0.87]
60	50	30	100	[-0.14 0.53 0.83]		290	135	210	165	[0.59 -0.71 0.36]
120	50	150	100	[-0.14 -0.53 -0.83]		110	45	150	107	[-0.16 -0.44 -0.87]
240	130	330	167	[0.64 0.64 -0.41]		250	135	330	165	[0.59 0.71 -0.36]

2.3.4 Polymer backbone conformation

The polyisocyanide backbone chain was modeled using the relative orientation angles of the ^{13}C CSA tensors and the ^{13}C-^{15}N CSA-DD orientation angles. In the first step, using the C1═N1 dipolar orientation angles obtained from the 2D-SLF data the C1═N1 bond of

the first monomer unit (*M1*) was oriented in the C1 CSA frame with the azimuthal ($\gamma_{\mathrm{D}}^{\mathrm{C1N1}} = 90^{o}$) and the polar ($\beta_{\mathrm{D}}^{\mathrm{C1N1}} = 80^{o}$) angles as shown in Figure 2.12(a). In the second step, the coordinates of the monomer *M1* were rotated using the Euler rotation matrix R_{CSA}^{C1C2}, obtained from the DOQSY analysis, to determine the coordinates of the neighboring monomer unit *M2* (Figure 2.12b). Successive body fixed rotations produced the coordinates for *M2→M3, M3→M4.....M(n-1)→Mn*. The rotations occur at the origin (coinciding with the position of carbon C1) hence the position coordinates of the successive carbons C1, C2, C3,....Cn are fixed at the origin and the remaining atoms of the sidechain change position, giving for example the position of the subsequent nitrogens N2, N3,...Nn etc.. In the third step, the monomer units have to be translated away from the origin. To do this we use the earlier deduced information of the orientation of carbon C2 in the principal axis frame of the C1 carbon CSA tensor depicted in
Figure 2.11 based on the sp^2 hybridization of the backbone carbons and the orientation of the C1=N1 bond. The monomer unit *M2* is translated in the direction of ^{13}C1─^{13}C2 dipolar coupling i.e. in the direction of C1---*p*, so that the translation amounts to the C─C bond length of 1.5Å which is essentially the position of the point '*p'* (Figure 2.12c). The monomer units *M1* and *M2* are then translated together in the opposite direction (p---C1) so as to place C2 at the origin. Subsequently rotation of the point 'p' over R_{CSA}^{C1C2} results in the coordinate point '*q'* which represents the position of the backbone carbon of the monomer unit *M3* (Figure 2.12e). The above procedure is repeated where the monomer unit *M3* is first translated to the point '*q'* and following which the entire chain consisting of *M1*, *M2* and *M3* is moved so as to move carbon C3 of the monomer unit *M3* to the origin and so on. This ultimately produces the entire polymer chain. The same procedure was used to build models for all the eight angle combination that fitted the DOQSY spectrum. Table 2-2 lists the resulting bond angle $\measuredangle C_nC_{n+1}N_{n+1}$ for the 8 models. Only four minima produce geometrically favorable bond angles $\measuredangle C_nC_{n+1}N_{n+1}$ resulting in two isotactic helical polymer models corresponding to relative rotation angles of 100^{o} and 90^{o}. The geometrically favorable angle $\measuredangle C_nC_{n+1}N_{n+1}$ also imply that in these models the helix axis [n_x n_y n_z] and the ^{13}C═^{15}N bond vector are perpendicular to each other. The other minima which do not form geometrically favorable $\measuredangle C_nC_{n+1}N_{n+1}$ angles were discarded as unphysical solutions.

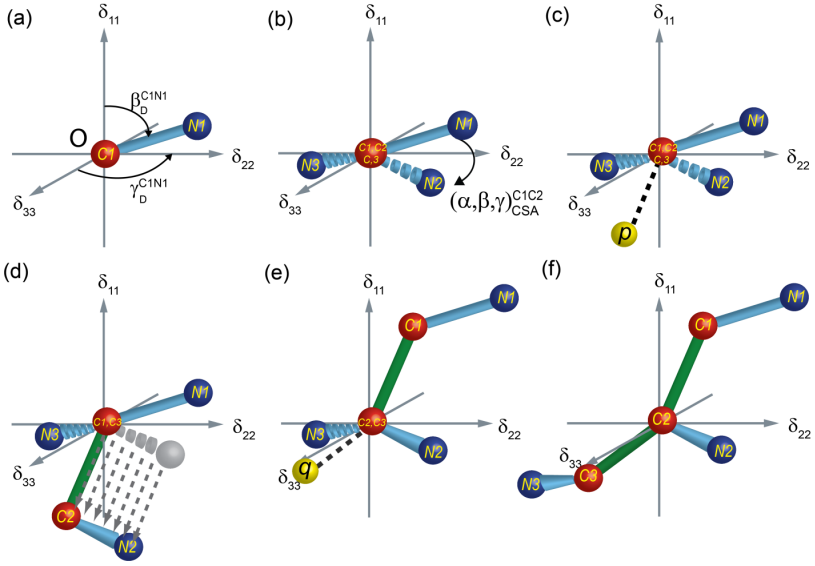

Figure 2.12 Illustration of polymer chain building starting from a single monomer unit using relative CSA-CSA and CSA-Dipolar angles. The position '*p*' represents the carbon atom bonded to C1 and lies in the sp^2 plane defined by C1-N1-p.

Table 2-2. List of Euler angle combinations $(\alpha,\beta,\gamma)_{CSA}^{C1C2}$ and relative rotation angle θ obtained from fitting the DOQSY spectra and the resulting bond angle ∠CnCn+1Nn+1 extracted from the polymer model based on these data (see text). The highlighted combinations lead to geometrically acceptable polymer models with a realistic ∠CnCn+1Nn+1 bond angle for a sp2 hybridized atom. All angles are in degrees.

	α_{CSA}^{C1C2}	β_{CSA}^{C1C2}	γ_{CSA}^{C1C2}	θ	∠$C_nC_{n+1}N_{n+1}$		α_{CSA}^{C1C2}	β_{CSA}^{C1C2}	γ_{CSA}^{C1C2}	θ	∠$C_nC_{n+1}N_{n+1}$
1	240	50	30	100	123		250	45	30	90	118
2	120	130	210	132	57		110	135	210	138	62
3	60	130	330	132	57		70	135	330	138	62
4	300	50	150	100	123		290	45	150	90	118
5	300	130	210	167	143		290	135	210	165	138
6	60	50	30	100	37		70	45	30	107	42
7	120	50	150	100	37		110	45	150	107	42
8	240	130	330	167	143		250	135	330	165	138

We started by generating polymer models with a helical angle equivalent to 90° and 100° i.e. 4_1 and 18_5 helices respectively, that were further subjected to molecular modeling

studies. Since the side chain orientations are unknown, for each of the polymer backbone models multiple structures with varying side chain orientations were built where the side chains were arbitrarily rotated around the C═N bond in steps of 30^{o}. This is done since in the complete polymer the side chains have less spatial freedom and hence may fall into local minima because the barrier leading to the proper energy minimum is too high to overcome in the modeling procedure. The molecular modeling studies were performed using the corrected Dreiding force field which was previously applied successfully for polyisocyanides.[2] To allow the polymer to easily rotate along the backbone and to minimize finite size effects along the polymer, a polymer with 100 repeat units without periodic boxes was used. The modeling was performed in three consecutive steps for every polymer structure. First, these structures were geometrically optimized at 0K to correct for any remaining artifacts from the structure generation process. Subsequent Molecular Dynamics simulation at 293K added enough energy to allow the polymer to explore a large conformational space and was used to determine the stability of the polymers. Finally, the resulting structure after 3ns of Molecular Dynamics simulation was again geometrically optimized at 0K. The resulting structures were analyzed with respect to the backbone C─C─C─C backbone dihedral angle and the hydrogen bond parameters between the N─H and C═O groups of the side chains. Both the initial helical 4_1 and 18_5 models converged to a ~15_4 helix (~96^{o} helical angle) with a mean C─C─C─C backbone dihedral angle of 79^{o}. The repeat unit corresponds to 3.75 units per turn. Figure 2.13 shows the side view and top view of one complete rotation of the 15_4 helix. The helix angle can be compared to that of the theoretical value of ~95^{o} obtained for poly(*tert*-butylisocyanide) (see figure 5c in ref [12]). Very recently the molecular modeling calculations of the polyisocyanide with a L-alanine substituent also yielded a helical structure with a rotation angle of ~96^{o}.[2] The optimized models obtained in the present study show regular hydrogen bonds between the side chains of the polymer. Hydrogen bond distances (N----O) in the polymer models showed a mean value of ~2.5-2.7Å and are largely unidirectional. This is in line with the earlier observed downfield shifted solid state amide proton chemical shifts of 9.2ppm.[14] To verify the model building approach used here we also built polymer models with helix angles of 70^{o}, 80^{o}, 110^{o} and 120^{o} and the models were subjected to molecular modeling studies. However, these structures showed very irregular and weaker (large N----O distance) hydrogen bonds and also showed large variations in C─C─C─C backbone dihedral angle. In the current approach,

the backbone conformation of the polymers is determined experimentally and only fine tuning of the backbone conformation and optimization of the orientation of the sidechain groups is done using modeling studies which takes less computational time. This approach is of particular value when determining the structure of functional polyisocyanides with large side chain substituents such as carbazole, perylene or porphyrin groups since they lead to additional interactions such as the aromatic π—π interactions, steric interactions etc. that can potentially influence the backbone conformations. For example, in the carbazole functionalized polyisocyanide, discussed in chapter 5, a markedly different chemical shift (δ=8.1ppm) for the NH proton as compared to L,D-PIAA (δ=9.2ppm) indicating that the hydrogen bonding strengths might be different in the two polyisocyanide analogues, raising questions towards possible structural differences in the polymer backbone conformation.[14, 54]

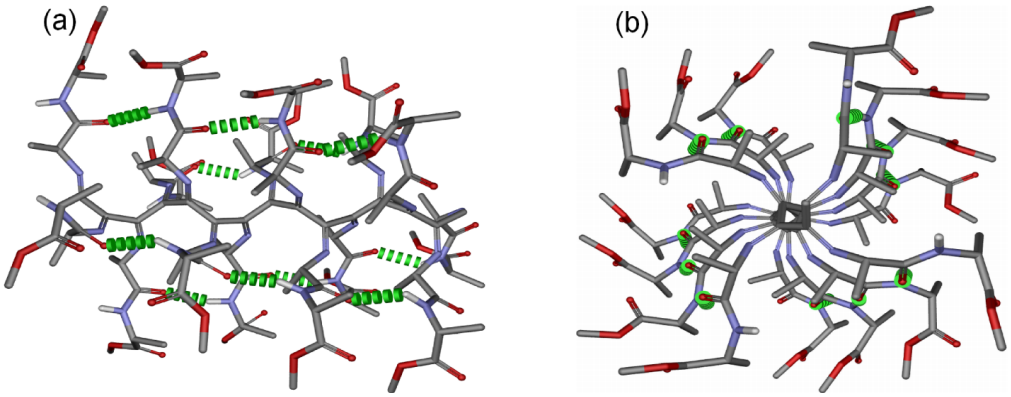

Figure 2.13 (a) side view and (b) top view of one complete helical turn of the geometry optimized L,D-PIAA polymer.

2.4 Conclusions

The structural studies of the hydrogen bond stabilized isocyanodipeptide polymer (L,D-PIAA) is carried out using 1D and 2D solid-state NMR experiments. Some of the key features observed in the NMR spectra of the polymer such as (1) The amide proton chemical shifts indicate presence of strong hydrogen bonds between the side chains in the L,D-PIAA. (2) The line widths of the ^{13}C CPMAS NMR spectrum are narrow with line widths of the order of ~100 Hz. (3). The 2D-SLF and DOQSY show well defined powder

ridge patterns that are reproduced very well in the SIMPSON simulations. The above three spectral features suggest a stable, strong and a regular structural conformation for the isocyanodipeptide polymer L,D-PIAA. The 2D-SLF experimental analysis revealed the orientation of the backbone carbon tensor in the molecular frame, while the DOQSY experiment was used to determine the relative ^{13}C-^{13}C CSA tensor orientation of neighboring carbons. Polymer models were built using the above NMR structural restraints. The polymer models of L,D-PIAA were subsequently energy minimized to refine the structure. We have determined the backbone conformation of the hydrogen bond stabilized isocyanodipeptide polymer (L,D-PIAA) to be an isotactic 15_4 helix. To the best of our knowledge this is the first direct structure determination of the polyisocyanopeptides which are a promising class of materials which are targeted as a scaffold for a host of functional materials. The question arises whether the exact helical structure is preserved when functional materials with for instance bulky aromatic functional groups are synthesized. Since such a system can lead to an interplay between aromatic interactions, steric interactions and hydrogen bonding in the stabilization of the polymer backbone. The approach followed in this study is independent of the pendant groups used in the polymer and hence is an efficient method for the structure determination of polymers with increasing structural complexity. A complete solid state NMR study analoguous to the one described in this study can shed more light on the precise molecular organization in these functionalized polymers. A suite of diverse NMR experiments combined with intelligent labelling strategies can help in deciphering not only the backbone conformation but explicity reveal conformation of sidechains and inter-sidechain interactions.

2.5 References

[1] P.A.J. de Witte, M. Castriciano, J.J.L.M. Cornelissen, L. Monsù Scolaro, R.J.M. Nolte, A.E. Rowan, Helical Polymer-Anchored Porphyrin Nanorods, Chemistry – A European Journal, 9 (2003) 1775-1781.

[2] E. Schwartz, V. Palermo, C.E. Finlayson, Y.-S. Huang, M.B.J. Otten, A. Liscio, S. Trapani, I. González-Valls, P. Brocorens, J.J.L.M. Cornelissen, K. Peneva, K. Müllen, F.C. Spano, A. Yartsev, S. Westenhoff, R.H. Friend, D. Beljonne, R.J.M. Nolte, P. Samorì, A.E. Rowan, "Helter-Skelter-Like" Perylene Polyisocyanopeptides, Chemistry – A European Journal, 15 (2009) 2536-2547.

[3] E. Schwartz, E. Lim, C.M. Gowda, A. Liscio, O. Fenwick, G. Tu, V. Palermo, R. de Gelder, J.J.L.M. Cornelissen, E.R.H. Van Eck, A.P.M. Kentgens, F. Cacialli, R.J.M. Nolte, P. Samori, W.T.S. Huck, A.E. Rowan, Synthesis, Characterization, and Surface Initiated Polymerization of Carbazole Functionalized Isocyanides, Chemistry of Materials, 22 (2010) 2597-2607.

[4] J.A.A.W. Elemans, R. Van Hameren, R.J.M. Nolte, A.E. Rowan, Molecular materials by self-assembly of porphyrins, phthalocyanines, and perylenes, Advanced Materials, 18 (2006) 1251-1266.

[5] M. Clericuzio, G. Alagona, C. Ghio, P. Salvadori, Theoretical Investigations on the Structure of Poly(iminomethylenes) with Aliphatic Side Chains. Conformational Studies and Comparison with Experimental Spectroscopic Data, Journal of the American Chemical Society, 119 (1997) 1059-1071.

[6] F. Millich, Rigid rods and the characterization of polyisocyanides, in: Polymerization Reactions, Springer Berlin / Heidelberg, 1975, pp. 117-141.

[7] W. Drenth, R.J.M. Nolte, Poly(iminomethylenes): Rigid rod helical polymers, Accounts of Chemical Research, 12 (1979) 30-35.

[8] R.J.M. Nolte, Vanbeijn.Aj, W. Drenth, Chirality in Polyisocyanides, Journal of the American Chemical Society, 96 (1974) 5932-5933.

[9] A.J.M. Van Beijnen, R.J.M. Nolte, W. Drenth, A.M.F. Hezemans, Screw sense of polyisocyanides, Tetrahedron, 32 (1976) 2017-2019.

[10] A.J.M. Van Beijnen, R.J.M. Nolte, A.J. Naaktgeboren, J.W. Zwikker, W. Drenth, A.M.F. Hezemans, Helical configuration of poly(iminomethylenes). Synthesis and CD spectra of polymers derived from optically active isocyanides, Macromolecules, 16 (1983) 1679-1689.

[11] M.M. Green, R.A. Gross, F.C. Schilling, K. Zero, C. Crosby, Macromolecular stereochemistry: effect of pendant group structure on the conformational properties of polyisocyanides, Macromolecules, 21 (1988) 1839-1846.

[12] C. Kollmar, R. Hoffmann, Polyisocyanides: electronic or steric reasons for their presumed helical structure?, Journal of the American Chemical Society, 112 (1990) 8230-8238.

[13] J.J.L.M. Cornelissen, J.J.J.M. Donners, R. de Gelder, W.S. Graswinckel, G.A. Metselaar, A.E. Rowan, N.A.J.M. Sommerdijk, R.J.M. Nolte, β-Helical Polymers from Isocyanopeptides, Science, 293 (2001) 676-680.

[14] J.J.L.M. Cornelissen, W.S. Graswinckel, P.J.H.M. Adams, G.H. Nachtegaal, A.P.M. Kentgens, N.A.J.M. Sommerdijk, R.J.M. Nolte, Synthesis and characterization of polyisocyanides derived from alanine and glycine dipeptides, Journal of Polymer Science Part A: Polymer Chemistry, 39 (2001) 4255-4264.

[15] J.J.L.M. Cornelissen, W.S. Graswinckel, A.E. Rowan, N.A.J.M. Sommerdijk, R.J.M. Nolte, Conformational analysis of dipeptide-derived polyisocyanides, Journal of Polymer Science Part A: Polymer Chemistry, 41 (2003) 1725-1736.

[16] T. Gullion, J. Schaefer, Rotational-echo double-resonance NMR, Journal of Magnetic Resonance (1969), 81 (1989) 196-200.

[17] S.L. Grage, A. Watts, Applications of REDOR for Distance Measurements in Biological Solids, in: G.A. Webb (Ed.) Annual Reports on NMR Spectroscopy, Academic Press, 2006, pp. 191-228.

[18] L. Odgaard, M. Bak, H.J. Jakobsen, N.C. Nielsen, 13C Chemical Shift and 13C-14N Dipolar Coupling Tensors Determined by 13C Rotary Resonance Solid-State NMR, Journal of Magnetic Resonance, 148 (2001) 298-308.

[19] T. Robert, P.W. David, E.B. Alan, Investigation of molecular structure in solids by two-dimensional NMR exchange spectroscopy with magic angle spinning, in, AIP, 1996, pp. 7915-7930.

[20] F.J. Blanco, R. Tycko, Determination of Polypeptide Backbone Dihedral Angles in Solid State NMR by Double Quantum 13C Chemical Shift Anisotropy Measurements, Journal of Magnetic Resonance, 149 (2001) 131-138.

[21] K. Schmidt-Rohr, Torsion Angle Determination in Solid 13C-Labeled Amino Acids and Peptides by Separated-Local-Field Double-Quantum NMR, J Am Chem Soc, 118 (1996) 7601-7603.

[22] K. Schmidt-Rohr, H.W. Spiess, Multidimensional solid-state NMR and polymers, Academic Press, London, 1994.

[23] T. Nakai, C.A. McDowell, Characterization of homonuclear spin pairs from two-dimensional spin-echo NMR powder patterns, J Am Chem Soc, 116 (1994) 6373-6383.

[24] X. Feng, M. Eden, A. Brinkmann, H. Luthman, L. Eriksson, A. Graslund, O.N. Antzutkin, M.H. Levitt, Direct Determination of a Peptide Torsional Angle Ïˆ by Double-Quantum Solid-State NMR, Journal of the American Chemical Society, 119 (1997) 12006-12007.

[25] J.M. Goetz, J. Schaefer, Orientational Information in Solids from REDOR Sidebands, Journal of Magnetic Resonance, 129 (1997) 222-223.

[26] S. Dusold, E. Klaus, A. Sebald, M. Bak, N.C. Nielsen, Magnitudes and relative orientations of chemical shielding, dipolar and J coupling tensors for isolated 31P-31P spin pairs determined by iterative fitting of 31P MAS NMR spectra, Journal of the American Chemical Society, 119 (1997) 7121-7129.

[27] D. Weliky, R. Tycko, Determination of Peptide Conformations by Two-Dimensional Magic Angle Spinning NMR Exchange Spectroscopy with Rotor Synchronization, Journal of the American Chemical Society, 118 (1996) 8487-8488.

[28] K. Schmidt-Rohr, A Double-Quantum Solid-State NMR Technique for Determining Torsion Angles in Polymers, Macromolecules, 29 (1996) 3975-3981.

[29] D.S. Wishart, B.D. Sykes, F.M. Richards, The chemical shift index: A fast and simple method for the assignment of protein secondary structure through NMR spectroscopy, Biochemistry®, 31 (1992) 1647-1651.

[30] H.B. Le, J.G. Pearson, A.C. De Dios, E. Oldfield, Protein structure refinement and prediction via NMR chemical shifts and quantum chemistry, J Am Chem Soc, 117 (1995) 3800-3807.

[31] J.D. van Beek, L. Beaulieu, H. Schafer, M. Demura, T. Asakura, B.H. Meier, Solid-state NMR determination of the secondary structure of Samia cynthia ricini silk, Nature, 405 (2000) 1077-1079.

[32] T. Nakai, J. Ashida, T. Terao, Measurements of Two-Dimensional Nmr Powder Patterns in Rotating Solids, Journal of Chemical Physics, 88 (1988) 6049-6058.

[33] M. Linder, A. Hohener, R.R. Ernst, ORIENTATION OF TENSORIAL INTERACTIONS DETERMINED FROM 2-DIMENSIONAL NMR POWDER SPECTRA, Journal of Chemical Physics, 73 (1980) 4959-4970.

[34] M. Bak, J.T. Rasmussen, N.C. Nielsen, SIMPSON: A General Simulation Program for Solid-State NMR Spectroscopy, Journal of Magnetic Resonance, 147 (2000) 296-330.

[35] G. De Paepe, B. Elena, L. Emsley, Characterization of heteronuclear decoupling through proton spin dynamics in solid-state nuclear magnetic resonance spectroscopy, Journal of Chemical Physics, 121 (2004) 3165-3180.

[36] A.J. Shaka, J. Keeler, R. Freeman, Evaluation of a New Broad-Band Decoupling Sequence - Waltz-16, Journal of Magnetic Resonance, 53 (1983) 313-340.

[37] A.E. Bennett, C.M. Rienstra, M. Auger, K.V. Lakshmi, R.G. Griffin, Heteronuclear decoupling in rotating solids, The Journal of Chemical Physics, 103 (1995) 6951-6958.

[38] D. Marion, K. Wüthrich, Application of phase sensitive two-dimensional correlated spectroscopy (COSY) for measurements of 1H-1H spin-spin coupling constants in proteins, Biochemical and Biophysical Research Communications, 113 (1983) 967-974.

[39] S. Cadars, J. Sein, L. Duma, A. Lesage, T.N. Pham, J.H. Baltisberger, S.P. Brown, L. Emsley, The refocused INADEQUATE MAS NMR experiment in multiple spin-systems: Interpreting observed correlation peaks and optimising lineshapes, Journal of Magnetic Resonance, 188 (2007) 24-34.

[40] H.W. Long, R. Tycko, Biopolymer Conformational Distributions from Solid-State NMR: α-Helix and 310-Helix Contents of a Helical Peptide, Journal of the American Chemical Society, 120 (1998) 7039-7048.

[41] J.D. van Beek, matNMR: A flexible toolbox for processing, analyzing and visualizing magnetic resonance data in Matlab®, Journal of Magnetic Resonance, 187 (2007) 19-26.

[42] Y. Hase, K. Nagai, H. Iida, K. Maeda, N. Ochi, K. Sawabe, K. Sakajiri, K. Okoshi, E. Yashima, Mechanism of Helix Induction in Poly(4-carboxyphenyl isocyanide) with Chiral Amines and Memory of the Macromolecular Helicity and Its Helical Structures, J Am Chem Soc, 131 (2009) 10719-10732.

[43] J. Herzfeld, A.E. Berger, Sideband Intensities in Nmr-Spectra of Samples Spinning at the Magic Angle, Journal of Chemical Physics, 73 (1980) 6021-6030.

[44] N.A. Davies, R.K. Harris, A.C. Olivieri, The effects of interplay between quadrupolar, dipolar and shielding tensors on magic-angle spinning NMR spectra: shapes of spinning sidebands, Molecular Physics, 87 (1996) 669-677.

[45] M. Edén, Computer simulations in solid-state NMR. I. Spin dynamics theory, Concepts in Magnetic Resonance Part A, 17A (2003) 117-154.

[46] M. Edén, M.H. Levitt, Computation of Orientational Averages in Solid-State NMR by Gaussian Spherical Quadrature, Journal of Magnetic Resonance, 132 (1998) 220-239.

[47] J.D. van Beek, B.H. Meier, A DOQSY approach for the elucidation of torsion angle distributions in biopolymers: Application to silk, Journal of Magnetic Resonance, 178 (2006) 106-120.

[48] Note:, The Euler angles in the SIMPSON spinsys relate the coordinate transformation from the principal axis frame to the laboratory frame., in, pp. simpson euler angles.

[49] S.L. Altmann, Rotations, quaternions, and double groups, Clarendon Press ;
Oxford University Press, Oxford
New York, 1986.

[50] A.M. Orendt, J.C. Facelli, A.J. Beeler, K. Reuter, W.J. Horton, P. Cutts, D.M. Grant, J. Michl, Low-temperature carbon-13 magnetic resonance. 8. Chemical shielding anisotropy of olefinic carbons, Journal of the American Chemical Society, 110 (1988) 3386-3392.

[51] R.D. Curtis, G.H. Penner, W.P. Power, R.E. Wasylishen, Dipolar-Chemical Shift Nmr-Spectra of the Carbon Nitrogen Linkage in Benzylideneaniline - Carbon and

Nitrogen Chemical Shielding Anisotropies, Journal of Physical Chemistry, 94 (1990) 4000-4006.

[52] R.E. Wasylishen, G.H. Penner, W.P. Power, R.D. Curtis, Dipolar NMR spectra of the oxime moiety in (E)-acetophenone oxime. Carbon and nitrogen chemical shielding anisotropies, Journal of the American Chemical Society, 111 (1989) 6082-6086.

[53] W.S. Veeman, Carbon-13 chemical shift anisotropy, Progress in Nuclear Magnetic Resonance Spectroscopy, 16 (1984) 193-235.

[54] C.M. Gowda, F. Vasconcelos, E. Schwartz, E.R.H. van Eck, M. Marsman, J.J.L.M. Cornelissen, A.E. Rowan, G.A. de Wijs, A.P.M. Kentgens, Hydrogen bonding and chemical shift assignments in carbazole functionalized isocyanides from solid-state NMR and first-principles calculations, Physical Chemistry Chemical Physics, 13 (2011) 13082-13095.

Chapter 3

Sensitivity enhancement of double quantum NMR Spectroscopy by modified CPMG

Chandrakala M. Gowda, Vipin Agarwal and Arno P. M. Kentgens

Journal of Magnetic Resonance 2012, vol. 223, pg. 11-19

3.1 Introduction

Solid-state NMR spectroscopy, is an invaluable technique for structural studies of biomolecules and materials.[1-9] Along with solution-state like isotropic interactions, the presence of anisotropic interactions in the solid-state provides additional information for structure and dynamics characterization. Anisotropic interactions such as chemical shift anisotropy (CSA), quadrupolar interaction and dipolar coupling interactions provide a means to access the spatial orientation of molecular segments and distance measurements between nuclei facilitating structure characterization of polymers, biomolecules and various other materials.[1, 3, 5, 7, 10] However, one of the limitations of solid-state NMR is that of sensitivity. Many biologically important nuclei such as carbon-13 and nitrogen-15 are only 1.1% and 0.36% naturally abundant. In addition to this the low gyromagnetic ratios of ^{13}C and ^{15}N, $\gamma_C = 6.72\times10^7$ rad s^{-1} $T^{-1}$and $\gamma_N = 2.71\times10^7$ rad s^{-1} T^{-1}, leads to intrinsically low sensitivity. In some other cases the nuclei have very long spin-lattice relaxation time leading to excessive experimental times. Several techniques have been designed to overcome the low sensitivity issue. One of the prominent and routinely applied techniques is Magic Angle Spinning (MAS).[11-13] The magic angle spinning method averages anisotropic interactions and preserves the isotropic information of the nuclear spin interactions. The extent to which the interactions are averaged depends on the spinning speed and the magnitude of the anisotropy of the interaction. Magic angle spinning is particularly important for two distinct reasons. 1. Samples consisting of multiple chemical sites such as the proteins, peptides, pharmaceutical compounds, host of inorganic molecules and other macro molecules show substantial overlap of lines. Most

of these lines can be resolved by magic angle spinning which are otherwise anisotropically broadened and overlapping. 2. The sensitivity of the MAS experiments is considerably higher since the signal intensity of the nuclei is concentrated in a single or a few lines with the line width dictated by the spin-spin relaxation time of the nuclei. In case of experiments such as REDOR-sideband dephasing, 2D-MAS Exchange etcetera the magic angle spinning speed is set lower to the magnitude of the anisotropic interaction so as to preserve the anisotropy information.[14, 15] The spinning sidebands are then used to recover the anisotropy information.[16, 17] A second technique, which is also applied routinely, is Cross Polarization (CP) where magnetization is transferred from highly sensitive nuclei such as protons to low sensitive nuclei such as carbon, silicon, nitrogen etcetera providing a factor of γ_H/γ_x gain in the signal intensity. The third technique developed to enhance sensitivity in solid-state NMR experiments is the CPMG pulse sequence.[18-22] The CPMG pulse sequence is applicable to nuclear spins with long transverse relaxation time (T_2) compared to the signal decay due to inhomogeneous broadening. Transverse magnetization dephased by inhomogeneous interactions can be refocused repeatedly using refocusing pulses to create echoes of the signal.[23] Carr and Purcell extended the use of this method to study the effects of diffusion on spin-spin relaxation time (T_2) in liquids. This repeated echo sequence was later modified by Meiboom-Gill to remove the π pulse imperfection effects on the T_2 measurements. The modified sequence came to be known as the Carr-Purcell-Meiboom-Gill (CPMG) sequence.[24, 25] In recent times the application of the CPMG sequence in ssNMR has increased in order to measure T_2 or to boost sensitivity of static or MAS spectra.[20, 26] The extension of the method to achieve sensitivity enhancement for spectra of quadrupolar nuclei is called the QCPMG sequence.[18, 22]

In solid-state NMR spectroscopy, CSA-CSA correlation experiments such as the 2D-DOuble Quantum SpectroscopY (DOQSY), Double quantum CSA spectroscopy with MAS (DQCSA) and variations of these experiments have been used extensively to obtain torsion angles of peptides, backbones of synthetic and biopolymers and molecular fragments.[3, 6, 9, 15, 27, 28] The MAS and static version of the double-quantum single-quantum (DQ-SQ) experiments have different advantages and limitations. The MAS DQ-SQ experiments have higher sensitivity and higher spectral resolution as compared to that of the static experiment.[9, 15] On the other hand, static experiments provide higher

angular resolution as compared to MAS experiments. The MAS based DQ filtered experiments involve employing tedious setting of multiple pulse sequences for the excitation and reconversion of double quantum coherences and are prone to RF imperfections. The static experiment is relatively straightforward to setup on the instrument and the spectral analysis is also very simple. In case of samples with coinciding chemical shift values, the 'n = 0' rotary resonance condition broadens the lines which severely reduce the sensitivity in the MAS experiments. This is also a drawback for samples with small chemical shift anisotropy and strong dipolar couplings in which case slow MAS is essential to retain anisotropy information. The slow MAS leads to poor sensitivity. This complication does not arise for a static experiment and therefore the 2D-DOQSY spectrum has become popular for obtaining relative tensor orientations in solid-state NMR. However, acquiring spectra with sufficient signal to noise in these experiments requires long instrument time particularly for samples with sparse isotope labeling and for samples with large molecular weights. For example, ^{13}C DOQSY spectra of isotopically labeled silk and polyisocyanides have been reported to take as much as 6 to 7 days of measurement time.[6, 28] In cases of limited sample quantities and lowly abundant low gamma nuclei this experiment is far from achievable, and therefore signal enhancement in these experiments is highly desired.

As the FID in these experiments evolves under the homonuclear dipolar coupling and chemical shift Hamiltonians, simultaneous refocusing of these interactions is necessary in order to recover the magnetization. Signal enhancement using the principle of the CPMG/QCPMG for spin-½ and quadrupolar nuclei involves the use of a series of 180^o pulses or a series of 90^o pulses.[18, 20, 22] The chemical shift Hamiltonian has linear spin operator terms whereas the homonuclear dipolar coupling Hamiltonian has bilinear terms in the same spin type. A Hahn-echo or a solid-echo does not fully refocus the magnetization that has a combination of the linear and bilinear terms of the same spin type. Hence the CPMG sequence in its current form will not suffice to achieve sensitivity enhancement for dipolar coupled homonuclear spin pairs.

In this chapter, we describe the use of the Hahn-solid-Hahn pulse combination which was initially introduced by Schmidt Rohr, to form a CPMG type of pulse train echo that enables recovery of dephased magnetization for dipolar coupled homonuclear spin

pairs.[3, 29] The new CPMG sequence is dubbed as Hahn-solid-Hahn Carr-Purcell-Meiboom-Gill (HSHCPMG) sequence. The HSHCPMG pulse train refocuses both the chemical shift anisotropy and the dipolar coupling interactions. The Fourier transform of HSHCPMG FID results in a spikelet spectrum where the intensities that are normally spread over the continuous powder line shape are concentrated in narrow spikelets. The envelope of these spikelets matches the trace of the powder line shape pattern. The spikelet spectrum was optimized to recover anisotropic information available from static powder line shapes. We apply the HSHCPMG sensitivity enhancement to the 2D-DOQSY experiment and determine the relative ^{13}C CSA tensor orientations of the carbonyl and alpha carbon of glycine. The CSA tensor relative orientation angles obtained using the sensitivity-enhanced spectrum will be compared with angles obtained from a 2D DOQSY spectrum without sensitivity enhancement. This comparison demonstrates the reproducibility of the orientation information with appreciable accuracy in the sensitivity enhanced spectrum.

3.2 Experimental Section

Samples: U-[$^{13}C_2$,^{15}N]-glycine was mixed with unlabeled glycine in the ratio of 1:19 and dissolved in distilled water. The solution was slowly evaporated at room temperature to obtain [5% $^{13}C_2$-^{15}N]-glycine crystals. The crystals were ground to fine powder and subsequently used for the NMR measurements.

Experiments: All experiments were recorded in static mode on a Varian VNMRS 400 MHz spectrometer using a 3.2 mm double resonance MAS probe. The proton and carbon 90^o pulse lengths were 2.9 μs and 3.7 μs respectively. The proton and carbon RF field for spinlock during cross polarization was set to 45 kHz each. TPPM decoupling was applied to achieve proton decoupling using radio frequency field strength of 70 kHz during the excitation, evolution and acquisition time.[30] The 2D-DOQSY and the 2D-DOQSY-HSHCPMG spectra were acquired under the same conditions except for the changes during the acquisition time. The double quantum excitation and reconversion time(2τ) were set to 160μs. Quadrature detection in the ω_1 dimension was achieved using the time proportional phase increment (TPPI) method.[31] The indirect dimension consists of 48 t_1 increments using 256 scans for each increment.

Simulation: The simulations of the 1D double quantum filtered CP-HSHCPMG, 2D-DOQSY and the 2D-DOQSY-HSHCPMG experiment were done using the SIMPSON simulation program.[32] Powder averaging was performed using the zcw4180 crystal file. Simulations of the DOQSY and DOQSY-HSHCPMG spectra were run with $\alpha_{\mathrm{CSA}}^{\mathrm{C1C2}}$ and $\beta_{\mathrm{CSA}}^{\mathrm{C1C2}}$ varying from 0^{o} to 90^{o} and $\gamma_{\mathrm{CSA}}^{\mathrm{C1C2}}$ varying from 0^{o} to 180^{o} and in steps of 10^{o} each. The 2D-DOQSY and 2D-DOQSY-HSHCPMG spectra were processed using the matNMR processing toolbox in Matlab.[33, 34]

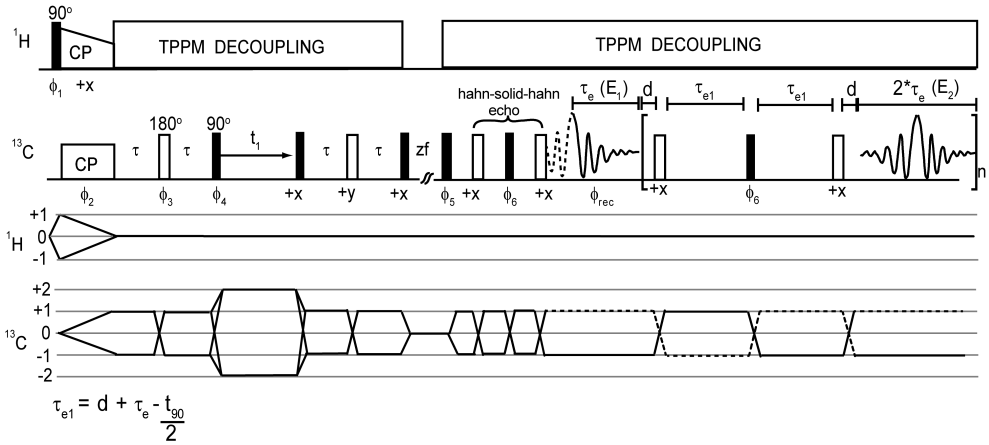

Figure 3.1 Sensitivity enhanced DOQSY sequence. 2×τ represents the double quantum excitation and reconversion time while t_1 is the indirect dimension evolution time. The z-filter (zf) time was set to 1ms during which unwanted coherences are dephased due to the heteronuclear dipolar coupling to protons. The pulse phases ϕ_2, ϕ_3 and ϕ_4 are cycled in four steps to select double quantum coherences. ϕ_1=(1,3); ϕ_2=(1,1, 2,2, 3,3, 0,0); ϕ_3=(0,0,1,1,2,2,3,3, 1,1,2,2,3,3,0,0, 2,2,3,3,0,0,1,1, 3,3,0,0,1,1,2,2); ϕ_4=(0,0,1,1,2,2,3,3); ϕ_5=(2_{32}, 3_{32}, 0_{32}, 1_{32}); ϕ_6=(1_{32}, 2_{32}, 3_{32}, 0_{32}, 3_{32}, 0_{32}, 1_{32}, 2_{32}); ϕ_{rec}= $(0,2,2,0, 0,2,2,0, 2,0,0,2, 2,0,0,2)_2$ $(1,3,3,1, 1,3,3,1, 3,1,1,3, 3,1,1,3)_2$ $(2,0,0,2, 2,0,0,2, 0,2,2,0, 0,2,2,0)_2$ $(3,1,1,3, 3,1,1,3, 1,3,3,1, 1,3,3,1)_2$.

3.3 Pulse sequence and Simulations

3.3.1 Pulse Sequence

The U-$^{13}C_2$-^{15}N-glycine sample was diluted with natural abundance glycine to obtain 5% $^{13}C_2$-^{15}N-glycine in order to avoid intermolecular ^{13}C-^{13}C dipolar coupling. The static CP spectrum of 5% $^{13}C_2$-^{15}N-glycine will have a considerable contribution from natural abundant carbon signals. The dipolar coupled carbon spin pairs are selected using the double quantum filtering sequence shown in Figure 3.1 The (^{1}H 90^o-CP$_{HX}$)-τ-180^o-τ-90^o represents the double quantum excitation block. After the initial ^{1}H 90^o pulse and the CP, the transverse magnetization evolves under the influence of homonuclear dipolar coupling and the chemical shift Hamiltonian during the delay τ. The magnetization evolves only in the presence of ^{13}C-^{13}C dipolar couplings as the chemical shift Hamiltonian is refocused by application of a 180^o pulse. The dipolar coupling terms evolve to give rise to antiphase terms ($I_xS_z + S_xI_z$) which can be converted to double quantum coherences by the application of a 90^o pulse. The DQ coherences evolve under the sum of the chemical shift Hamiltonian of the two coupled spins during the incremented time delay t_1.[3, 7] The second 90^o-τ-180^o-τ-90^o block converts the DQ coherences to observable single quantum coherences with the final 90^o pulse flipping the magnetization from the transverse plane to the z-direction. A z-filter time without proton decoupling is added to dephase any unwanted coherences that remain in the transverse plane.[35, 36] Finally, the magnetization along the z direction is flipped to the transverse plane using a 90^o pulse for signal detection. Thus the resulting fid consists of the signal from dipolar coupled spin pairs which evolve under the Hamiltonian of the individual chemical shifts of the nuclei and the homonuclear dipolar coupling Hamiltonian.

The signal decays very rapidly in static solid-state NMR experiments hence echo acquisition is necessary to avoid distortion caused by the dead time delay at the start of the acquisition. The Hahn-echo and solid-echo are the most commonly used methods that are used to refocus magnetization in solid-state NMR. The Hahn echo consists of a τ - 180^o - τ block, the 180^o pulse refocuses evolution of spin operators in the time delay 2*τ that are linear in I_z such as the chemical shift terms, heteronuclear dipolar couplings etc.[7, 23, 29] The echo maximum appears at time τ after the 180^o pulse. For a bilinear operator such as $I_zS_z - \boldsymbol{I}.\boldsymbol{S}$ the 180^o pulse produces $(-I_z)(-S_z) - (-\boldsymbol{I}).(-\boldsymbol{S})$.

Therefore, the Hamiltonian remains unchanged due to the pulse and hence does not cancel itself in the overall propagator. A solid-echo consists of a τ - 90^o - τ block, the 90^o pulse refocuses the evolution of operators under the Hamiltonian which are bilinear in the same spin type I_aI_b (a, b = x, y, z) such as the Homonuclear dipolar interaction ($3I_zI_z + I.I$). The 90^o pulse in the solid echo is applied in the direction of the magnetization.[7, 29] A Hahn echo and solid echo pulse sequence is shown in Figure 3.2.

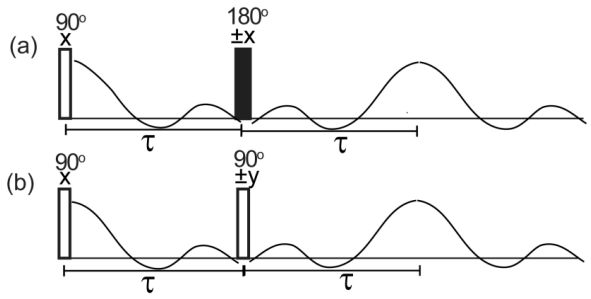

Figure 3.2 (a) Hahn echo pulse sequence. (b) Solid echo pulse sequence

Application of either a Hahn echo or a solid echo independently would fail to fully refocus the magnetization in a dipolar coupled spin pair system. To overcome this problem, Schmidt Rohr used a combination of solid echo and Hahn echo (τ - 180^o - τ - 90^o - τ - 180^o - τ), dubbed as Hahn-solid-Hahn echo, to refocus magnetization evolving under the chemical shift and homonuclear dipolar coupling Hamiltonian.[3, 29] The solid-echo occurs unperturbed in the case of strongly coupled or weakly coupled isolated spin pairs.[29] For intermediate couplings the solid-echo time has to fulfill the condition $\Delta\omega_{cs} \times t_{echo} \ll 2\pi$ and $\Delta\omega_{dip} \times t_{echo} \ll 2\pi$ to form echoes. The $^{13}C\alpha$—^{13}CO spin pairs in glycine are directly bonded with a dipolar coupling of ~2200 Hz and have large chemical shift difference of 133 ppm (~13 kHz)which makes the homonuclear dipolar coupling fall in the weak coupling limit hence making it possible to obtain an undistorted Hahn-solid-Hahn echo of the carbon spin pair. The acquisition of an echo train can increase the sensitivity of the double quantum filtered signals to a large extent. To achieve this we have replaced the Hahn echo/solid echo element of the CPMG sequence by the Hahn-solid-Hahn echo element as shown in Figure 3.1. The HSHCPMG consists of the first echo E_1, which is acquired for the acquisition time τ_e and the '*n*' number of echoes E_n of duration 2*τ_e each. The delay, *d*, is adjusted to account for the dead time delay (*d*) after

the second 180^{o} pulse in the HSHCPMG block. The Fourier transformation of the double quantum filtered HSHCPMG FID gives rise to a spikelet spectrum separated by the time period (1 / (2 × (τ_e + d))). Higher sensitivity enhancement can be achieved by decreasing the τ_e time since shorter echo time intervals imply a larger frequency separation between the spikelets.[18, 37, 38] However, decreasing the echo time excessively could result in loss of spectral resolution and anisotropic information contained in the spectrum (see also data processing section).[18, 37, 38] The HSHCPMG acquisition is a trade-off between sensitivity and anisotropy information. This was optimized through simulations and is discussed in the next section. Signal enhancement using multiple echo acquisition aims to achieve higher signal to noise ratio without seriously compromising the anisotropy information that can be obtained from the spectrum.

3.3.2 Echo time optimization and data processing

In the previous section it was discussed that sensitivity gain achieved by refocusing the (truncated) FIDs at the cost of spectral resolution and anisotropy information. The effects of truncated echo acquisition and zero-filling in the double quantum filtered CP-HSHCPMG acquisition in the glycine spectrum (Figure 3.3). The simulations are performed with 'np1' acquisition points during E_1 and '2np1' acquisition points during each of the echoes E_2, E_3….E_n. In the processing of normal FID acquisitions line shape definition can be improved by addition of zero filling points at the end of the FID. In the case of CPMG/HSHCPMG type of acquisition this can be slightly modified to benefit in an additional way. By addition of zero filling evenly in between consecutive echoes in the FID the length of the echoes are artificially increased there by increasing the time period between the echoes.[39] The Fourier transformation of this zero-filled HSHCPMG FID leads to a spikelet spectrum with frequency lines separated by smaller frequency interval which results in a better tracing of the powder line shape (Figure 3.3). The HSHCPMG FIDs processed using the above method with varying number of zero filling points are shown in Figure 3.3. The τ_e period corresponding to the number of np1 points is given by (dwell time) × np1. The dwell time used in each case of simulations here is 8μs. The spectra with only 8 np1 points of acquisition lose anisotropy information to a large extent as shown in Figure 3.3(i). This illustrates lack of complete anisotropy information in the excessively truncated HSHCPMG echoes. The spectra with longer echo acquisition time corresponding to np1=16 points and np1 =21 show better accuracy in tracing out the

powder line shape (see Figure 3.3 (vi, vii)). An echo acquisition of ~170 μs for the E_1 is sufficient to acquire the anisotropy information of the tensors. In the case of np1=8 the shape of the spikelet envelope does not improve upon zero filling (see Figure 3.3 (ii, iii)) whereas the zero filling improves the appearance of the powder line shapes for np1=16 and 21 (see Figure 3.3 (v, vi, viii, ix)). The zero filling procedure does not add additional information but delivers a visually perceivable spectrum that is easier to compare to the outline of the powder line shapes.

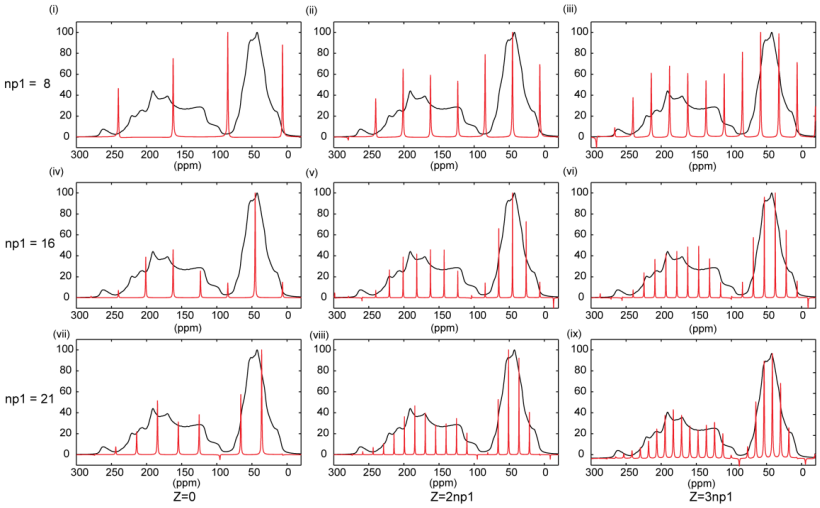

Figure 3.3 Double quantum filtered CP and CPHSHCPMG simulations with np1 points during E1 and 2np1 points during each of the E2, E3…En echoes. i, iv, and vii represent spectra acquired using np1= 8, 16, 21 points respectively. The spectra along the three successive columns are processed using Z=0, 2×np1, 3×np1 zero filling points in between the HSHCPMG echoes respectively.

3.3.3 Practical considerations for 2D DOQSY-HSHCPMG simulations

The 2D-DOQSY-HSHCPMG spectrum that is described in the section below is used to obtain relative tensor orientation angles by means of least square fitting of the experimental spectrum with that of the simulated spectra. Before directly embarking on performing the simulations of these spectra certain practically relevant factors have to be considered; 1. Simulations of powder spectra require powder averaging over a large

number of crystal orientations which are time consuming calculations. 2. HSHCPMG acquisition involves acquisition of the echoes over repeated cycles consequently adding to the computational time for the simulations which can be enormous for a 2D data with 3 spin system (explained below) 3. The simulations are to be spanned over a range of Euler angles with a fine grid to obtain reliable orientation angles hence involve simulations of large number of spectra. The three factors above make the simulation procedure extremely time demanding. A workaround for these problems was proposed earlier in the case of QCPMG simulations.[18] The method involved the simulation of a single echo (E_1) and subsequent generation of a full-echo (E_2) followed by replication of E_2 to generate the E_3, E_4,…E_n echoes of the FID. However, the echoes can only be replicated if the effects of each RF pulse on the spectrum is negligible i.e. the RF pulse strengths are sufficiently high so as to be the dominant interaction during the pulse. In the case of spin-½ nuclei this condition translates to $H_{rf} \gg H_{CSA}$ and $H_{rf} \gg H_{dip}$. The simulations of the 1D double quantum filtered HSHCPMG spectra of glycine using real pulses and ideal pulses are shown in Figure 3.4. The differences between the spectra are very small and can be neglected. Thus, all the 1D double quantum filtered CP-HSHCPMG and the 2D DOQSY-HSHCPMG simulations are performed using ideal pulses and echoes E_1 and E_2 only are simulated whilst E_3, E_4,…E_n are replicated from echo E_2 to obtain the full acquisition. All simulations are performed using SIMPSON simulation package.

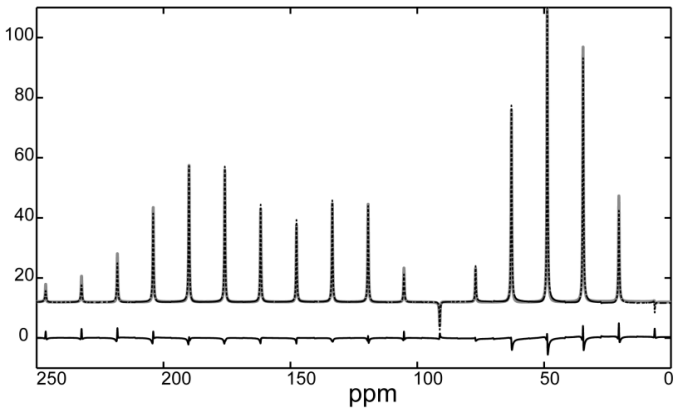

Figure 3.4 Simulation of the 13C2-15N-a-glycine double quantum filtered CP-HSHCPMG spectrum using real (black dotted) and ideal (gray line) pulses. The difference spectrum is shown below.

3.4 Results and discussions

3.4.1 Sensitivity enhancement in double quantum filtered 1D static CP spectrum using HSHCPMG acquisition

The dipolar coupled carbon spin pairs are selected using the double quantum filtering sequence shown in Figure 3.1. The double quantum filtered 1D static CP spectrum is shown in

Figure 3.5a. The powder line shapes corresponding to the alpha and the carbonyl carbon of glycine are well separated. The carbonyl carbon exhibits a large anisotropy of -71.5 ppm and the alpha carbon has a relatively small anisotropy of -19.6 ppm.[40] The double quantum filtered CP-HSHCPMG spectrum is shown in

Figure 3.5b. The spectrum was acquired with parameters obtained from simulation as discussed above. We have acquired 21 points in the E_1 echo time in the double quantum filtered CP-HSHCPMG spectrum. With an echo separation of ~334 μs in the time domain the spikelets appear at ~m×2987 Hz, m = 0, 1, 2… relative to the transmitter frequency position in the frequency domain. On zero filling of each echo, the spectral outline of the spikelet spectrum improves visually

Figure 3.5c). A well-defined envelope of the spikelets mimicking the powder line shape indicates that the anisotropy information is not compromised under the given sampling conditions.

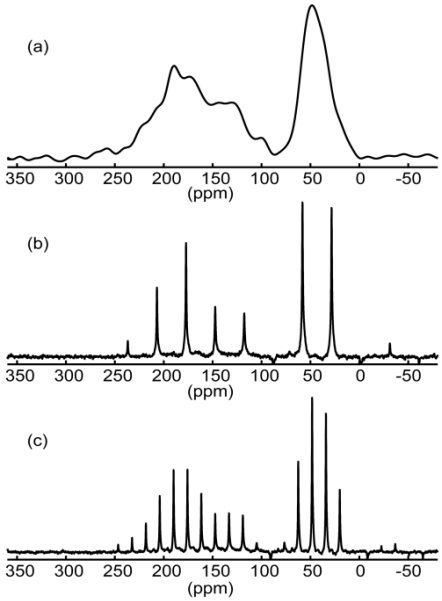

Figure 3.5 (a) 1D double quantum filtered CP and (b) double quantum filtered CP-HSHCPMG spectrum without zero filling. The spikelets in (b) are sparsely distributed over the span of the powder pattern. (c) The number of spikelets defining the powder pattern is improved upon zero filling with 46points.

Comparison of the signal to noise ratio of two spectra acquired with and without HSHCPMG type of acquisition is not straightforward. This is because the FID decay profile is considerably different in the two cases and hence the percentage of noise contribution to the FID is very different in the two spectra. In addition, the effective signal to noise ratio (S/N) of the spectra are also influenced by the processing steps such as the apodization functions used prior to the Fourier transformation of the FID which in turn also depends on the FID decay profile. However a pragmatic approach is made to provide a reasonable comparison of the two spectra. The static spectra are processed in two different ways. In the first method, the length of the FID is fixed at a point where the signal has almost reached the noise level. This corresponds to an acquisition time of ~1 ms and ~40 ms for DQ filtered CP and CP-HSHCPMG FIDs respectively. The 40 ms acquisition time comprises of the 21 points in the first half-echo and 56 full-echoes of 42 points each and 46 zero points in between the echoes. Zero filling points are used in each case at the end of the FID to obtain a total of 2^n points in the FID. The two FIDs are then

Fourier transformed without applying any apodization function Figure 3.6a and c. In the second method, all the steps in the previously described method are followed and at last a suitable apodization function is applied to both the FIDs prior to Fourier transformation. The FID of the DQ filtered CP of 1 ms acquisition length is multiplied by a cosine function. The cosine function matches the FID decay profile and reduces the noise in the static spectrum to a considerable extent without compromising the powder line shape features in the spectrum (Figure 3.6b). The DQ filtered CP-HSHCPMG FID of ~40 ms acquisition length is multiplied by exponential function to obtain best sensitivity (see Figure 3.6d). The application of apodization function improves the signal to noise ratio of each spectrum.

The S/N of the NMR spectra in Figure 3.6 are measured using the equation

$$\frac{Signal}{Noise} = \frac{Signal\ peak\ amplitude}{rms\ noise\ amplitude}.[41]$$

The alpha carbon amplitude at the maximum position is considered for the calculation of the signal to noise.

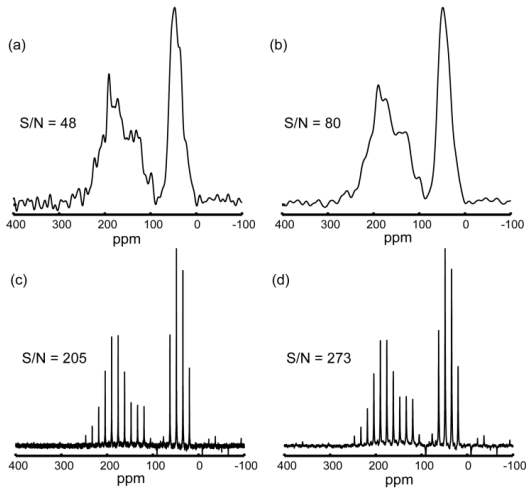

Figure 3.6 Double quantum filtered CP spectra (a) processed without line broadening and (b) processed with a cosine apodization function. Double quantum filtered CP-HSHCPMG spectra (c) processed without line broadening (d) processed with an exponential function with 36 Hz line broadening.

In the case of the spectra processed without any apodization function applied to the FID the signal to noise ratio of the spectrum with HSHCPMG acquisition improves by ~4.2. And for the spectra processed with apodization functions the CP-HSHCPMG spectrum shows a signal to noise gain of ~3.4. The improvement obtained compares well to the theoretical maximum of 7.4 (i.e. the square root of the number of echoes acquired). It is not possible to achieve the theoretical maximum due to the factors such as T_2 relaxation of spins, pulse imperfections, probe limitations on the proton decoupling power used etc.

3.4.2 2D Double-quantum single-quantum spectrum

The relative tensor orientations of the carbonyl and the alpha carbon of glycine are obtained using the sensitivity enhanced 2D DOQSY spectrum and the results are compared to that obtained using the 2D DOQSY spectrum obtained without sensitivity enhancement. The glycine sample was chosen in view of the fact that the tensor orientations of both the alpha and the carbonyl carbon is available for the glycine single crystal and hence is a good test sample.[42] Secondly, it has two carbons one of which has very large anisotropy and the other has a small anisotropy and hence forms a good example to show that the method is useful for samples with varying anisotropies. The 2D-DOQSY and 2D-DOQSY-HSHCPMG spectra are shown in Figure 3.7a and c respectively. The powder line shape in the direct dimension is determined by the ^{13}C CSA and ^{13}C-^{13}C dipolar coupling while the powder line shape in the indirect dimension depends of the sum of the ^{13}C CSA tensors only. The DQ excitation efficiency depends on the magnitude and orientation of the ^{13}C—^{13}C dipolar couplings. To obtain a uniform DQ excitation throughout the powder pattern, several spectra at varying excitation times ($2\times\tau$) have to be recorded and summed as described in reference [3]. Here we use only a single DQ excitation time of 160μs. The spectral patterns are thus strongly affected by the ^{13}C—^{13}C dipolar coupling. The dipolar coupling effects are accounted for in the simulations by using the ^{13}C—^{13}C dipolar coupling magnitude and orientations obtained from the single crystal NMR data.[42]

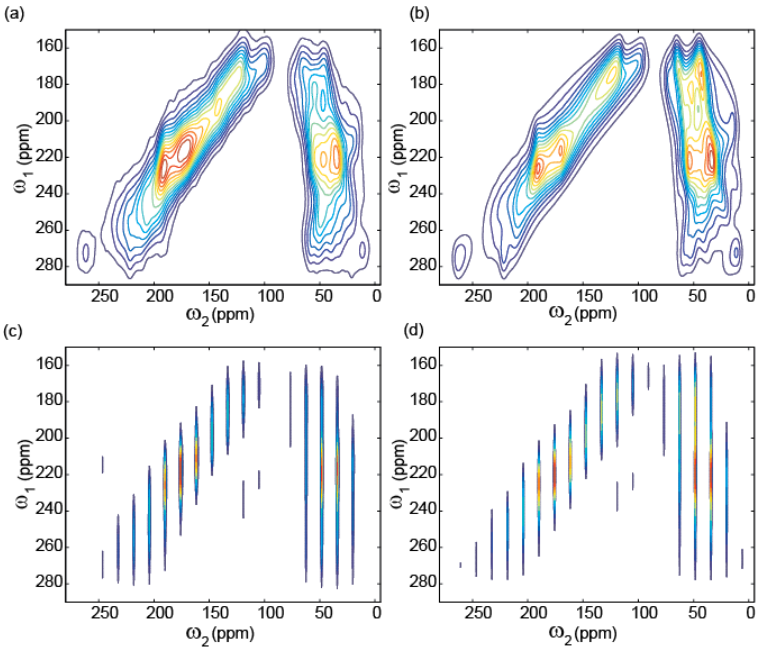

Figure 3.7 (a) Static DOQSY spectrum and (b) the best matching simulation corresponding to the Euler angles [0 80 220]. (c) The DOQSY-HSHCPMG spectrum and (d) the best matching simulation corresponding to the angle Euler angles [0 80 200].

SIMPSON simulations are performed to extract the relative tensor orientation of the carbonyl and the alpha carbons from the DOQSY-HSHCPMG spectrum of glycine. The spin system of $^{13}C_2$—^{15}N-glycine is subject to the following NMR interactions: 1. The CSA interactions of alpha and carbonyl carbon. 2. The ^{13}Ca—^{13}CO homonuclear dipolar coupling interaction of magnitude ~2142 Hz. 3. The ^{13}CO---^{15}N and $^{13}C\alpha$—^{15}N heteronuclear dipolar coupling of magnitude ~199 Hz and ~954 Hz respectively. The ^{13}CO—^{15}N heteronuclear dipolar couplings are generally weak compared to that of the anisotropy tensors and can be neglected. In case of glycine $^{13}C\alpha$-^{15}N dipolar coupling magnitude is comparable to the anisotropy of the alpha carbon and hence have to be taken into account during simulation. When the magnitude and orientation of the heteronuclear dipolar coupling between two spins is unavailable they can be removed experimentally using decoupling schemes such as WALTZ.[43] The dipolar coupling values of the ^{13}CO---^{15}N, ^{13}CO—$C\alpha$ and $C\alpha$—^{15}N was obtained using the distance information from the crystal structure of glycine.[44] The ^{13}CO tensor is fixed as the reference frame in the

SIMPSON simulation spin system. In the SIMPSON spin system this translates to representing the Euler angles of the 13CO PAS as [0 0 0]. The other NMR interaction tensor orientations are expressed relative to this frame of reference.

The orientation of the 13CO tensor in the molecular frame has been determined earlier in the single crystal NMR data.[42] In the ^{13}CO CSA tensor PAS, ^{13}Cα-^{13}CO dipolar coupling has an orientation of $\beta_{dip}\sim95^{o}$, $\gamma_{dip}\sim179^{o}$as deduced from the single crystal structure.[42, 44] Similarly, the dipolar coupling orientations of the ^{13}CO─^{15}N and ^{13}Cα─^{15}N heteronuclear dipolar coupling in the reference frame can be deduced to be (75^{o}, 147^{o}) and (70^{o}, 112^{o}). All the above information was used in the SIMPSON input to obtain simulated data.

A closer inspection of 1D traces from experimental and simulated DOQSY-HSHCPMG spectra reveal that the line shapes of spikelets in the experimental spectrum are broader at the base compared to that of the spikelets in the simulations. The line shape distortion is not reproduced in the simulations. Hence, to obtain a reliable fit the experimental 2D spectral spikelets are represented using stick plot where the line integrals of each spikelet in the direct dimension are used for least squares fitting.[18] The symmetry considerations for exchange patterns of CSA yield 16 equivalent Euler angle sets which relate the orientation of the one CSA PAS frame with the other CSA PAS frame. These Euler angles can be listed as $[\alpha,\beta,\gamma]$, $[\alpha,\beta,180+\gamma]$, $[180+\alpha,\beta,\gamma]$, $[180+\alpha,\beta,180+\gamma]$; $[-\alpha,\beta,-\gamma]$, $[-\alpha,\beta,180-\gamma]$, $[180-\alpha,\beta,-\gamma]$, $[180-\alpha,\beta,180-\gamma]$; $[-\alpha,180-\beta,+\gamma]$, $[-\alpha,180-\beta,180+\gamma]$, $[180-\alpha,180-\beta,\gamma]$, $[180-\alpha,180-\beta,180+\gamma]$; $[\alpha,180-\beta,-\gamma]$, $[\alpha,180-\beta,180-\gamma]$, $[180+\alpha,180-\beta,-\gamma]$, $[180+\alpha,180-\beta,180-\gamma]$.[7] The ^{13}C-^{13}C dipolar coupling introduced in the SIMPSON simulations do not affect the 16 symmetry angle sets since $\beta_{dip}\sim95^{o}$, $\gamma_{dip}\sim179^{o}$ are very close to $\beta_{dip}=90^{o}$, $\gamma_{dip}=180^{o}$ which do not affect the spectral symmetry. Hence the simulations were performed for [α, β, γ] ranging from [0^{o}, 0^{o}, 0^{o}] to [90^{o}, 90^{o}, 90^{o}] in steps of 10^{o} each for the DOQSY and DOQSY-HSHCPMG spectra. Least squared fitting of the DOQSY spectrum yields the minima corresponding to the Euler angles equivalent to [0^{o} 80^{o} 220^{o}] and is shown in Figure 3.7b. The minima of the DOQSY-HSHCPMG spectrum is obtained for the Euler angles equivalent to [0^{o} 80^{o} 200^{o}]

which is shown in Figure 3.7c. The accuracy of the fitted angles in the DOQSY as well as the DOQSY-HSHCPMG spectrum is about 10 degrees each for alpha, beta and gamma angles. The angles obtained compare well to the angles [~0^o 88^o 214^o] derived from the single crystal NMR data. The angle minima obtained are easy to visualize when expressed in the axis-angle notation in which the Euler angles represent a net rotation of ϕ degrees about an unique axis [nx ny nz].[45] The minima of the DOQSY and the DOQSY-HSHCPMG here correspond to a net rotation angle of 206±5 and 202±8 degrees respectively. The Euler angles obtained from the single crystal data yield a net rotation angle of 203 degrees.

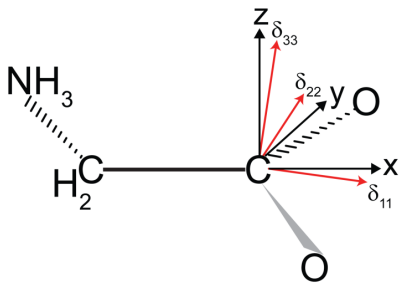

Figure 3.8 PAS orientation in the molecular frame for the carbonyl carbon in glycine. The principal axes δ_{11}, δ_{22}, δ_{33} make an angle of ~3^o each with x, y, z axis respectively. The Z-axis is perpendicular to the plane consisting of O-C=O, X-axis bisects the COO angle and is in the CO_2 plane and Y-axis is perpendicular to these two directions. The figure is adapted from ref [42].

The experimental sensitivity of the HSHCPMG block in our case was limited by the performance of the probe. The limitation of the probe is two folds: one the amplitude of applied proton RF fields for decoupling and two the duration for which proton decoupling pulses can be applied without damaging the probe. For static powder samples, heteronuclear decoupling has not been issue due to limitation of residual line broadening imposed by anisotropic interaction. However, in the HSHCPMG experiment the T_2 of a sample is very crucial in defining the experimentally achievable sensitivity. In solids, the proton RF amplitude during heteronuclear decoupling is very critical in determining the effective T_2 of carbon resonances. Our group recently demonstrated that life times of coherences could be enhanced several folds for carbons strongly coupled to proton by increasing the amplitude of proton RF fields during heteronuclear decoupling.[46] The

enhanced T_2 opens up the possibility to acquire more echoes and therefore boost sensitivity of the HSH-CPMG block by several folds.

As described in chapter 2, the 2D DOQSY experiment was used to determine the torsion angle of the polyisocyanodipeptide which has a rigid and stable helical structure.[28] The polyisocyanodipeptides are used as structural backbone for the development of range of functional materials that have potential applications as chromophoric and optoelectronic molecular machines.[47, 48] The backbone carbons in this class of polymers have degenerate chemical shifts where the n= 0 rotary resonance condition under MAS would result in broad lines. Backbone torsion angle determination is crucial for the understating the functioning of these materials and also for the design of new functional materials based on this scaffold. The sensitivity enhanced DOQSY experiment will make the measurement of backbone torsion angles possible in such classes of useful materials where the signal to noise is not very large owing to the bulky nature of the molecules and in addition the sample quantities can as well be limited.

3.4.3 Conclusions

A new Hahn-solid-Hahn CPMG pulse sequence for the sensitivity enhancement of the dipolar coupled spin pair is demonstrated. The experiment yielded an increase in the S/N of approximately 4.2. It is shown that the HSHCPMG acquisition can be conveniently applied to 2D-DOQSY type of experiments where the sensitivity factor is very important. The angular information has been retrieved from the sensitivity enhanced 2D DOQSY spectrum of glycine for which the single crystal structure and single crystal NMR data is available. Comparison of the result obtained from the DOQSY, DOQSY-HSHCPMG and the single crystal data shows that reliable angular information can be extracted from the sensitivity enhanced spectrum. The 4 times increase in S/N leads to a reduction in experimental time by a factor of 16. The number of HSHCPMG echoes acquired in this case was limited by the decoupling performance of the probe at very long acquisition. In principle on probes with better decoupling performance samples with long T_2 values will result in higher sensitivity gains.

3.5 References

[1] I. Schnell, A. Watts, H.W. Spiess, Double-quantum double-quantum MAS exchange NMR spectroscopy: Dipolar-coupled spin pairs as probes for slow molecular dynamics, Journal of Magnetic Resonance, 149 (2001) 90-102.

[2] A. Ramamoorthy, Y.F. Wei, D.K. Lee, PISEMA solid-state NMR spectroscopy, Ann R Nmr S, 52 (2004) 1-52.

[3] K. Schmidt-Rohr, A Double-Quantum Solid-State NMR Technique for Determining Torsion Angles in Polymers, Macromolecules, 29 (1996) 3975-3981.

[4] G. Terry, Chapter 4 Recent Applications of REDOR to Biological Problems, in: A.W. Graham (Ed.) Annual Reports on NMR Spectroscopy, Academic Press, 2009, pp. 111-137.

[5] S.L. Grage, A. Watts, Applications of REDOR for Distance Measurements in Biological Solids, in: G.A. Webb (Ed.) Annual Reports on NMR Spectroscopy, Academic Press, 2006, pp. 191-228.

[6] J.D. van Beek, L. Beaulieu, H. Schafer, M. Demura, T. Asakura, B.H. Meier, Solid-state NMR determination of the secondary structure of Samia cynthia ricini silk, Nature, 405 (2000) 1077-1079.

[7] K. Schmidt-Rohr., H.W. Spiess, Multidimensional Solid-State NMR and Polymers, Academic Press, 1996.

[8] H. Kaji, K. Schmidt-Rohr, Conformation and dynamics of atactic poly(acrylonitrile). 2. Torsion angle distributions in meso dyads from two-dimensional solid-state double-quantum C-13 NMR, Macromolecules, 34 (2001) 7368-7381.

[9] F.J. Blanco, R. Tycko, Determination of polypeptide backbone dihedral angles in solid state NMR by double quantum C-13 chemical shift anisotropy measurements, Journal of Magnetic Resonance, 149 (2001) 131-138.

[10] J. Goetz, Orientational Information in Solids from REDOR Sidebands, Journal of Magnetic Resonance, 129 (1997) 222-223.

[11] C.M. Gowda, F. Vasconcelos, E. Schwartz, E.R.H. van Eck, M. Marsman, J.J.L.M. Cornelissen, A.E. Rowan, G.A. de Wijs, A.P.M. Kentgens, Hydrogen bonding and chemical shift assignments in carbazole functionalized isocyanides from solid-state NMR and first-principles calculations, Physical Chemistry Chemical Physics, 13 (2011) 13082-13095.

[12] R.K. Harris, Applications of solid-state NMR to pharmaceutical polymorphism and related matters, Journal of Pharmacy and Pharmacology, 59 (2007) 225-239.

[13] A. Rapp, I. Schnell, D. Sebastiani, S.P. Brown, V. Percec, H.W. Spiess, Supramolecular Assembly of Dendritic Polymers Elucidated by 1H and 13C Solid-State

MAS NMR Spectroscopy, Journal of the American Chemical Society, 125 (2003) 13284-13297.

[14] J.M. Goetz, J. Schaefer, Orientational Information in Solids from REDOR Sidebands, Journal of Magnetic Resonance, 129 (1997) 222-223.

[15] D. Weliky, R. Tycko, Determination of Peptide Conformations by Two-Dimensional Magic Angle Spinning NMR Exchange Spectroscopy with Rotor Synchronization, Journal of the American Chemical Society, 118 (1996) 8487-8488.

[16] J. Herzfeld, A.E. Berger, Sideband Intensities in Nmr-Spectra of Samples Spinning at the Magic Angle, J Chem Phys, 73 (1980) 6021-6030.

[17] HBA 1.6.12 K. Eichele, R. E. Wasylishen Dalhousie University & Universit¨at T¨ubingen, 2010.

[18] F.H. Larsen, H.J. Jakobsen, P.D. Ellis, N.C. Nielsen, Sensitivity-enhanced quadrupolar-echo NMR of half-integer quadrupolar nuclei. Magnitudes and relative orientation of chemical shielding and quadrupolar coupling tensors, J Phys Chem A, 101 (1997) 8597-8606.

[19] R. Siegel, T.T. Nakashima, R.E. Wasylishen, Signal-to-noise enhancement of NMR spectra of solids using multiple-pulse spin-echo experiments, Concept Magn Reson A, 26A (2005) 62-77.

[20] M. Goswami, P.K. Madhu, J. Dittmer, N.C. Nielsen, S. Ganapathy, Sensitivity enhancement of (29)Si double-quantum dipolar recoupling spectroscopy by Carr-Purcell-Meiboom-Gill acquisition method, Chem Phys Lett, 478 (2009) 287-291.

[21] I. Hung, A.J. Rossini, R.W. Schurko, Application of the Carr-Purcell Meiboom-Gill pulse sequence for the acquisition of solid-state NMR spectra of spin-1/2 nuclei, J Phys Chem A, 108 (2004) 7112-7120.

[22] F.H. Larsen, H.J. Jakobsen, P.D. Ellis, N.C. Nielsen, QCPMG-MAS NMR of half-integer quadrupolar nuclei, Journal of Magnetic Resonance, 131 (1998) 144-147.

[23] E.L. Hahn, Spin Echoes, Phys Rev, 80 (1950) 580-594.

[24] H.Y. Carr, E.M. Purcell, Effects of Diffusion on Free Precession in Nuclear Magnetic Resonance Experiments, Phys Rev, 94 (1954) 630-638.

[25] S. Meiboom, D. Gill, Modified Spin-Echo Method for Measuring Nuclear Relaxation Times, Rev Sci Instrum, 29 (1958) 688-691.

[26] G.J. Kennedy, J.W. Wiench, M. Pruski, Determination of Si-Al connectivities in zeolites with 2D Al-Si RAPT CPMAS CPMG HETCOR NMR techniques., Stud. Surf. Sci. Catal., 174 (2008) 769-774.

[27] A.R. Albunia, R. Graf, A. Grassi, G. Guerra, H.W. Spiess, Geometry of Complex Molecular Motions of Guest Molecules in Polymers from Solid State (2)H NMR, Macromolecules, 42 (2009) 4929-4931.

[28] C.M. Gowda, E.R.H. van Eck, A.M. van Buul, E. Schwartz, G.W.P. van Pruissen, J.J.L.M. Cornelissen, A.E. Rowan, R.J.M. Nolte, A.P.M. Kentgens, Direct Backbone Structure Determination of Polyisocyanodipeptide Using Solid-State Nuclear Magnetic Resonance, Macromolecules, 45 (2012) 2209-2218.

[29] K. Schmidt-Rohr, Complete Dipolar Decoupling of 13C and Its Use in Two-Dimensional Double-Quantum Solid-State NMR for Determining Polymer Conformations, Journal of Magnetic Resonance, 131 (1998) 209-217.

[30] A.E. Bennett, C.M. Rienstra, M. Auger, K.V. Lakshmi, R.G. Griffin, Heteronuclear decoupling in rotating solids, The Journal of Chemical Physics, 103 (1995) 6951-6958.

[31] D. Marion, K. Wüthrich, Application of phase sensitive two-dimensional correlated spectroscopy (COSY) for measurements of 1H-1H spin-spin coupling constants in proteins, Biochemical and Biophysical Research Communications, 113 (1983) 967-974.

[32] M. Bak, J.T. Rasmussen, N.C. Nielsen, SIMPSON: A General Simulation Program for Solid-State NMR Spectroscopy, Journal of Magnetic Resonance, 147 (2000) 296-330.

[33] J.D. van Beek, matNMR: A flexible toolbox for processing, analyzing and visualizing magnetic resonance data in Matlab®, Journal of Magnetic Resonance, 187 (2007) 19-26.

[34] MATLAB, Version 7.10.0.499; The Mathworks Inc., in.

[35] O.W. Sorensen, M. Rance, R.R. Ernst, Z-Filters for Purging Phase-Distorted or Multiplet-Distorted Spectra, Journal of Magnetic Resonance, 56 (1984) 527-534.

[36] S. Cadars, J. Sein, L. Duma, A. Lesage, T.N. Pham, J.H. Baltisberger, S.P. Brown, L. Emsley, The refocused INADEQUATE MAS NMR experiment in multiple spin-systems: Interpreting observed correlation peaks and optimising lineshapes, Journal of Magnetic Resonance, 188 (2007) 24-34.

[37] K.K. Dey, J.T. Ash, N.M. Trease, P.J. Grandinetti, Trading sensitivity for information: Carr--Purcell--Meiboom--Gill acquisition in solid-state NMR, The Journal of Chemical Physics, 133 (2010) 054501-054510.

[38] R. Lefort, J.W. Wiench, M. Pruski, J.P. Amoureux, Optimization of data acquisition and processing in Carr-Purcell-Meiboom-Gill multiple quantum magic angle spinning nuclear magnetic resonance, J Chem Phys, 116 (2002) 2493-2501.

[39] A.S. Lipton, J.A. Sears, P.D. Ellis, A general strategy for the NMR observation of half-integer quadrupolar nuclei in dilute environments, Journal of Magnetic Resonance, 151 (2001) 48-59.

[40] M. Strohmeier, D.W. Alderman, D.M. Grant, Obtaining molecular and structural information from C-13-N-14 systems with C-13 FIREMAT experiments, Journal of Magnetic Resonance, 155 (2002) 263-277.

[41] R.R. Ernst, G. Bodenhausen, A. Wokaun, Principles of nuclear magnetic resonance in one and two dimensions, Clarendon Press, Oxford, 1987.

[42] R.A. Haberkorn, R.E. Stark, H. Vanwilligen, R.G. Griffin, Determination of Bond Distances and Bond Angles by Solid-State Nuclear Magnetic-Resonance - C-13 and N-14 Nmr-Study of Glycine, Journal of the American Chemical Society, 103 (1981) 2534-2539.

[43] A.J. Shaka, J. Keeler, R. Freeman, Evaluation of a New Broad-Band Decoupling Sequence - Waltz-16, Journal of Magnetic Resonance, 53 (1983) 313-340.

[44] R.E. Marsh, A Refinement of the Crystal Structure of Glycine, Acta Crystallogr, 11 (1958) 654-663.

[45] S.L. Altmann, Rotations, quaternions, and double groups, Clarendon Press ;
Oxford University Press, Oxford
New York, 1986.

[46] S.K. Vasa, H. Janssen, E.R.H. Van Eck, A.P.M. Kentgens, High-resolution solid-state 13C μmAS NMR with long coherence life times, Physical Chemistry Chemical Physics, 13 (2011) 104-106.

[47] E. Schwartz, E. Lim, C.M. Gowda, A. Liscio, O. Fenwick, G. Tu, V. Palermo, R. de Gelder, J.J.L.M. Cornelissen, E.R.H. Van Eck, A.P.M. Kentgens, F. Cacialli, R.J.M. Nolte, P. Samori, W.T.S. Huck, A.E. Rowan, Synthesis, Characterization, and Surface Initiated Polymerization of Carbazole Functionalized Isocyanides, Chem Mater, 22 (2010) 2597-2607.

[48] E. Schwartz, V. Palermo, C.E. Finlayson, Y.-S. Huang, M.B.J. Otten, A. Liscio, S. Trapani, I. González-Valls, P. Brocorens, J.J.L.M. Cornelissen, K. Peneva, K. Müllen, F.C. Spano, A. Yartsev, S. Westenhoff, R.H. Friend, D. Beljonne, R.J.M. Nolte, P. Samorì, A.E. Rowan, “Helter-Skelter-Like” Perylene Polyisocyanopeptides, Chemistry - A European Journal, 15 (2009) 2536-2547.

Chapter 4

Chemical shift analysis to obtain structural insight of polyisocyanodipeptides

Chandrakala M. Gowda, Vipin Agarwal, Ernst R. H. van Eck and Arno P. M. Kentgens

4.1 Introduction

Natural biopolymers such as proteins and peptides are known to be very stable and are designed to fulfill specific and complex functions. There is a growing trend to design molecules that perform specific tasks, called synthetic functional materials. The polyisocyanides have attracted interest in the research community due to their stability and rigid rod like helical structure.[1-3] Since the polymer helices are chiral in nature, they have been used as enantiomer selective groups in chromatography and as enantio-selective catalysts.[4] The basic molecular skeleton of the polyisocyanides can be represented as shown in Figure 4.1a. The structure allows a variety of chemical groups to be substituted as -R groups leading to the synthesis of a wealth of polymers with different applicability. The structural conformation of the polyisocyanides has been in the focus for several decades. Initial studies based on X-ray diffraction, viscosity measurements, circular dichroism (CD) spectroscopy etcetera suggested tightly coiled 4_1 helical conformation for the polyisocyanides such as the α-phenylethylisocyanides and poly-(*tert*-butyl isocyanide).[3, 5] The polyisocyanides were found to be stable when bulky sidechain groups were present in the sidechains such as the poly-(*tert*-butyl isocyanide). When the sidechain substituents were not bulky enough they were found to uncoil upon standing in solutions as in the N-phenly substituted polyisocyanides.[6] Solution state NMR studies by Green et al. showed that a regular and rigid helical conformation did not strictly exist even for the polymers such as the α-phenyl ethyl isocyanide which is

claimed to have rigid 4_1 helical conformation.[7] Theoretical studies on small molecular fragments of polyisocyanides with substituents of varying sizes indicated that the polyisocyanides with bulkier substituents adapted a 4_1 helical conformation whilst the polymers with less bulkier substituents were found to have more loose helical configuration.[8] With the above mentioned studies it was clear that the structural regularity and conformation of the polyisocyanides has been an open question for long time where the different nature of the sidechains plays an important role. Thus, with the aim of creating more stable and rigid polyisocyanides which can possess well defined secondary structure Cornelissen et al. synthesized peptide derived polyisocyanides. Inspired by the natural molecules such as proteins and other biomolecules they incorporated a similar design into the polyisocyanides. Amino acids such as alanine and glycine were used to form peptide derived polyisocyanides.[9] The isocyano monomer unit molecule, L-isocyanoalanyl-D-alanine methyl ester (L,D-IAA), is shown in Figure 4.1b, and the corresponding polymer is shown in Figure 4.1. The amino acids are chiral in nature. These chiral monomeric units bias the polymerization process leading to preferential formation of polymers of one screw sense over the other. The alanine-alanine derived polyisocyanides lead to four stereoisomers based on the '*L*' and '*D*' conformation of the two alanines. These polymers are named here as L,L-PIAA, L,D-PIAA, D,L-PIAA and D,D-PIAA for convenience. Several techniques such as CD spectroscopy, Infrared spectroscopy (IR), X-ray diffraction, atomic force microscopy (AFM) and nuclear magnetic resonance (NMR) spectroscopy have been applied for the structural characterization of the dipeptide derived polyisocyanides.[9] AFM and X-ray diffraction studies showed that these polymers are rigid rod like structures with lengths of about ~200 nm. The introduction of amino acids resulted in N-H---C=O hydrogen bonding between the 'n' and 'n+4' sidechains of the polymer thus stabilizing the helix.[10, 11] Fast-magic angle spinning (MAS) ^{1}H NMR in the solid-state and IR measurements of the four stereoisomers has revealed strong hydrogen bonding in the four stereoisomers.[9, 11, 12] A sketch of the L,D-PIAA polymer showing a hydrogen bond array between the sidechains 'n' and 'n+4' is shown in Figure 4.1d. The peptide derived polyisocyanides provide a possibility for adding larger chemical groups as sidechains with a hydrogen bond stabilized backbone. This has paved way for the realization of a number of functional materials which are useful in the design of electrochromic devices such as LEDs and optoelectronic devices, solar cells, conducting 'nanowires', field effect

transistors (FETs) etcetera.[13-15] Polyisocyanides possessing functional groups without the dipeptide sidechains have been reported to be structurally non rigid and possess irregularities in structure.[16]

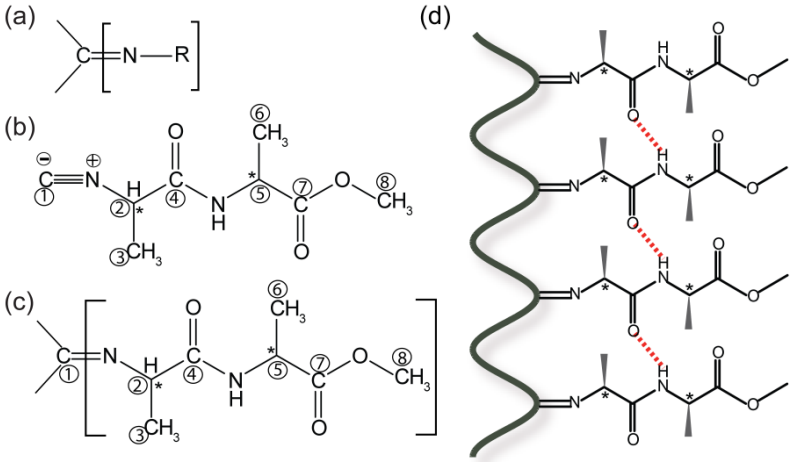

Figure 4.1 (a) Basic isocyanide polymer skeleton. (b) L-isocyaoalanyl-D-alanine methyl ester (L,D-IAA) monomer unit and (c) L-isocyanoalanyl-D-alanine methyl ester polymer (L,D-PIAA). The carbon positions are numbered in (b) and (c) for convenience in discussions. The NH proton will be designated as NH proton. (d) Sketch of the L,D-PIAA polymer showing the hydrogen bonds between 'n' and 'n+4' side chains. The asterisks in (b) and (c) indicate chiral centers in the amino acids.

Several experimental studies of the dipeptide derived polyisocyanides show that they have different physical properties such as viscosity, polymer lengths, molecular weights, aggregation behavior, polymerization rates and stability.[9, 12]. Previous molecular modeling studies of L,D-PIAA and L,L-PIAA proposed that the L,L-PIAA polymer has unfavorable steric interactions due to the orientation of the methyl groups of the sidechains making it less stable than the L,D-PIAA polymer.[11] On the other hand, thermal stability studies showed that the L,D-PIAA polymer decomposed faster than the L,L-PIAA and D,D-PIAA polymers indicating lower stability for the L,D-PIAA polymer. There is no experimental evidence that support significant structural differences between the stereoisomers of the dipeptide derived polyisocyanides. Understanding of the structural differences could provide a means to understand the underlying differences in

the physical properties of these polymers and assist in future design of new functional materials.

In chapter 2 we have shown that the backbone structure of one of the stereoisomer, L,D-PIAA, is a 15_4 helix.[10] However, structural analysis of the side chain arrangement in the L,D-PIAA and the other stereoisomers has not been described yet. The chemical shift interaction of nuclei is sensitive to the chemical environment and is anisotropic in nature i.e., it depends on the orientation of the particular molecular segment.[17] The chemical shift anisotropy (CSA) tensor analysis has proved to be a useful tool for structural and dynamics studies.[18, 19] In this study we have used solid-state NMR spectroscopy to obtain structural information from the chemical shift studies of the four stereoisomers L,L-PIAA, L,D-PIAA, D,L-PIAA and D,D-PIAA. Previous solid-state NMR studies of the polymers (L,L-PIAA, L,D-PIAA, D,L-PIAA and D,D-PIAA) and the monomers (L,L-IAA, L,D-IAA and D,L-IAA), only give partial assignments of the peaks and lack any structural insights.[9] Here we provide a detailed description of the chemical shifts and we identify and highlight certain spectral features that throw light on the structural configuration of the polymers. We have also used high resolution ^{1}H-^{13}C heteronuclear correlation experiments for the spectral analysis of L,D-PIAA and the L,L-PIAA polymers. In a ^{1}H-^{13}C heteronuclear correlation experiment the proton magnetization is transferred to the carbons that are spatially close using the ^{1}H-^{13}C dipolar coupling interaction. The observed correlations help in identifying the carbon and proton nuclei that are spatially close to each other. The heteronuclear correlation experiments also reveal interesting effects in the NH proton chemical shifts which will be discussed below.

We systematically compare the isotropic chemical shifts and chemical shift anisotropy tensors of the carbons in the four stereoisomers, L,L-PIAA, L,D-PIAA, D,L-PIAA and D,D-PIAA, and the monomers, L,L-IAA, L,D-IAA and D,L-IAA with each other. The chemical shift differences and similarities between the various monomers and polymers are correlated to the molecular structure of the polymers. The tensor analysis of the carbonyl carbon (C4) is only performed for the L,D-PIAA polymer as it requires specifically ^{13}C enriched polymer at the C4 position. The carbonyl tensor parameters of the polymer are compared to that of the L,D-IAA monomer. We analyze the chemical shifts of the hydrogen bonding moieties NH proton and C═O carbon (C4) with high resolution ^{1}H-^{13}C

heteronuclear correlation experiment and 1D CPMAS spectra of specific site enriched L,D-PIAA respectively which reveals structural details in the L,D-PIAA polymer.

4.2 Experiment

The isocyanoalanyl-alanine methyl ester monomers, L,D-IAA, L,L-IAA, D,L-IAA and the polymers of isocyanoalanyl-alanine methyl ester, L,D-PIAA, L,L-PIAA, D,L-PIAA and D,D-PIAA were synthesized as described previously.[9] The 1D ^{13}C CPMAS spectra of the polymers (L,L-PIAA, L,D-PIAA, D,L-PIAA and D,D-PIAA) and the monomers (L,L-IAA, L,D-IAA and D,L-IAA) were obtained with a 4 mm HXY probe at a MAS frequency of 6000 Hz and 6200 Hz on a 14.1 T Varian VNMRS system. A ^{1}H spinlock pulse of approximately 50 kHz was used for the cross polarization. Proton decoupling was achieved using continuous modulation (CM) decoupling at a 76 kHz RF field.[20] A L,D-PIAA polymer ^{13}C enriched specifically at the carbonyl position (C4) (Figure 4.1c) was used to determine the CSA tensor of the carbonyl carbon in the polymer. The spectra are externally referenced using the CH_2 carbon peak of adamantane at 38.48 ppm as a secondary reference.

2D ^{1}H–^{13}C heteronuclear correlation spectra of the polymers, L,D-PIAA and L,L-PIAA were recorded on a 9.4 T Varian VNMRS system using a 3.2 mm probe at 10 kHz sample spinning speed.[21] A CP contact time of 150 μs and 300 μs was used to acquire the spectra. Heteronuclear proton decoupling was achieved using TPPM proton decoupling in the direct (^{13}C) dimension while Frequency Switched Lee–Goldburg (FSLG) homonuclear decoupling was applied in the indirect (^{1}H) dimension with a ^{1}H field strength of 75 kHz and 86 kHz respectively.[22, 23] The FSLG scaling factor was determined to be 0.57 by comparing the ^{1}H peak positions in the heteronuclear correlation spectrum to that of the fast-MAS 1D ^{1}H NMR spectrum. 1.Quadrature detection in the indirect dimension was achieved using the States method.[24] CSA tensors were determined using the Herzfeld Berger spinning sideband Analysis software package.

4.3 Results and Discussions

4.3.1 Comparison of 13C spectra of L,D-IAA and L,L-IAA

An overlay plot of the 1D ^{13}C CPMAS spectra of the L,L-IAA and L,D-IAA monomers is shown in Figure 4.2. The line widths of the various carbon peaks are narrow with line widths of about 48 Hz and 20 Hz for the narrowest lines for L,L-IAA and L,D-IAA respectively. Except for the ester carbon (C7) and alpha carbon of the first alanine (C2) the chemical shifts of all the other carbon atoms differ slightly for the L,L-IAA and L,D-IAA monomers. These differences in chemical shifts could originate from differences in crystal structure packing of the two monomers or due to difference in orientation of various chemical moieties in the stereoisomers or both. It is intriguing to note that carbon atoms directly attached to nitrogen atoms show different line shapes. The C1 carbon of the L,D-IAA monomer shows a lorentzian line shape while the same carbon atom in the L,L-IAA monomer exhibits a broader distorted line shape. This distortion in line shape for the C1 carbon of the L,L-IAA monomer most likely results from the residual dipolar coupling due to a second-order cross term between ^{13}C-^{14}N heteronuclear dipolar couplings and the ^{14}N quadrupolar coupling. [26] For the L,D-IAA monomer the alpha carbon of the second alanine (C5) and the carbonyl carbon (C4) exhibit line splitting. It is not clear if the L,L-IAA monomer also exhibits line splitting at these carbons as the lines are slightly broadened. The residual dipolar couplings are small and cause only line splitting of the order of ~20 Hz in the L,D-IAA monomer. The D,L-IAA monomer spectrum is similar to that of the L,D-IAA monomer and is not shown here.

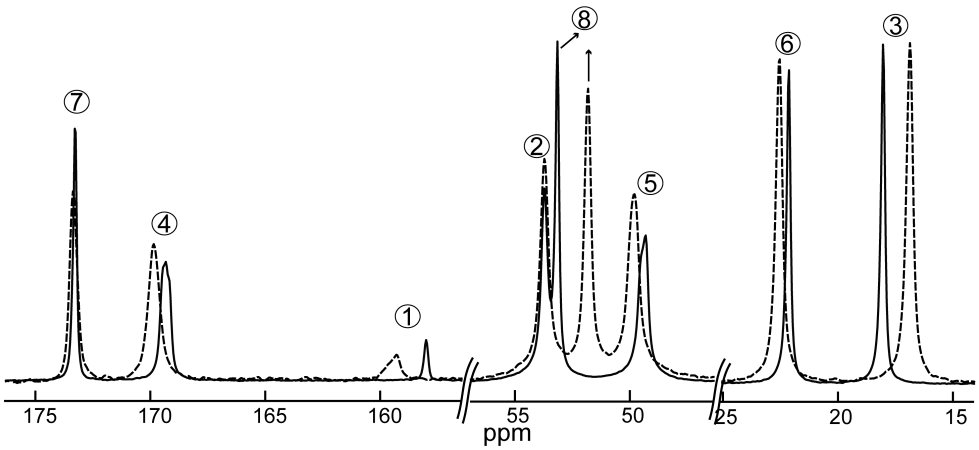

Figure 4.2 1D ^{13}C CPMAS spectra of the monomers L,D-IAA (solid) and L,L-IAA (dashed) recorded at the spinning speed of 6200 Hz. The numbers indicate the assignment of the peaks to the respective carbons in Figure 4.1.

4.3.2 Comparison of chemical shielding in L,D-IAA monomer and L,D-PIAA polymer

The ^{13}C CPMAS NMR spectra of the monomer L,D-IAA and the polymer L,D-PIAA shown in Figure 4.3a and c respectively. The ^{13}C isotropic chemical shift assignments for the monomer and the polymer are summarized in

Table 4.1. Several differences are evident immediately on examining the monomer and polymer spectra. The monomers shows narrower lines compared to that of the polymers indicating the crystalline state of the monomer while broader resonances in the polymer are indicative of a disordered state. In general the ^{13}C line width varies between 20-40 Hz for all the peaks of the monomer while for the polymer a narrowest line width of approximately 258 Hz is observed for the backbone carbon (C1). Beside changes in line width, the chemical shift of all carbons changes on polymerization. As expected, the most dramatic changes in chemical shift are observed near the chemical moiety ($^{-}C \equiv N^{+}$) involved in polymerization. The chemical shift of the C1 carbon changes by about 2.9 ppm whereas the chemical shift of the C2 carbon moves downfield by about 11.4 ppm. These large chemical shifts originate from the change in hybridization state of the C1 carbon upon polymerization and the associated changes in currents originating from the π

electrons of the $^{-}C \equiv N^{+}$ moiety. In addition there will be a change in chemical shift of all chemical moieties due to changing packing environment going from crystalline monomer phase to the amorphous polymer state. All other chemical shift changes on polymerization are summarized in

Table 4.1. The chemical shift anisotropies of the sp^2 hybridized carbons C1, C4 and C7 are about 80-100 ppm which are larger than the rate of magic angle spinning and hence are not averaged out. This gives rise to spinning sidebands on either side of the isotropic chemical shift position. The intensities of these sidebands have been used to deduce the magnitude of the CSA tensors through Herzfeld and Berger spinning sideband analysis.[27]

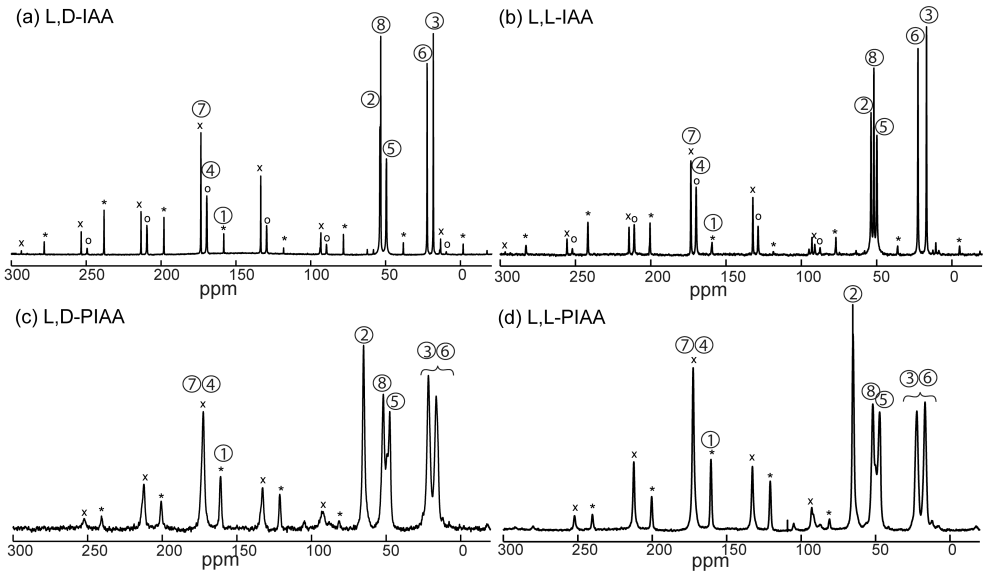

Figure 4.3 1D ^{13}C CPMAS spectra of (a) L,D-IAA (b) L,L-IAA. (c) L,D-PIAA and (d) L,L-PIAA. The 'x', 'o' and '*' marks denote the spinning sidebands of C7, C4 and C1 respectively in the monomers and 'x' and '*' marks denote the spinning sidebands of C7/C4 and C1 respectively in the polymers. *note*: The assignments of C3 and C6 remain ambiguous in the polymer.

Previously we demonstrated that the amide protons form strong hydrogen bonds on polymerization.[9] From that study it was clear that the amide proton is the hydrogen

bond donor but the study was not conclusive as to which carbon, C4 or C7, participated in the hydrogen bond as a hydrogen acceptor. The carbonyl and ester carbons (C4 and C7) are well separated in the monomers whereas for the polymers the carbonyl and ester carbons (C4 and C7) overlap to a large extent giving a single line in the spectrum. The ester carbon (C7) undergoes a small upfield change in chemical shift of about 0.8 ppm while the carbonyl carbon (C4) carbonyl undergoes a larger downfield shift of about 3.2 ppm and 2.6 ppm respectively for the L,D-PIAA and L,L-PIAA polymers. This implies that the C4 acts as the hydrogen acceptor in the N─H----C═O hydrogen bond. This hypothesis was independently verified by preparing a ^{13}C enriched L,D-PIAA polymer at C4 position and comparing the changes in the CSA tensor components of the carbon with that of the L,D-IAA monomer. An extract from the ^{13}C CPMAS spectrum of ^{13}C enriched L,D-PIAA polymer at the carbonyl position (C4) is shown in Figure 4.4. The ^{13}C line shape for the C4 carbon in the L,D-PIAA polymer shows a prominent shoulder with an approximate intensity distribution of 1:2. This indicates that on polymerization the C4 carbon has at least two different chemical environment in the L,D-PIAA polymers. The carbonyl carbons are sp^2 hybridized and the electrons in the sp^2 plane are affected significantly due to hydrogen bond.[28] The CSA tensor values for the carbonyl carbon from the isotopically enriched sample were extracted using spinning sideband analysis. The line was also deconvoluted into two separate peaks and the tensor values of the individual lines were obtained. The values of the isotropic chemical shift and chemical shift anisotropy tensors of the carbonyl carbon (C4) both with and without deconvolution of the peak, of the polymer L,D-PIAA and the monomer L,D-IAA are listed in Table 4.2.

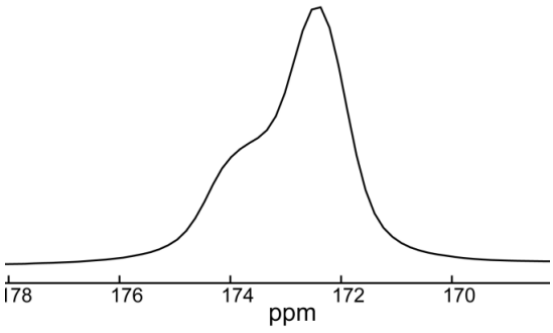

Figure 4.4 the line shape of the C4 carbon obtained from the ^{13}C enriched sample at the C4 position.

Table 4.1 Isotropic chemical shift values of the stereoisomers of isocyanide polymers and the monomers. All values are in ppm

Carbon	Polymers				Monomers	
	L,D-PIAA	D,L-PIAA	L,L-PIAA	D,D-PIAA	L,D-IAA	L,L-IAA
C1	160.9	160.9	160.5	160.6	158	159
C2	65.1	65.0	65.1	65.1	53.7	53.7
C3	21.6/16.4	21.5/15.4 and 16.2	22.3/16.8	22.3/16.8	18.0	16.9
C4	172.5	172.4	172.5	172.5	169.3	169.9
C5	47.5 and 49.4	47.4 and 49.3	47.2 and 50.2	47.4 and 50.0	49.4	49.8
C6	21.6/16.4	21.5/15.4 and 16.2	22.3/16.8	22.3/16.8	22.1	22.5
C7	172.5	172.4	172.5	172.5	173.3	173.4
C8	51.9	51.7	51.8	51.8	53.1	51.8

**The shaded region in the table indicate ambiguity in the assignment of C3 and C6 carbons in the polymers.

Table 4.2 Chemical shift tensors of the carbonyl carbon (C4) measured using the ^{13}C enriched sample at the C4 position. The principal tensor components are expressed in ppm.

Carbonyl carbon (C4)		δ_{iso}	δ_{11}	δ_{22}	δ_{33}	Anisotropy ζ_δ	Asymmetry η_δ
L,D-PIAA	The integral of the peak considered as a single peak is used for fitting	172.4	245	182	90	-82	0.75
	deconvoluted peak integrals used for fitting at 172.42	172.4	241	188	88	-84	0.63
	deconvoluted peak integrals used for fitting at 173.7	173.7	247	181	92	-81	0.81
L,D-IAA		169.2	247	173	87	-82	0.91

In a carbonyl group the δ_{11} and δ_{22} component lie close to the sp^2 plane of the C═O carbon with δ_{22} approximately parallel to the C═O bond and therefore experiences the largest change in the tensor value upon hydrogen bonding. The δ_{33} component is mostly perpendicular to the sp^2 plane of the carbonyl carbon.[28] The tensor component δ_{22} shows a significant downfield shift of about 9 ppm in the polymer indicating stronger hydrogen bonding in the polymer than in the monomer crystal. Due to the perpendicular alignment only minor changes are observed in the δ_{11} and δ_{33} components of the carbonyl

tensor. This clearly establishes that on the side chains in the polymer are stabilized by hydrogen bonds. However, one must note that the presence of multiple CO peaks indicate that there exist more than one environment for the hydrogen bond.

4.3.3 Comparison of chemical shielding in L,L-IAA and L,L-PIAA

Similar to the effects described in the previous paragraph, the chemical shift of the C1 carbon moves downfield by 1.5 ppm in the L,L-PIAA polymer whereas the chemical shift of the C2 carbon moves downfield by about 11.4 ppm compared to that the of L,L-IAA monomer. The carbonyl carbon shows a downfield shift in the polymer of about 2.6 ppm. The tensor analysis of the carbonyl carbon in the L,L-PIAA polymer is not performed as it requires specific carbon labeling. However based on the downfield shift of the carbonyl carbon (C4) similar to that the L,D-PIAA polymer it can be concluded that the C4 carbon is the hydrogen bond acceptor also in the L,L-PIAA polymer.

4.3.4 Comparison of chemical shielding for the different stereopolymers

In this section first we compare the ^{13}C chemical shifts and principal CSA tensor values for two pairs of the enatiomeric polymers L,D-PIAA and D,L-PIAA and for L,L-PIAA and D,D-PIAA. In the second part we compare the similarities and difference in the ^{13}C spectra of the diastereoisomers L,D-PIAA and L,L-PIAA. Figure 4.5a and b show the overlay of the ^{13}C CPMAS spectra L,D-PIAA and D,L-PIAA polymers and L,L-PIAA and D,D-PIAA polymers respectively.

L,D-PIAA and the D,L-PIAA polymers: The intensities of both pairs of spectra were normalized to the intensity of the C2 carbon. The chemical shifts and line shapes of the different peaks in the L,D-PIAA and **D,L**-PIAA polymers are identical to each other. There are some differences in the intensities of the peak that could result from variations in CP conditions. The isotropic shift values for all the peaks are tabulated in

Table 4.1. The **D,L** -PIAA molecule shows exactly the same shift and peak shape for the C4 carbon attributed above to hydrogen bonding in case of the **L,D** -PIAA molecule. In

addition, one of the methyl groups shows a split resonance for both the polymer molecules. The chemical shift anisotropy tensor values for the backbone carbon (C1) in the **L,D** -PIAA and the **D,L** -PIAA polymer was extracted by means of Herzfeld-Berger spinning sideband analysis (see Table 4.3). [27] The spinning speed of the spectra is adjusted so that the sidebands have no or least overlap with other peaks. Within experimental accuracy the CSA tensor for the C1 carbon are similar. From the ^{13}C isotropic chemical shifts, CSA tensors and hydrogen bonding indication we can conclude that the backbone structure and details of side chain packing are identical in the two polymers.

L,L-PIAA and the D,D-PIAA polymers: From the ^{13}C isotropic chemical shifts, CSA tensors and line shape analysis of the L,L-PIAA and D,D-PIAA polymers, one can conclude that both the molecules have identical backbone structure and sidechain packing. As discussed in the introduction, previous studies have indicated striking differences in the physical and chemical properties of L,D-PIAA and L,L-PIAA polymers. The above analysis suggests that the structural configuration of the polymers L,L-PIAA and D,D-PIAA and that of L,D-PIAA and D,L-PIAA polymers are similar to each other.

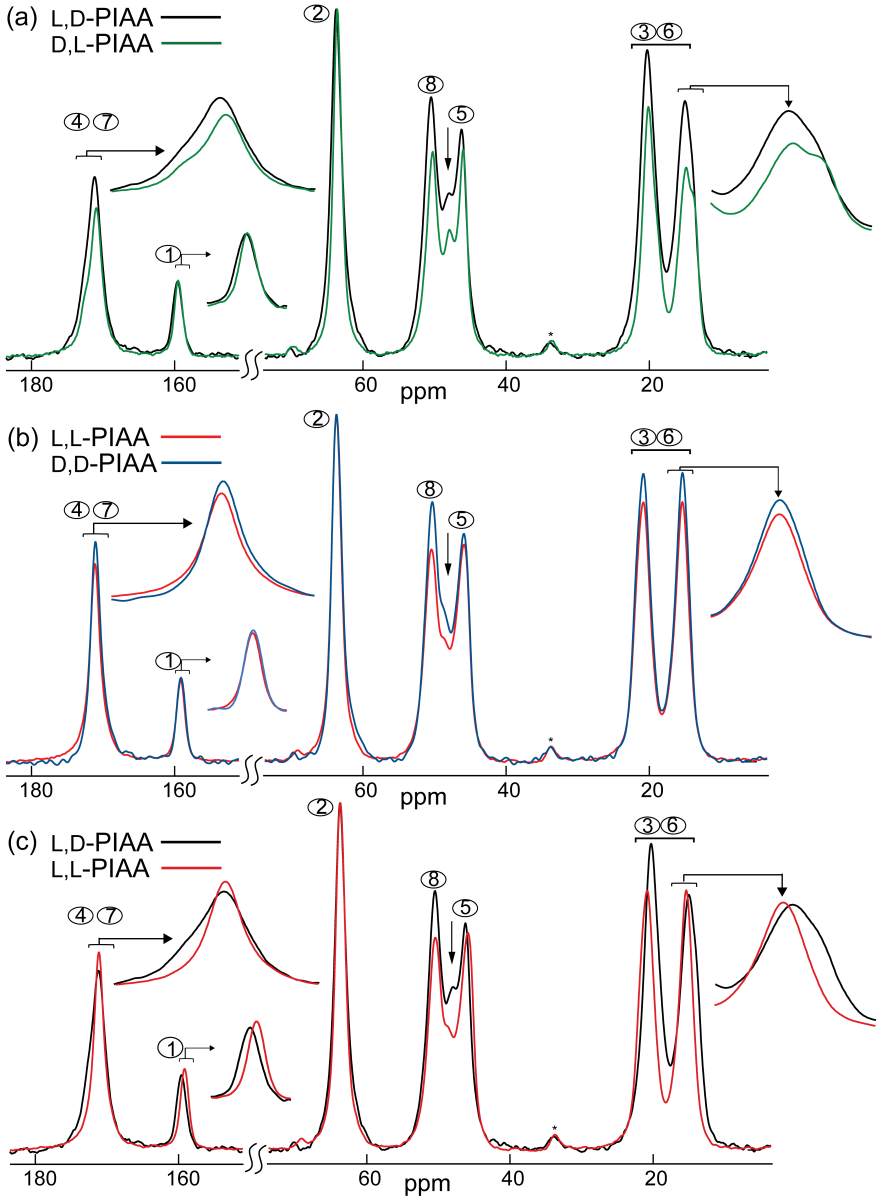

Figure 4.5 1D ^{13}C CPMAS spectra of (a) L,D-PIAA(black) and D,L-PIAA(green), (b) (a) L,L-PIAA(red) and D,D-PIAA(blue) and (c) L,D-PIAA(black) and L,L-PIAA(red) polymers. Only the isotropic chemical shifts are shown for clarity.

Table 4.3 Chemical shift tensors of the backbone carbon (C1). The principal tensor components are expressed in ppm.

Backbone Carbon (C1)	δ_{iso}	δ_{11}	δ_{22}	δ_{33}	Anisotropy ζ_δ	Asymmetry (η_δ)
L,D-PIAA	160.9	256	145	82	96	0.66
D,L-PIAA	160.9	258	143	82	97	0.63
L,L-PIAA	160.5	257	141	83	97	0.59
D,D-PIAA	160.5	254	146	81	94	0.69

L,L-PIAA and the L,D-PIAA polymers: The similarities and differences in the spectra of the polymers can be summarized as follows:

1. The backbone carbon (C1) shows a rather small difference of ~0.4 ppm between the L,D-PIAA and L,L-PIAA polymer. The CSA tensors of the C1 carbon shown in Table 4.3 have an accuracy of ±3 ppm. Within the experimental accuracy the tensor values do not indicate big structural differences in the polymer backbone conformations.
2. The alpha carbon of the first alanine that is close to the backbone of the polymers (C-2) shows identical chemical shifts in all the polymers.
3. The L,D-PIAA polymer show a prominent shoulder near the base of the line for the carbonyl carbon involved in hydrogen bond (highlighted in the inset of Figure 4.5a and c) while the L,L-PIAA shows a single Lorentzian line shape This indicates possible differences in the hydrogen bonding environment in the two polymers.
4. The line shapes of the CH_3 carbon at ~16 ppm (C3/C6) in L,D-PIAA polymer suggests more than one resonance for the CH_3 group while the L,L-PIAA shows a single peak. (shown in the inset in Figure 4.5)
5. There appears to be more than two peaks in the region between 40 ppm and 60 ppm whereas only two carbon peaks, C8 and C5, are expected in this region for the polymers. In L,D-PIAA polymer the additional peak appears at 49.4 ppm (indicated by arrow in Figure 4.5c) whereas in the L,L-PIAA polymers the same peak appears to have a shift of 50.2 ppm. Using the heteronuclear correlation experiment (Figure 4.6) we show that this additional peak can be assigned to the C5 carbon implying two chemical shift positions for the C5 carbon.

In the 2D heteronuclear correlation spectra, we particularly focus on the region between 42 ppm and 58 ppm which is enlarged for clarity in Figure 4.6a. From this region it can be seen that the ^{13}C peak at 49.4 ppm shows correlations to the NH protons at 9.3 ppm indicating that the peak is from the C5 carbon in L,D-PIAA. The methyl carbon from the ester group (C8) does not show correlations to the NH proton as they are far from NH. Similarly, in the L,L-PIAA ^{1}H-^{13}C heteronuclear correlation spectra (Figure 4.6b) the ^{13}C peak at 50.2 ppm correlates to the NH peak at 9.4 ppm indicating that the peak at 50.2 ppm is that of C5. Thus the CH carbon has at least two chemical shift values in the polymers. Now having established two peaks for the C5 carbon the question arises whether these peaks originate from two different conformations of the C5 carbon or due to the residual dipolar coupling of C5 to ^{14}N that causes line shape distortion.[26] The magnitude of the splitting of the alanine moiety ~1.84 ppm (280 Hz) is unusually large at 14.1 T field to be caused by the residual dipolar-quadrupolar cross term.[29] To eliminate this ambiguity a 1D ^{13}C CPMAS spectrum of L,D-PIAA sample was measured at a field strength of 9.4 T and compared with that of the spectra measured at 14.1 T. The residual dipolar couplings have an inverse dependence on the magnetic fields. Thus the splitting should increase in magnitude when measured at lower magnetic field. The spectrum at 9.4 T retains the 1.84 ppm splitting. This eliminates the possibility of splitting of the C5 carbon due to residual ^{14}N dipolar couplings. Thus the C5 carbon exhibits different chemical shifts within the polymer in both the L,D-PIAA and L,L-PIAA. It is worth noting that a similar splitting was observed for the C4 carbonyl carbon involved in formation of hydrogen bond in L,D-PIAA.

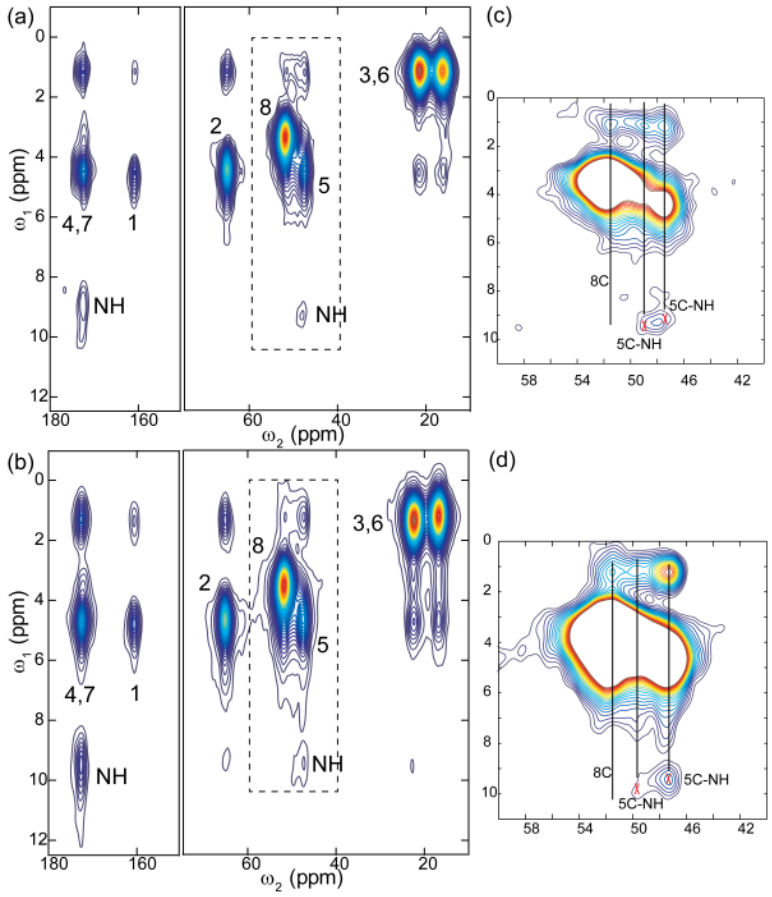

Figure 4.6 ^{1}H-^{13}C heteronuclear correlation spectra of (a) L,D-PIAA and (b) L,L-PIAA. The spectra are recorded using 150μs contact time. The spectra within the rectangular box are shown with lower contour levels for clarity in (c) and (d). (The contour levels in the two spectra are different due to differences in signal to noise ratio of the spectra)

From the shifts of the carbons close to the backbone such as those of C1 and C2 it appears that the backbone structure is well defined in all the polymers and the backbone conformation is similar to each other. The chemical shift distribution in the sidechains particularly in the region away from the backbone i.e., C4, C5, C3/C6 and C8 suggest 'local' structural irregularities. This structural irregularity seems to be larger in the L,D-PIAA than in the L,L-PIAA as can be concluded from the broader and multiple lines in sidechain carbons of the L,D-PIAA.

In order to obtain further evidence for the structural irregularity exhibited in the polymer sidechains we have performed the heteronuclear correlation experiment at a longer mixing time to check the behavior of the -NH proton chemical shifts. The longer mixing time spectrum reveals correlations of the NH protons to the carbons which are farther away from the NH proton.

As seen from the heteronuclear correlation spectra the C4---NH cross peaks are centered at 9.2 ppm for L,D-PIAA and at 9.5 ppm for L,L-PIAA. The NH proton shifts indicate similar hydrogen bonding strengths in the two polymers. Since the L,D-PIAA polymer exhibit larger line widths in the carbon spectra and also shows split resonances a heteronuclear correlation spectra for the L,D-PIAA polymer was measured with 300 μs contact time to elucidate more information of the NH proton chemical shifts. The changes in the NH proton chemical shifts reflect changes in the hydrogen bond strength. The heteronuclear correlation spectrum of L,D-PIAA polymer measured at 300 μs correlation time (see Figure 4.7) reveals that the correlations to the NH proton indicate more than one chemical shift value for the NH proton. The cross peaks appearing at (65, 9.3), (49.4, 9.4), (47.5, 9.3), (21, 9.7), (15.7, 9.2), (16.2, 9.4) clearly indicate these different NH proton chemical shifts. The C5 carbon which occurs at two chemical shift positions shows correlations to two different NH proton chemical shifts i.e., at (15.7, 9.2), (16.2, 9.4). Also the peak at ~16.4 ppm (C3/C6) which clearly shows split resonances in the carbon dimension (see Figure 4.5) shows NH correlations at different proton chemical shift values. The (C4/C7)----NH cross peak region is very intense and also broad. A similar spectrum of L,L-PIAA with a correlation time of 300 μs has not been recorded and hence a parallel comparison is not made here. Thus the NH proton chemical shifts and the carbonyl carbon (C4) chemical shift and tensor values suggest very strong hydrogen bonding in the polymer. At the same time they also implicate a ‘local’ structural irregularity.

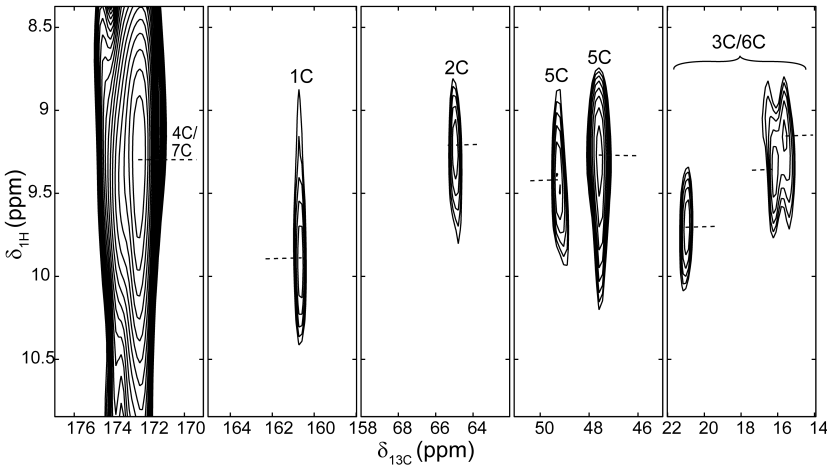

Figure 4.7 ^{1}H-^{13}C heteronuclear correlation spectra of L,D-PIAA showing the ^{13}C----NH correlations of the aliphatic carbons. The spectrum is recorded using 300μs contact time. The horizontal lines are indicated as guides to the center of the cross peaks.

The observation that (1) The chemical shift dispersion in the side chain carbon atoms predominantly occur in the sites farther away from the backbone, (2) split resonances of carbonyl carbon and multiple shifts of the NH proton are observed and suggest structural irregularities in the sidechains of the L,D-PIAA polymer. We hypothesize that the sidechains probably locally make small angular twists about the sidechain axis. This brings the NH proton closer to some groups in one instance and closer to other carbons in the other instances. We think the change is not completely random but somewhat periodic since NH proton chemical shifts and the carbons C5, C4 and C3/C6 appear as split lines rather than an averaged single broad peak (see Figure 4.7). The carbons close to the backbone such as the C1 and the C2 carbon on the contrary show the narrowest line widths. The well conserved chemical shift of the backbone carbons show that the backbone region preserves a uniform and well defined structure throughout.

Previous molecular modeling studies showed that the two methyl groups in the sidechains experience unfavorable steric interactions in case of the L,L-PIAA polymer while the L,D-PIAA is devoid of the steric interaction between the bulky methyl groups.[11] From this one can infer that the side chains in the L,D-PIAA polymer will be less restricted in terms of orientation compared to the L,L-PIAA polymer or in other words one can say that one

would see a larger distribution in the orientation of sidechains in case of L,D-PIAA polymer. This is corroborated by the larger chemical shift distribution of the side chain carbons and the C4 carbon observed for the L,D-PIAA polymer. The L,L-PIAA polymer in general exhibits narrower lines compared to that of L,D-PIAA polymer although at certain carbon positions such as the C5 the polymer exhibits a comparable distribution in chemical shifts. The larger distribution of chemical shifts in the L,D-PIAA indicates a lower steric interaction and a narrow distribution of chemical shifts in the L,L-PIAA indicates larger steric interaction. A higher steric interaction would impart restriction on the conformational freedom of the molecular groups which thus produces restricted geometry resulting in more uniformity in the structure.

4.4 Conclusions

The solid-state NMR ^{13}C chemical shift and CSA tensor analysis of the four stereoisomers of the alanine-alanine derived polyisocyanodipeptides show that the backbone conformation of the polymers are well defined and conserved through the length of the polymers. All the four polymers are stabilized by strong NH---C=O hydrogen bonding. The enantiomers L,D-PIAA and D,L-PIAA show identical chemical shift indicating a similar structure and likewise the enantiomers L,L-PIAA and D,D-PIAA are similar. It is indicated that the enantiomers L,D-PIAA/D,L-PIAA may exhibit a very small difference in the backbone conformation in comparison to L,L-PIAA/D,D-PIAA as is reflected by the small difference in isotropic shift (~0.4 ppm) of the backbone carbon. The difference is however too small to be detected in the CSA tensor analysis (within the experimental accuracy). Thus it can be concluded that overall the backbone conformations of the polymers are similar to each other. The sidechains in the L,D-PIAA show some structural irregularity as can be concluded from the sidechain carbons and NH proton chemical shift distribution. This structural irregularity is local and does not disturb the backbone conformation. The carbon lines of the L,L-PIAA/D,D-PIAA polymers are slightly narrower compared to that of the L,D-PIAA/D,L-PIAA particularly at the carbonyl carbon and seems to suggest more structural regularity compared to that of the L,D-PIAA/D,L-PIAA polymers. Nevertheless, there is some structural irregularity near sidechain region of the L,L-PIAA/D,D-PIAA.

4.5 References

[1] R.J.M. Nolte, A.J.M. van Beijnen, W. Drenth, Chirality in Polyisocyanides, J Am Chem Soc, 96 (1974) 5932-5933.

[2] W. Drenth, R.J.M. Nolte, Poly(iminomethylenes): Rigid rod helical polymers, Accounts of Chemical Research, 12 (1979) 30-35.

[3] F. Millich, Rigid rods and the characterization of polyisocyanides, in: Polymerization Reactions, Springer Berlin / Heidelberg, 1975, pp. 117-141.

[4] J.M. Van Der Eijk, R.J.M. Nolte, V.E.M. Richters, W. Drenth, Polymeric model system for protein-bilirubin interaction, Biopolymers, 19 (1980) 445-448.

[5] A.J.M. Van Beijnen, R.J.M. Nolte, W. Drenth, A.M.F. Hezemans, Screw sense of polyisocyanides, Tetrahedron, 32 (1976) 2017-2019.

[6] J.J.L.M. Cornelissen, W.S. Graswinckel, A.E. Rowan, N.A.J.M. Sommerdijk, R.J.M. Nolte, Conformational analysis of dipeptide-derived polyisocyanides, Journal of Polymer Science Part A: Polymer Chemistry, 41 (2003) 1725-1736.

[7] M.M. Green, R.A. Gross, F.C. Schilling, K. Zero, C. Crosby, Macromolecular stereochemistry: effect of pendant group structure on the conformational properties of polyisocyanides, Macromolecules, 21 (1988) 1839-1846.

[8] C. Kollmar, R. Hoffmann, Polyisocyanides: electronic or steric reasons for their presumed helical structure?, J Am Chem Soc, 112 (1990) 8230-8238.

[9] J.J.L.M. Cornelissen, W.S. Graswinckel, P.J.H.M. Adams, G.H. Nachtegaal, A.P.M. Kentgens, N.A.J.M. Sommerdijk, R.J.M. Nolte, Synthesis and characterization of polyisocyanides derived from alanine and glycine dipeptides, Journal of Polymer Science Part A: Polymer Chemistry, 39 (2001) 4255-4264.

[10] C.M. Gowda, E.R.H. van Eck, A.M. van Buul, E. Schwartz, G.W.P. van Pruissen, J.J.L.M. Cornelissen, A.E. Rowan, R.J.M. Nolte, A.P.M. Kentgens, Direct Backbone Structure Determination of Polyisocyanodipeptide Using Solid-State Nuclear Magnetic Resonance, Macromolecules, 45 (2012) 2209-2218.

[11] J.J.L.M. Cornelissen, J.J.J.M. Donners, R. de Gelder, W.S. Graswinckel, G.A. Metselaar, A.E. Rowan, N.A.J.M. Sommerdijk, R.J.M. Nolte, β-Helical Polymers from Isocyanopeptides, Science, 293 (2001) 676-680.

[12] J.J.L.M. Cornelissen, PhD thesis: Polymers and Block Copolymers of Isocyanopeptides Towards Higher Structural Order in Macromolecular Systems in: PhD Thesis: Polymers and Block Copolymers of Isocyanopeptides Towards Higher Structural Order in Macromolecular Systems 2001.

[13] E. Schwartz, V. Palermo, C.E. Finlayson, Y.-S. Huang, M.B.J. Otten, A. Liscio, S. Trapani, I. González-Valls, P. Brocorens, J.J.L.M. Cornelissen, K. Peneva, K. Müllen, F.C. Spano, A. Yartsev, S. Westenhoff, R.H. Friend, D. Beljonne, R.J.M. Nolte, P. Samorì, A.E. Rowan, "Helter-Skelter-Like" Perylene Polyisocyanopeptides, Chemistry – A European Journal, 15 (2009) 2536-2547.

[14] E. Schwartz, E. Lim, C.M. Gowda, A. Liscio, O. Fenwick, G. Tu, V. Palermo, R. de Gelder, J.J.L.M. Cornelissen, E.R.H. Van Eck, A.P.M. Kentgens, F. Cacialli, R.J.M. Nolte, P. Samori, W.T.S. Huck, A.E. Rowan, Synthesis, Characterization, and Surface Initiated Polymerization of Carbazole Functionalized Isocyanides, Chemistry of Materials, 22 (2010) 2597-2607.

[15] P.A.J. de Witte, M. Castriciano, J.J.L.M. Cornelissen, L. Monsù Scolaro, R.J.M. Nolte, A.E. Rowan, Helical Polymer-Anchored Porphyrin Nanorods, Chemistry – A European Journal, 9 (2003) 1775-1781.

[16] E. Gomar-Nadal, L. Mugica, J. Vidal-Gancedo, J. Casado, J.T.L. Navarrete, J. Veciana, C. Rovira, D.B. Amabilino, Synthesis and doping of a multifunctional tetrathiafulvalene-substituted poly(isocyanide), Macromolecules, 40 (2007) 7521-7531.

[17] R.K. Harris, NMR crystallography: The use of chemical shifts, Solid State Sciences, 6 (2004) 1025-1037.

[18] D.H. Barich, R.J. Pugmire, D.M. Grant, R.J. Iuliucci, Investigation of the structural conformation of biphenyl by solid state 13C NMR and quantum chemical NMR shift calculations, Journal of Physical Chemistry A, 105 (2001) 6780-6784.

[19] J. Heller, D.D. Laws, M. Tomaselli, D.S. King, D.E. Wemmer, A. Pines, R.H. Havlin, E. Oldfield, Determination of dihedral angles in peptides through experimental

and theoretical studies of α-carbon chemical shielding tensors, J Am Chem Soc, 119 (1997) 7827-7831.

[20] G. De Paepe, B. Elena, L. Emsley, Characterization of heteronuclear decoupling through proton spin dynamics in solid-state nuclear magnetic resonance spectroscopy, J Chem Phys, 121 (2004) 3165-3180.

[21] B.J. van Rossum, H. Förster, H.J.M. de Groot, High-Field and High-Speed CP-MAS13C NMR Heteronuclear Dipolar-Correlation Spectroscopy of Solids with Frequency-Switched Lee-Goldburg Homonuclear Decoupling, Journal of Magnetic Resonance, 124 (1997) 516-519.

[22] A. Bielecki, A.C. Kolbert, M.H. Levitt, Frequency-switched pulse sequences: Homonuclear decoupling and dilute spin NMR in solids, Chemical Physics Letters, 155 (1989) 341-346.

[23] M.H. Levitt, A.C. Kolbert, A. Bielecki, D.J. Ruben, High-resolution 1H NMR in solids with frequency-switched multiple-pulse sequences, Solid State Nuclear Magnetic Resonance, 2 (1993) 151-163.

[24] D.J. States, R.A. Haberkorn, D.J. Ruben, A two-dimensional nuclear overhauser experiment with pure absorption phase in four quadrants, Journal of Magnetic Resonance (1969), 48 (1982) 286-292.

[25] J.D. van Beek, matNMR: A flexible toolbox for processing, analyzing and visualizing magnetic resonance data in Matlab®, Journal of Magnetic Resonance, 187 (2007) 19-26.

[26] A. Naito, S. Ganapathy, C.A. McDowell, 14N quadrupole effects in CP-MAS 13C NMR spectra of organic compounds in the solid state, Journal of Magnetic Resonance (1969), 48 (1982) 367-381.

[27] J. Herzfeld, A.E. Berger, Sideband Intensities in Nmr-Spectra of Samples Spinning at the Magic Angle, J Chem Phys, 73 (1980) 6021-6030.

[28] Y. Wei, D.K. Lee, A. Ramamoorthy, Solid-State 13C NMR Chemical Shift Anisotropy Tensors of Polypeptides, in, 2001, pp. 6118-6126.

[29] L. Odgaard, M. Bak, H.J. Jakobsen, N.C. Nielsen, 13C Chemical Shift and 13C-14N Dipolar Coupling Tensors Determined by 13C Rotary Resonance Solid-State NMR, Journal of Magnetic Resonance, 148 (2001) 298-308.

Chapter 5

Hydrogen Bonding AND Chemical Shift Assignments in Carbazole Functionalized Isocyanides from Solid-State NMR and First-Principles Calculations

Chandrakala M. Gowda, Filipe Vasconcelos, Erik Schwartz, Ernst R. H. van Eck, Martijn Marsman, Jeroen J. L. M. Cornelissen, Alan E. Rowan, Gilles A. de Wijs, and Arno P. M. Kentgens, *Physical Chemistry Chemical Physics 2011, vol. 13, pg. 13082–13095*

5.1 Introduction

Carbazole based materials are known for their favourable hole-transport and electroluminescent properties. The development of systems in which chromophores are ordered in a well-defined manner is of great interest for chemistry and material science.[1, 2] To achieve the ordering polyisocyanopeptides, are often used as framework for supporting the functional groups.[3] Recently, carbazole functionalized polyisocyanopeptides synthesized on silicon wafer surface to form a brush like patterned surface have shown to exhibit opto-electronic properties.[4] The AFM scanned morphology of the surface of these brushes is shown in Figure 5.1. However, the correlation of the function and physical properties with the conformation of these macromolecular chains is not well understood. In the solid state, molecular interactions such as hydrogen bonding and the weak interactions such as the aromatic σ- π/π–π interactions play significant role in defining and tuning the overall molecular arrangement and consequently the macroscopic properties of the material. We wish to obtain insight into structure, dynamics, and molecular interactions in the native state of the compound. Experimental studies combined with theoretical analysis have often helped in understanding the complex molecular behavior which otherwise cannot be accomplished by any of the techniques alone. Solid-state NMR ^{1}H and ^{13}C NMR chemical shifts of

powders combined with quantum mechanical calculations have enabled to predict crystal structures of molecular solids.[5] Theoretical assignments of solid-state NMR spectra from first-principles calculations (*ab-initio* or DFT) can be routinely used in solid-state NMR. Several methods are available to obtain chemical shift tensors of extended systems from periodical first-principles calculations. For example, the linear-response approach by Mauri et al.[6] and its GIPAW[7] (Gauge-Including Projector Augmented Wave) extension have been successfully applied to organic[8, 9] and inorganic crystalline materials[10, 11]. The recently introduced 'converse' approach, based on the modern theory of orbital magnetization[12], also permits to get accurate isotropic chemical shifts[13, 14]. These theoretical methods allow to unambiguously assign the chemical shifts in crystals to the NMR spectrum of a given compound. The approach also allows to quantitatively separate intra-molecular and inter-molecular interactions responsible for NMR parameters such as J-coupling and chemical shift.[15] For example, in a recent combined experimental and computational study the ability to quantify weak CH----X hydrogen bonding in uracil and 4-cyano-4′-ethynylbiphenyl *via* the calculated Nuclear Independent Chemical Shifts (NICS) was demonstrated.[9]

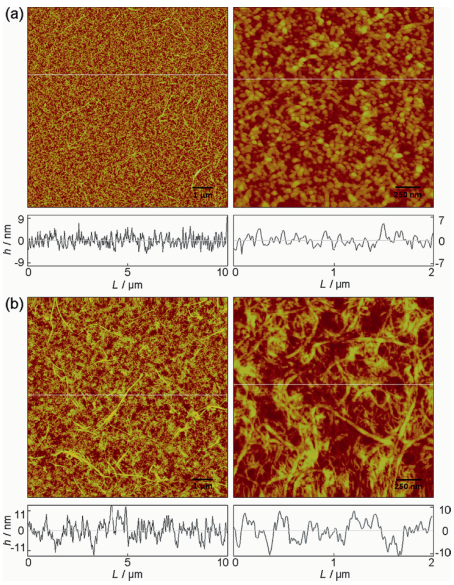

Figure 5.1 The AFM morphology of the carbazole polymer brushes grown on a silicon wafer with film thicknesses of (a) 9 nm and (b) 73 nm. (Figure adapted from reference 4)

In this chapter we use 1D cross polarization-magic angle spinning (CP-MAS), two-dimensional ^{1}H-^{13}C heteronuclear correlation and double-quantum single-quantum homonuclear correlation solid-state NMR spectroscopy for an in depth structural study of the crystalline isocyanide monomer bearing a carbazole moiety and its polymer. The experiments are combined with first-principles calculations of isotropic chemical shifts to assign all resonances in the spectra. We use the NICS approach to identify the structure stabilizing interactions in the crystal structure and also understand the influence of the molecular packing in the crystal structure on the chemical shift data observed in the NMR spectra. Finally, we extend the chemical shift analysis of the monomer to gain insight in the structural conformation of the polymer.

5.2 Methods

5.2.1 Synthesis and chemical structure of monomer (1) and polymer (2)

The molecular structure of monomer **1** and the carbazole functionalized polyisocyanide **2** is shown in Figure 5.2. The monomer was synthesized following a similar strategy to that described for the synthesis of perylene functionalized polymers as is described in.[4, 16] In short, an amine functionalized carbazole was coupled to Boc-L-alanine-OH. After removal of the Boc protecting group with acid, the amine was formylated and subsequently dehydrated using diphosgene and *N*-methylmorpholine. The isocyanide monomer was polymerized with 1 mol% $Ni(ClO_4)_2 \cdot 6H_2O$ in dichloromethane. After stirring for 5 minutes, the off-white precipitate was filtered off, washed with methanol and subsequently dried, offering **2** as a cream solid with satisfactory purity according to elemental analysis. The polymer was found to be insoluble in most common organic solvents. A detailed procedure for the polymer synthesis has been reported by Schwartz et al.[4] The monomer **1** crystal data shows that the crystal structure is orthorhombic, with space group *P*212121, and unit cell parameters of a = 9.0264(8), b = 9.9060(4), c = 16.8195(10) Å, α = 90, β = 90, γ = 90°. The experimental details of X-Ray crystallography and other crystal data such as the bond lengths and angles are also described in the publication by Schwartz et al.[4]

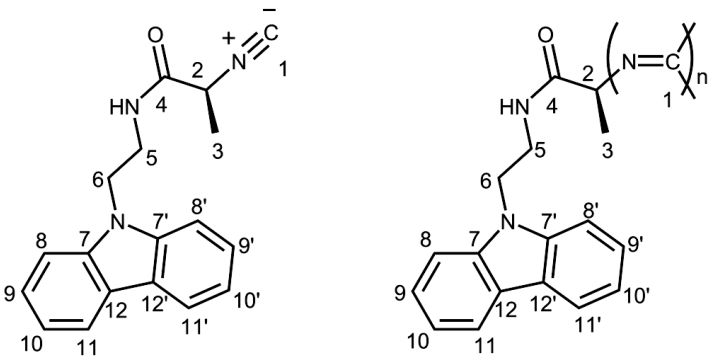

Figure 5.2 Isocyanoalanyl carbazole amide monomer **1** and polymer **2**. The positions are numbered for convenience in assignments. In the discussions below carbons will be referred to as C1, C2… and protons as H1, H2.... The NH proton is not numbered and will be designated as NH proton.

5.2.2 Solid-State NMR

Conventional one dimensional carbon spectra and two dimensional ^{1}H-^{13}C heteronuclear correlation and ^{1}H-^{1}H double quantum-single quantum correlations were recorded for the monomer 1 and the polymer 2. The 1D ^{13}C Cross Polarisation with Magic Angle Spinning (CPMAS) spectra of the monomer were recorded using a 4mm HXY MAS probe at a spinning speed of 7.3 kHz on a 7.05T Varian VNMRS system. The CPMAS spectrum of the polymer was obtained with a 4mm HXY probe at a MAS frequency of 14 kHz on a 14.1T Varian VNMRS system. A ^{1}H spinlock pulse of about 45 kHz was used for the cross polarisation. Two separate experiments with a short and a long CP contact time were recorded for the monomer 1 and the polymer 2. Two pulse phase modulation[17] (TPPM) decoupling at 78 kHz field strength was applied during acquisition in all cases. The spectra are referenced to the CH_2 carbon peak of adamantane at 38.48ppm.

Single pulse proton NMR spectra of the monomer 1 and polymer 2 were recorded at a MAS frequency of 40 kHz at 14.1T field using a Varian 1.6mm Fast-MAS probe.

2D ^{1}H-^{13}C heteronuclear correlation[18] spectra of the monomer 1 and the polymer 2 were recorded on a 9.4T Varian VNMRS system using a 3.2 mm probe with 12 kHz sample spinning speed. The CP contact time was 600 μs. Heteronuclear proton decoupling in the direct (^{13}C) dimension was achieved using TPPM proton decoupling and Frequency Switched Lee-Goldburg decoupling (FSLG)[19, 20] was applied in the indirect (^{1}H) dimension. For both sequences the RF field strength was 80 kHz, ^{1}H π/2 pulses of 3.1 μs were used. States[21] acquisition was done to achieve quadrature detection in the indirect dimension.

The 2D ^{1}H-^{1}H double quantum-single quantum correlation spectra were recorded at 18.8T with a Varian infinity+ console using a homebuilt double resonance probe equipped with a 1.8mm Samoson design stator. [22-25] The experiment was recorded at a magic angle spinning frequency of 40 kHz. The proton π/2 pulse length amounted to 2.3 μs in this case. For the detailed description and a more elaborate explanation of the pulse sequence used here, see Brinkmann et al.[24]

5.2.3 Chemical Shift Calculation

The calculation of NMR chemical shielding parameters for extended systems has recently undergone a new development with the so-called "converse" approach by Thonhauser et al.[13] It is fundamentally different from the other solid state methods that calculate the induced magnetic fields at the nuclear positions in response to an applied, uniform magnetic field within a linear response framework[6, 26]. In the converse approach the NMR shielding tensor $\sigma_{s,\alpha\beta}$ of a particular nucleus *s* is obtained from the total orbital magnetization $\mathbf{M}^{\mathrm{ind}}$ induced by a magnetic dipole $\mathbf{m}_s$ placed at the position of that particular nucleus, as

$$\sigma_{s,\alpha\beta} = -\Omega \frac{\partial M_{\beta}^{ind}}{\partial m_{s,\alpha}} \quad .$$

where $\boldsymbol{\alpha}, \boldsymbol{\beta} = \{\boldsymbol{x}, \boldsymbol{y}, \boldsymbol{z}\}$ are the Cartesian components and Ω the unit cell volume. Here a linear response treatment of the electronic states is circumvented. The ground state Bloch functions of the "perturbated" Hamiltonian, i.e. including the vector potential of the magnetic dipole $\mathbf{m}_s$, are calculated and their k-gradients are used to obtain the induced

orbital magnetization[12] which is a ground state quantity. This method can be applied in the framework of the GIPAW, where it is used to calculate a pseudopotential contribution to the shielding tensor. As for the linear response methods, also here a PAW[27] reconstruction in the core region is needed to obtained accurate shieldings. The complete derivation of this converse approach in the GIPAW framework was recently presented by Ceresoli et al.[14]

As the isotropic chemical shielding is given by the trace of the chemical shielding tensor ($\sigma_{iso} = \frac{1}{3}(\sigma_{xx} + \sigma_{yy} + \sigma_{zz})$), in general three calculations are needed (one for each direction of the applied magnetic dipole) to obtain the isotropic chemical shift. It is worth noting that experimental isotropic chemical shifts δ_{iso} and absolute isotropic chemical shielding σ_{iso} are related through the definition of an isotropic reference shielding σ_{ref} defined by $\delta_{iso} = \sigma_{ref} - \sigma_{iso}$. Experimentally the reference is set according to an external compound; in a theoretical approach it is more convenient to use a well-defined internal reference site. Here the recently implemented converse approach for crystals in the Vienna Ab-initio Simulation Package (VASP) is used for calculation purposes[28-32]. All the calculated values were obtained using the PBE[33, 34] functional for the exchange and correlation approximation. The norm-conserving PAW data sets used for the chemical shift calculation require a large kinetic energy cut-off on the plane wave basis set. In all the following calculations we used a cut-off of 1000 eV. For the reciprocal space integration, a 2×2×1 k-point grid was used for the monomer structure considering a single unit-cell whereas for the NICS calculations defined in a 2×2×1 supercell only one gamma centered k-point was considered. It is worth noting that the unit cell of the monomer **1** contains 156 atoms (440 electrons) and the super cell 624 atoms (1760 electrons). Although such calculations are not anymore really challenging for DFT, it is more difficult for a linear response calculation to converge when dealing with such big systems. Here the converse approach has shown to be very useful. A preliminary calculation on the experimental diffraction structure of monomer **1** shows large forces (~4 eV/Å) on several atoms. This was expected as the protons are known to be ill-resolved by diffraction techniques. Therefore we used energy minimization procedures to optimize the structures and reduced forces about two orders of magnitude**.** Two procedures were used for this aim: (i) only protons and (ii) all the atomic positions were optimized in a

fixed (experimental) simulation cell. These optimisations were carried out within PBE using standard ultra-soft PAW data sets. A cut-off energy of 400 eV and 2×2×1 k-point grid were used. Theoretical methods have the advantage that they can be used to calculate the chemical shift at any point in space. In the converse approach, this evaluation is easily performed by putting the perturbing magnetic moment in vacuum at any desired position. Thus one obtains the Nuclear Independent Chemical Shift (NICS). This quantity has been used extensively to quantify the aromaticity of organic molecules.[35] In section 4, it is described as to how it can be used to separate non-bonding and bonding contributions to the chemical shift in a molecular complex.

5.3 Results

5.3.1 One dimensional NMR experiments

Figure 5.4 shows the 1D ^{13}C CPMAS spectra of the monomer **1** and the polymer **2** recorded using the pulse sequence shown in Figure 5.3(a). In a CPMAS experiment, the magnetization transfer from protons to carbons depends on the strength of their dipolar coupling, which is inversely proportional to the cube of the distance between the two nuclei. The stronger the dipolar coupling, the more efficient the CP transfer is. This basic principle is used in identifying quaternary carbons of the molecules that lack directly bonded protons. Figure 5.4 shows the overlay of short (black) and long (red) CP contact time spectra of monomer **1** and the polymer **2**. The monomer **1** shows narrower lines since it is crystalline, whereas polymer **2** shows broad lines. The monomer **1** has 6 quaternary carbons that do not have a directly bonded proton (i.e. C1, C4, C7/C7', C12/C12'). These carbons rely on long distance transfer of magnetization and hence CP is less efficient resulting in weak or no signals when the CP contact time is short. The line at 24.3 ppm also shows a weak intensity in the monomer at short contact times, which allows an assignment to methyl (C3) as the fast methyl rotation around the symmetric axis of the CH_3 group partially averages dipolar interactions. The signals at 37.6 ppm and 42.2 ppm show broader peaks and strong CP transfer even at short contact times characteristic for CH_2 groups, and can therefore be identified as the C5 and C6 carbons. The line at 52.1 ppm is assigned to the CH (C2) carbon. These assignments are verified

by semi-empirical chemical shift assignment rules.[36] Indeed, the lines between 100 ppm and 135 ppm that are of the carbons in the carbazole ring, show extensive overlap making unambiguous assignment difficult in that region of the spectrum. The total number of lines does not exceed the number of carbon sites in one monomer unit, implying that the monomer crystal packing has one molecule per asymmetric unit of the unit cell. Figure 5.4(b) presents the ^{13}C CPMAS spectrum of the polymer **2**, which is clearly much less resolved than the monomer spectra. Moreover various lines are substantially shifted with respect to the monomer spectra. Nevertheless, many resonances are well separated and the assignments of the quaternary carbons, methyl carbon, cyano carbon and the C7/C7' can be done using the same considerations as for the analysis of the monomer **1** spectra. Figure 5.5 shows the fast-MAS (40 kHz) single pulse NMR spectrum of the monomer **1** and the polymer **2**. The methyl (H3) protons at 1.2 ppm in the monomer and 0.6 ppm in the polymer can be identified in both the spectra that are relatively narrow due to their fast CH_3 rotation. The broad profile of proton resonances arises due to large homonuclear dipolar couplings of protons that has not been fully averaged even at the 40 kHz MAS. As in the ^{13}C spectra, the proton lines of the monomer are narrower than those of the polymer. Obtaining individual proton shifts from such a broad profile is not straightforward; therefore, in order to facilitate the assignment of the protons and those of the carbons in the ring, ^{1}H-^{13}C heteronuclear correlation spectra and ^{1}H-^{1}H double quantum-single quantum correlation spectra were acquired.

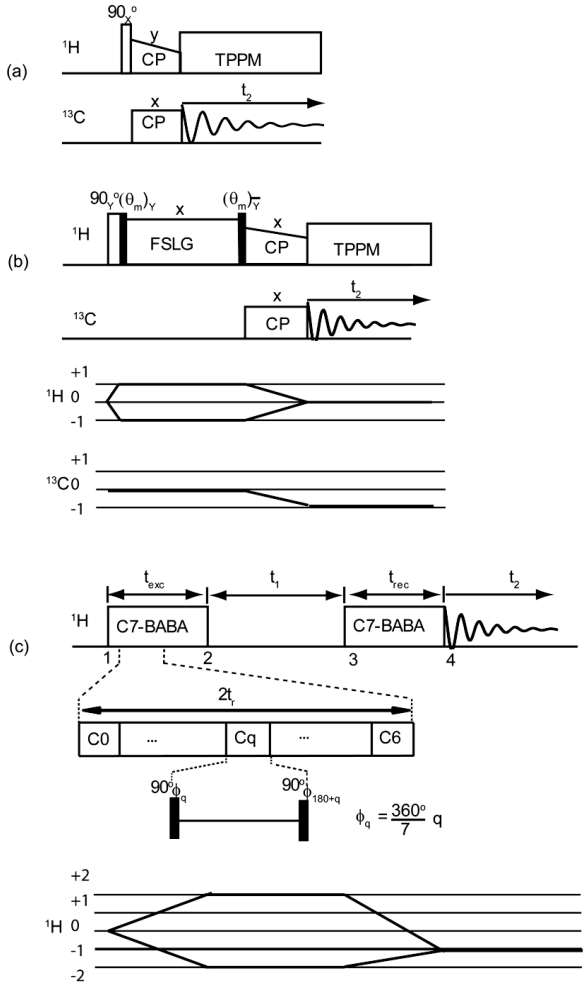

Figure 5.3 (a) CP pulse sequence with an RF amplitude ramp on the proton contact pulse used to obtain the CPMAS spectra shown in Figure 5.4. (b) Pulse sequence for the ^{1}H-^{13}C 2D correlation experiment. The θm pulses correspond to a proton flip angle of 54.74°. Phase sensitive detection in F1 was achieved using states method. The sequence is adapted from [18]. (c) Pulse sequence to obtain ^{1}H-^{1}H DQ-SQ correlation spectra. The C7-BABA DQ excitation block has phases ϕ_q as indicated in the figure which change for each ϕ_q block. The C7-BABA reconversion block has the phase ϕ_q+90 again changing for each of the ϕ_q blocks as indicated in the figure. The BABA basic element has two 90° pulses with phases shifted by 180°. Here we have used the complete 7 blocks of the C7-BABA element so as to take full advantages of the C7 symmetry. A TPPI acquisition is used for quadrature detection in the F2 dimension. The pulse sequence is adapted from[24].

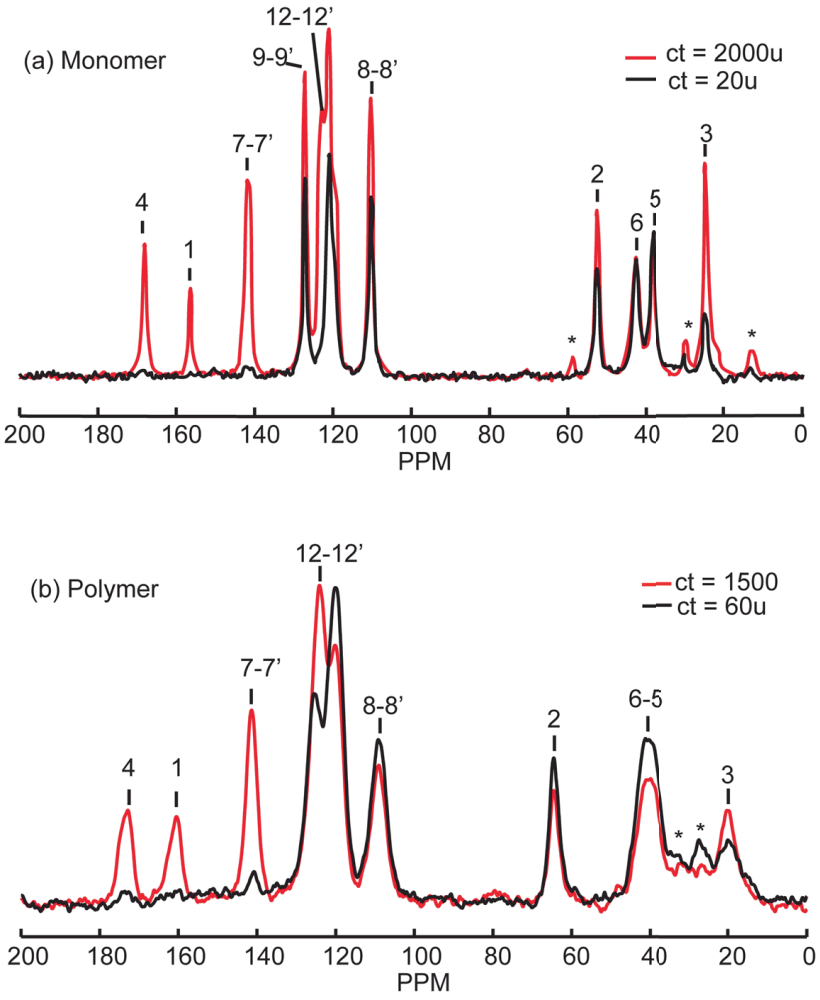

Figure 5.4. (a) CPMAS spectrum of monomer 1 obtained at MAS speed of 7.3 kHz at 7.05T field. (b) CPMAS spectrum of polymer 2 obtained at a speed of 14 kHz at 14.1T field. The two spectra show an overlay of a short and long CP contact time spectrum. Two pulse phase modulation (TPPM) decoupling of 78 kHz field strength was applied during acquisition in all the cases.

* spinning sidebands

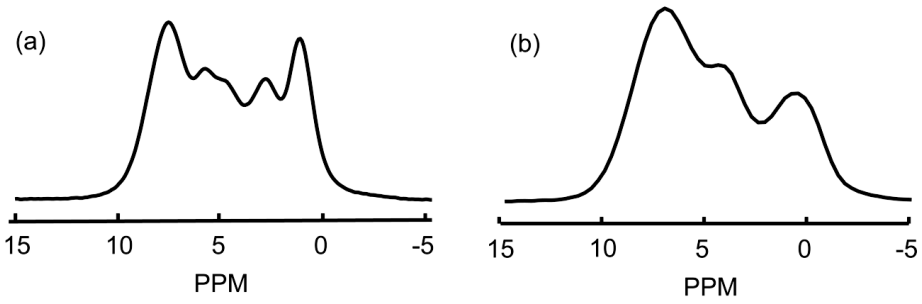

Figure 5.5. Single pulse excitation fast-MAS proton NMR spectrum of monomer 1 (a) and polymer 2 (b) recorded at a spinning speed of 40 kHz at a field of 14.1T.

5.3.2 Two-dimensional NMR experiments

A Heteronuclear Correlation

The ^{1}H-^{13}C heteronuclear correlation experiment shown in Figure 5.6 was acquired using pulse sequence shown in Figure 5.3b[18]. In the spectrum of the monomer **1**, shown in Figure 5.6a, a relatively long contact time of 600μs is used to also build up long range correlations between protons and carbons. This long range correlation is essential to obtain cross peaks for the quaternary carbons and to observe protons of the NH which are not directly bonded to a carbon. The carbonyl carbon C4 shows two long distance correlations in the spectrum one connecting to the methyl protons (H3) at 1.2 ppm and the other at 5.4 ppm is thought to originate from a contact to NH proton. The NH proton is significantly shifted upfield in comparison to the commonly observed 7-8ppm shift for NH protons in alanine residues in proteins, peptides or organic molecules.[37] The aromatic region of the spectrum is magnified and shown for clarity in the figure. At first glance, one can see that the proton and carbon peaks of the ring show doublet patterns for most lines, indicating that the primed and unprimed sites in the carbazole ring are not equivalent. There appears a set of protons between 4 - 6 ppm substantially shifted upfield compared to the usual range of chemical shifts of aromatic rings around ~7 ppm. The assignment of the C12 and C12' carbons as discussed earlier (Figure 5.4) enables the identification of the cross correlations C12-H11 and C12'-H11'. Red lines in the spectrum mark these correlations. With this we see that one of the protons H11/H11' has a chemical shift of 5.8 ppm whilst the other proton resonates at the usual aromatic

chemical shift value of 7.7 ppm. This is attributed to different ring current shifts experienced by the two halves of the carbazole unit related to the packing of the molecules in the unit cell (vide infra). The cross peak at (126.7 ppm, 4.8 ppm) identifies one of the two possible cross correlations C9─H10 or C9'─H10'. Both these correlations are marked with blue lines. This indicates that the protons H10 and H10' have chemical shifts of 4.8 ppm and 7.3 ppm, so again one of the protons experiences a significant upfield shift compared to the corresponding proton on the other ring of the carbazole unit. The carbon pairs C10/C10' and C11/C11' also show differences in chemical shifts. The long distance correlations C7─H8 and C7'─H8' are marked with green lines. A comparison of the peak widths in the ^{1}H dimension indicates that, although not resolved, the resonances of H9 and H9' also differ from each other, roughly to the same extent as that of H8 and H8' and hence are seen to be inequivalent. The assignments of the heteronuclear correlation spectrum prove that the two six member rings of the carbazole unit (marked by primed and unprimed numbers in Figure 5.2) are not equivalent.

The ^{1}H-^{13}C heteronuclear correlation spectrum of the polymer **2** is shown in Figure 5.6(b). Spectral assignment was done on a similar basis as that of the monomer. The broad lines prohibit unambiguous assignment of the peaks of the ring, however. The distinguishing feature of the polymer **2** is that there are no strongly upfield-shifted protons in the carbazole ring of the polymer. The carbonyl carbon (C4) shows cross correlation to the N─H protons at 8.1ppm, which in contrast to the monomer, is in the 'typical' regime for hydrogen bonded NH protons in alanines. The cross peak at (20.0 ppm, 0.6 ppm) shows the C3-H3 correlation. The two CH_2 correlations (C5-H5, C6-H6) overlap to a large extent with the poorly separated cross peaks appearing at (40.1 ppm, 3.7 ppm) and (41.4 ppm, 4.0 ppm). It is not possible to assign them uniquely to sites 5 and 6. The C2-H2 cross peak is at (64.5 ppm, 4.0 ppm). The assignments made are shown in Figure 5.6b.

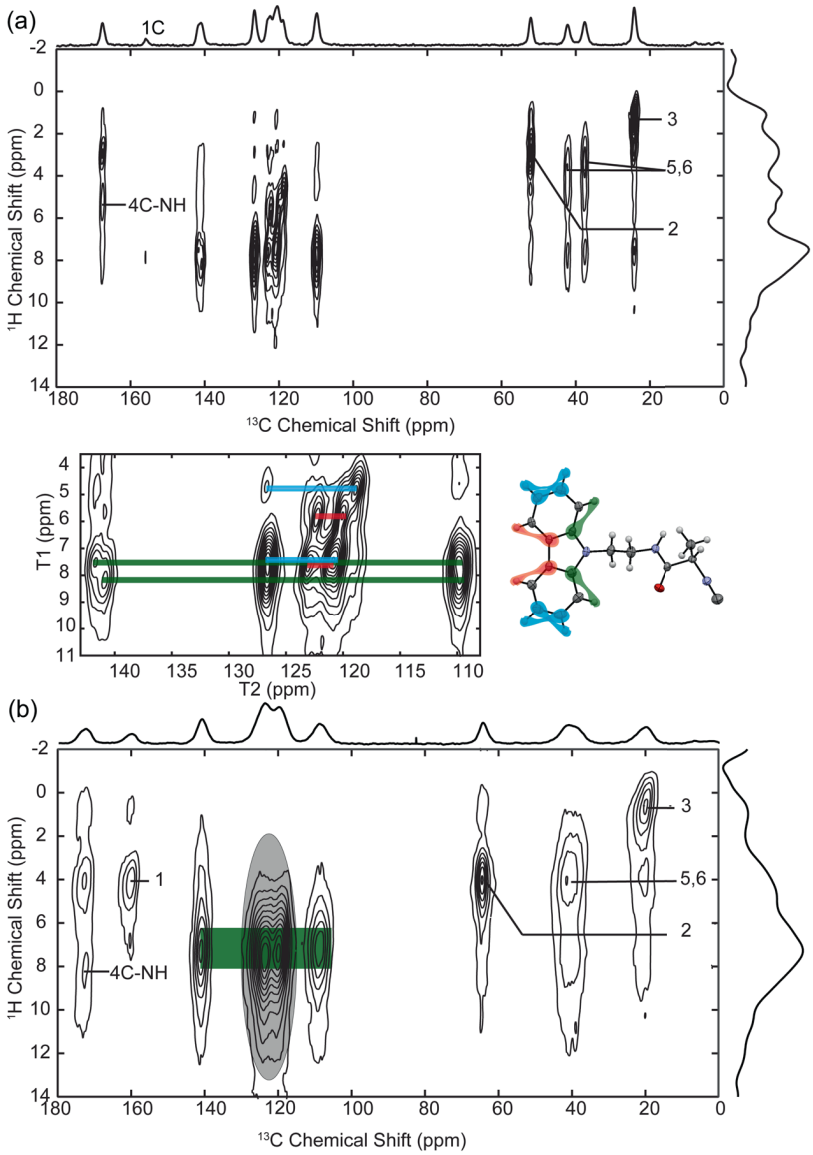

Figure 5.6 Heteronuclear correlation spectra of the monomer (a) and the polymer (b). In (a) The line at position (126.7ppm, 4.7ppm) indicates one of the two (H9-C10)/(H9'-C10') cross correlations. The cross correlations between various carbons and protons in the carbazole ring are illustrated with colors (see text). The cross correlations C8-H9, C8'-H9', C9-H8, and C9'-H8' are not shown for clarity. In (b) the shaded region in the polymer spectrum shows the unresolved correlations of the carbazole ring carbons and protons which includes the sites 9/9', 10 /10', 11/11' and 12/12'.

B Homonuclear 1H-1H Double Quantum-Single Quantum Correlation

In the analysis based on the heteronuclear correlation spectra discussed in the previous section, we cannot assign the protons and carbons of the carbazole unit unambiguously to either the primed or the unprimed sites of the carbazole rings. To remove this ambiguity a ^{1}H-^{1}H DQ-SQ correlation spectrum was recorded using the pulse sequence shown in Figure 5.3(c). In a DQ-SQ correlation spectrum dipolar coupled nuclei with chemical shifts f1 and f2 are excited to form double quantum coherences using a double quantum excitation pulse sequence block such as the C7 sequence using Back-to-Back(BABA) sequence as the basic element (Figure 5.3(c)). [24, 38] The double quantum coherences evolve with the sum frequency of the two coupled nuclei (f1+f2) during the evolution period t_1 and are then converted back to single quantum coherence using the same sequence phase shifted by 90^{o} with respect to the excitation block (between points 3 and 4 in Figure 5.3(c)). These single quantum coherences evolve at the respective frequencies f1 and f2 for each nucleus during the detection period t_2. This gives rise to cross peaks at (f1+f2, f1) and (f1+f2, f2) in a two dimensional spectrum. The selective observation of spatially proximal protons leads to less overlap of the spectral peaks, making assignments easier. Figure 5.7 shows the ^{1}H-^{1}H DQ-SQ correlation spectra of the monomer **1** and the polymer **2**. The monomer spectrum shows all short range intramolecular proton spin pairs along with a few intermolecular short range proton correlations. The H3-H3 correlations appear strong and is along the 'diagonal' (f1=2·f2) of the spectrum. The strong correlation of the protons at about 7ppm in the F2 and 14ppm in the F1 dimension establishes that the protons of one of the six member rings of the carbazole unit resonate around 7ppm. A very important contribution of this spectrum is the appearance of the cross peaks at (5.8, 10.4) and (4.8, 10.7) (indicated with blue line) which means that the protons with shifts of 5.8 ppm and 4.8 ppm lie spatially close to each other i.e., on the same ring. The intramolecular distances between two protons on the same ring, $d_{H10'-H11'}$ or $d_{H10-H11}$, is 2.32 A^{o} whereas the shortest intermolecular distance between these protons is at least $3.6A^{o}$. Thus the peak at 4.8 ppm can be assigned to H10' and 5.8 ppm to H11' protons (primed notation is chosen arbitrarily for the upfield shifted resonances). The protons H8' and H9' on the other hand do not show upfield shifted chemical shift values. The other intramolecular ^{1}H-^{1}H correlations are indicated with colored lines. Almost all nearest neighbour cross correlations such as the NH-H2/NH-H5(red), NH-H3(beige), H6-H8/H6-H8'(green), H9'-H10'(burnt umber), H5-H6(pink) and H2-H3(purple) are clearly seen as

well resolved peaks in the monomer spectrum. The protons in the carbazole ring that are not indicated with any color code appear in the broad region centered at ~ (7.7 ppm, 15.5 ppm). The cross peaks at (1.2 ppm, 8.7 ppm) and (7.4 ppm, 8.8 ppm) are due to the intermolecular correlations of the methyl (H3) protons with the protons of the carbazole unit of neighbouring molecules. Taking these assignments back to the ^{1}H-^{13}C heteronuclear correlation spectrum of Figure 5.6a makes it possible to assign the carbon resonances at 118.9 ppm, 120.0 ppm, 120.8 ppm and 120.9 ppm to C10', C11', C10 and C11 respectively. The protons and carbon chemical shifts for the sites 8/8', 7/7', 9/9', 5/6 in the monomer **1** cannot be uniquely assigned on the basis of the NMR data alone. However, understanding the interactions in the crystal requires the assignment of all resonances in the monomer unit of the crystal. To complete the assignments and to identify the unusual upfield shift of the NH proton and the inequivalence of the six member rings of the carbazole unit, bulk DFT calculations were performed as will be discussed in the next section.

The polymer ^{1}H-^{1}H DQ-SQ spectrum, Figure 5.7(b), although very broad and with less details, confirms the absence of upfield shifted ring proton resonances. This is significant as it can be used for the structural analysis of the side-chains orientation in the polymers which must be significantly different from the arrangement of the carbazole units in the monomer as will be discussed further below.

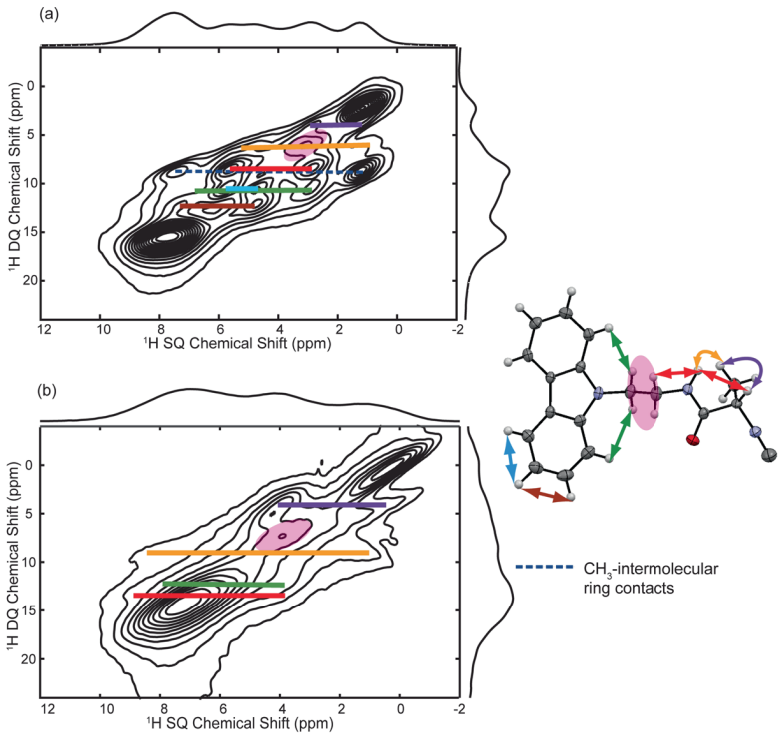

Figure 5.7 Double-Quantum Single-Quantum correlation spectra of the monomer 1 (a) and the polymer 2 (b). The spectra were recorded at 18.8T using a 40 kHz spinning speed. Double quantum excitation time of 50 ms was used in both the spectra corresponding to one complete cycle of the C7-BABA block and two rotational periods of the spinner. The cross peaks at (4.8ppm, 10.7ppm) and (5.8 ppm,10.4 ppm), indicated by the blue colored line, show that H10' and H11' are the upfield shifted protons in the monomer. The protons of the polymer ring do not show such upfield shifts.

5.4 DFT based assignments

Figure 5.8 presents the theoretical and experimental ^{13}C isotropic chemical shift correlation for the two energy minimization procedures of the XRD crystalline structure of monomer **1**. This figure uses the chemical shift assignments obtained from the 1D ^{13}C CPMAS, the 2D ^{1}H-^{13}C heteronuclear correlation and the ^{1}H-^{1}H DQ-SQ correlation experiments. An excellent correlation between the experimental and calculated values is observed. The calculation permits to completely remove any ambiguity in the carbon

assignment of the aromatic, CH_2, methyls and the cyano carbons. Of particular significance is the assignment of the H8/H8', H9/H9', C8/C8', C9/C9' C7/C7', H5/H6, C5/C6 which could not be resolved on the basis of the experimental data alone. When comparing the results of the two structure optimisations used (c.f. methods section), we see that the optimisation of all the atomic positions improves the linearity of the correlation. It is worth noting that the shift of the cyano carbon is clearly overestimated in this optimization procedure, which is attributed to an overestimation of the $^{-}C{\equiv}N^{+}$ bond length by DFT-PBE (~0.03Å). The optimization procedure improves the calculated carbon chemical shifts. Although no influence on the proton shifts was observed after optimization, in all the further calculations presented in this work only optimized structures were considered. Based on NMR experiments and DFT calculations we have been able to assign the carbon and proton chemical shifts of the monomer **1** and for the polymer **2**. The ^{13}C and ^{1}H chemical shifts of the monomer and the polymer are summarized in Table 5.1 and

Table 5.2 respectively. Solution state NMR chemical shifts of the monomer **1** in DMSO[4] solvent are also tabulated for comparison.

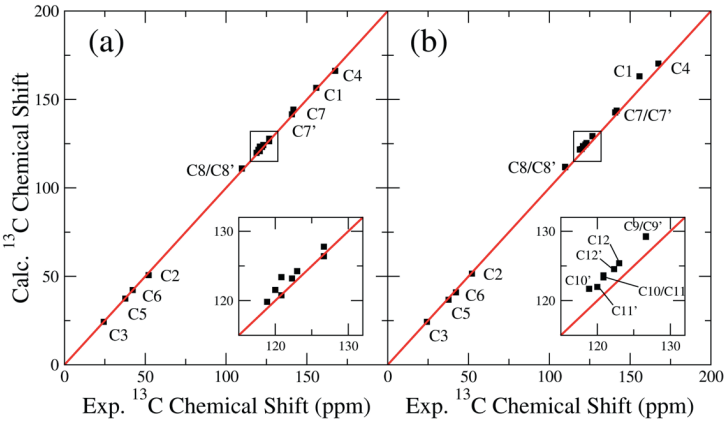

Figure 5.8 Experimental and calculated correlation of ^{13}C isotropic chemical shifts for two different crystal structures obtained by two different DFT energy minimization procedures: Starting from the XRD structure (a) only the protons or (b) all atoms were allowed to move. The inserts emphasises the carbazole ring carbons. The line represents the exact correlation between experimental and theoretical values. The internal chemical shift reference was set to the experimental value obtained for carbon C3.

Table 5.1 Experimental ^{13}C chemical shifts of the monomer 1 (in liquid and solid state) and polymer (solid state) together with the calculated chemical shifts referenced relatively to carbon site C3. (All values are in ppm).

Carbon site		monomer (liquid DMSO) δ_{exp}	monomer (solid) δ_{exp}	polymer (solid) δ_{exp}	Calculated monomer δ_{solid}
C1	C≡N	157.7	155.8	160.0	163.1
C2	CH	52.3	52.1	64.5	51.6
C3	CH3	19.2	24.3	20.0	24.3
C4	C=O	166.7	167.5	172.6	170.3
C5	CH2	38.4	37.6	40.1,41.4	36.8
C6	CH2	41.3	42.2	(overlapping)	41.0
C7/C7'	Ring	140.2	140.7/141.6	140.8	142.7/143.7
C8/C8'	Ring	109.1	109.8	108.6	111.7/111.9
C9/C9'	Ring	125.7	126.7		129.2/129.3
C10/C10'	Ring	118.9	120.8/118.9	123.6,119.8	123.6/121.7
C11/C11'	Ring	120.3	120.9/120.0	(overlapping)	123.3/122.0
C12/C12'	Ring	122.2	123/122.3	123.8	125.4/124.6

Table 5.2 Experimental ^{1}H chemical shifts of the monomer (in liquid and solid state) and polymer (solid state) together with the calculated chemical shifts referenced relatively to proton site H2. (All values are in ppm)

Proton site		Monomer (DMSO) δ_{exp}	Monomer (solid) δ_{exp}	Polymer (solid) (±0.2) δ_{exp}	Monomer δ_{solid} (calculated)
H3	CH3	1.21	1.2	0.6	1.0/0.9/0.6
H2	CH	4.25	2.7	4.0	2.7
H5	CH2	3.54	3.2	3.7,4.0	2.5/2.9
H6	CH2	4.49	3.6		4.3/3.5
H8	Ring	7.57	7.5	7.0 (broad lines)	7.2
H8'	Ring	7.57	8.1		8.5
H9	Ring	7.20	8.1		8.2
H9'	Ring	7.20	7.5		7.0
H10	Ring	7.45	7.3	7.1,7.2	7.4
H10'	Ring	7.45	4.8	(broad lines)	4.3
H11	Ring	8.14	7.7		7.5
H11'	Ring	8.14	5.8		5.3
NH	NH	8.37	5.4	8.1	5.6

5.5 Discussion

The chemical shifts listed in Table 5.1 show that protons and carbons in the carbazole unit of the monomer **1**, which are equivalent in the liquid state, exhibit significant differences in their chemical shift values in the solid state. Furthermore there are substantial changes in the chemical shifts of the protons and carbons at other chemical sites e.g. the NH proton, H10', H11', H2 and C3. These changes in the chemical shifts are to be expected as crystal packing effects are known to be extremely important in solid-state NMR. However, it is hard to interpret these experimental shifts through structural considerations, or even to attribute them to a specific interaction. Therefore, we make use of a theoretical approach to provide a way to distinguish which interactions are responsible for the observed crystal packing effects on the observed chemical shifts. Complementary to this chemical shift analysis, we discuss the relevant interactions individually using simple structural considerations and additional spectroscopic evidence.

5.5.1 Nuclear Independent Chemical Shift (NICS) approach

Crystal packing effects can be quantitatively understood by a theoretical solid-state approach. The intra-molecular and inter-molecular contributions can be separated by comparing the calculated shift values of an isolated molecule (δ_{mol}) with those obtained for the complete solid (δ_{solid}). The difference between these two quantities is a good estimation of the crystal packing effects. Local structural effects can be identified by comparing molecular calculations of the fully relaxed molecule (e.g. gas phase structure) and the molecule with the structural constraints found in the crystal.[15] We observed that such conformational contributions to the chemical shift are small in case of monomer **1**.

This simple comparison of molecular and solid-state chemical shift calculations underlines the importance of the bulk calculation to reproduce ssNMR observations. It is to be noted however, that this approach cannot reveal the nature of the intermolecular chemical shift contributions. Indeed, the chemical shift being an indirect probe it is influenced both by effects not related to intermolecular bonding (e.g. the ring-current fields arising from neighboring molecules) and by the intermolecular bonding itself (via the modified electronic structure of covalent bonds, H-bonds, van der Waals and even ionic bonds).

These two different contributions are quantitatively separated by evaluating the NICS at each nuclear position. If we consider a non-interacting molecular complex, the chemical shift of one site is given by the summation of two contributions: (i) the intra-molecular shift (δ_{mol}) and (ii) the shift induced at the site of the molecules by the neighboring molecules (δ_{NICS}) (with the molecule which belongs to this site removed). In case of an interacting system, the intra-molecular and induced shifts are not sufficient to describe the observed shifts in the interacting system (δ_{solid}), i.e. the solid state shifts in our case. The difference δ_{int} gives the specific contribution caused by the interactions between the molecules:

$$\delta_{\text{int}} = \delta_{solid} - (\delta_{mol} + \delta_{NICS})$$

This methodology is applied to analyze the ^{1}H chemical shifts of monomer **1.** The NICS values were obtained using the super-cell technique (i.e. removing one molecule out of the 2x2x1 supercell in real space) to prevent any interactions between the cavity created by the removed molecule and its images arising from the periodical boundary conditions. Also, for reliable comparison, each contribution of the interaction shift (molecule, bulk) has been calculated in the same super cell (see Figure 5.9) at the same level of convergence for the electronic structure (plane wave cut-off 1000 eV and Γ-point for the reciprocal space integration). For the calculation of δ_{int}, identical cutoffs and identical cells for the complete crystal, crystal with cavity and molecule has been used. All (virtual) atoms are kept at exactly the same positions. Thus, all calculations are carried with identical basis sets and small remaining errors due to interactions of the periodic images are removed. Table 5.3 shows the different molecular and NICS calculations (in absolute unreferenced values) for all ^{1}H sites of monomer **1** together with the previously defined solid-state contributions. From this the shifts resulting from interactions are calculated. We observe a considerable contribution of the crystal effect confirming the importance of a solid-state treatment for this system. For several of these protons the interaction contribution is rather small. For such sites, the crystal packing effect is completely given by the NICS, or in other words the chemical shifts are completely due to non-bonding interactions. For the H10' and H11' protons the shifts are attributed to large ring-current effects, according to the distance to the neighboring aromatic ring,

therefore the calculated NICS accounts for the crystal effect. For the other protons (H8', NH, H2, H3), the NICS analysis shows there must be a sizeable interaction contribution of ~1 ppm or more. For H8', the interaction contribution is attributed to the proximity of the cyano group (~2.7 Å), as the carbon of this group is negatively charged. In case of NH, H2 and H3, the local geometry permits us to attribute this interaction to the proximity of a CO group, revealing the hydrogen bond polarization of these protons to the neighboring molecule. For the other protons, the interaction contributions are non-negligible but more difficult to interpret in terms of precise electronic interactions between the neighboring molecules. It is worth noting that we checked convergence in the cutoff of the δ_{int} values comparing to values calculated at 800eV. For all relevant interactions (H8', NH, H2, H3) we observed changes of just 0.1ppm maximum. The largest difference of 0.3 ppm were observed for H5' and H9' for which the interactions are not discussed.

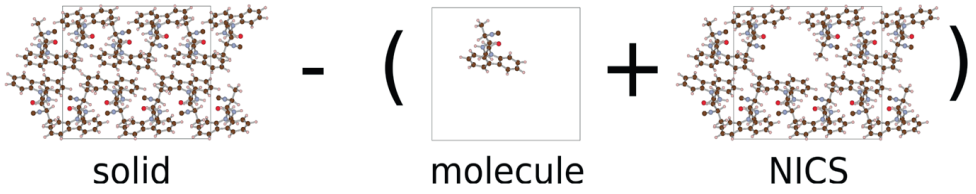

Figure 5.9 Schematic representation of the method used to reveal the interaction contributions to the observed chemical shifts. Each calculation is done in the same supercell (2×2×1) at the same level of accuracy for the electronic structure. (For visual convenience three molecules are removed in the NICS figure and of course only one molecule is removed for the actual calculation.)

Table 5.3 Calculated 1H isotropic chemical shifts of the monomer 1. Values for the solid, the molecule and the NICS are given in absolute chemical shift scale ($-\sigma_{iso}$). The crystal effect corresponds to the difference between the solid-state and the molecular calculation. The "interacting" contribution is defined by $\delta_{int} = \delta_{solid} - (\delta_{mol} + \delta_{NICS})$(see text). All values are given in ppm.

Label	δ_{solid}	$\delta_{molecule}$	δ_{NICS}	$\delta_{crystaleffect}$	$\delta_{interacting}$
H3	-22.6	-28.9	6.6	6.3	-0.3
H3'	-22.9	-28.9	6.4	6.0	-0.4
H3''	-23.1	-29.5	5.4	6.4	1.0
H2	-21.0	-26.5	4.6	5.5	0.9
H5	-21.2	-26.4	5.7	5.2	-0.5
H5'	-20.9	-27.7	6.6	6.8	0.2
H6	-19.4	-25.7	6.8	6.3	-0.5
H6'	-20.2	-26.7	6.0	6.5	0.5
H8	-16.5	-22.9	6.7	6.4	-0.3
H8'	-15.2	-23.4	6.4	8.2	1.8
H9	-15.5	-23.0	7.3	7.5	0.2
H9'	-16.8	-23.1	6.3	6.3	-0.0
H10	-16.3	-23.2	6.9	6.9	-0.0
H10'	-19.4	-23.2	3.8	3.8	0.0
H11	-16.2	-22.4	6.4	6.2	-0.2
H11'	-18.5	-22.4	4.2	3.9	-0.3
NH	-18.1	-24.9	5.2	6.8	1.6

5.5.2 N─H---O═C and C─H---O═C hydrogen bonding with Oxygen as common acceptor (Bifurcated hydrogen bond)

The crystal structure of the monomer **1** shows an array of molecules arranged to form a zigzag pattern of N─H---O═C and C─H---O═C bonds as shown in Figure 5.12. The presence of N─H and O═C groups often stabilize molecules such as proteins, macromolecules, organic and inorganic compounds by forming N─H---O═C hydrogen bonds whose strength varies from very weak to very strong.[39-41] The C─H---O=C

hydrogen bonding has been found to be a contributing factor in the stabilization of several molecular structures such as proteins and peptides and organic and inorganic molecules.[42-44] The hydrogen bonding motif as shown in Figure 5.12a, with the carbonyl oxygen accepting two protons, has been reported for protein structures and also in crystal structures of organic molecules.[39, 45] The strength of the hydrogen bonds formed depends on the geometrical parameters: (i) the hydrogen bond distance H----O, (ii) the distance D between the donor (C/N) and acceptor atoms (O) and (iii) the hydrogen bond angle ∠NHO/∠CHO. The survey of N─H---O═C hydrogen bonding moieties in organic crystals by Taylor et al. shows that the N─H protons have a tendency to lie close to the idealized oxygen lone pair directions.[39] The N---O distance (D) in the crystal structure of monomer **1** is 3.414 Å and the NH proton lies in the plane of C4─O─N─C2 (see Figure 5.12) with the hydrogen bonding angle ∠NHO of ~152^{o} and ∠C═O─H of 130^{o} (Figure 5.12b). The amide proton lies in the plane of the lone pair electrons of the oxygen and approaches the oxygen within 10^{o} of angular deviation from the lone pair direction. The C----O distance in the C─H---O═C linkage is 3.156 Å and ∠CHO is ~124^{o} (in-plane angle is 164^{o}). The C─H proton is inclined to the plane of C4─O─N─C2 by an angle of ~36^{o} (Figure 5.12c). The larger deviations in the angular parameters of the C─H proton in the C─H---O═C linkage indicates a weak hydrogen bonding for this proton. Geometrical studies of C─H---O═C hydrogen bonds have been reported and these studies show weak directionality exhibited by these hydrogen bonds.[46-48]

Usually, protons involved in hydrogen bonding are shifted downfield in an NMR spectrum. Therefore, it is expected that the C─H proton of monomer 1 would show a relative downfield shift if hydrogen bonded. We see from

Table 5.2 that the H2 proton of the monomer has a chemical shift of 4.25 ppm in solution and 4.0 ppm in the (solid) polymer. The H2 proton chemical shift of monomer **1** in the crystal structure is upfield shifted to 2.7 ppm, in contrast to our expectations. Along the same line for N─H---O═C hydrogen bonds the NH protons are known to have chemical shifts in the range of 8 ppm -10 ppm and higher. Chemical shifts of NH proton below 7 ppm range indicate weak or no hydrogen bonding.[49] The chemical shift of the N─H protons in the monomer **1** is shifted far up-field and has a value of only 5.4 ppm. Apparently, there seems to be a disagreement between the crystallographic data and the NMR chemical shifts. If we look at shift analysis (Table 5.3), however, we see indeed

positive (downfield) shift interaction contributions for the CH and NH protons, supporting the formation of C─H---O═C and N─H---O═C hydrogen bonds. This means that other non-interacting shift contributions such as ring current shifts from the neighboring carbazole rings are larger and therefore obscure the effects of hydrogen bonding when analyzing the spectra in a semi-empirical way. It can also be observed from Figure 5.12 that the N─H proton in the monomer is in close proximity of the $^{-}C{\equiv}N^{+}$─. To qualitatively understand the possible influence of the neighboring carbazole rings and the $^{-}C{\equiv}N^{+}$─ moieties on the N─H proton chemical shifts we consider the chemical shift pattern of some other protons that are in close proximity(intermolecular) to the $^{-}C{\equiv}N^{+}$─ moiety and the carbazole ring. The aromatic protons H8' and H8 are at a distance of 2.6Å and 3.2Å to the $^{-}C{\equiv}N^{+}$─ moiety making a ∠HC≡N angle of 165^{o} and 60^{o} respectively (see Figure 5.10). Assuming that the induced field profile of the $^{-}C{\equiv}N^{+}$─ moiety is similar (qualitatively) to that of a ─C≡C─ group, H8' is in the shielding region while the H8 is most likely in the deshielding region of the $^{-}C{\equiv}N^{+}$─ moiety (see Figure 5.10).[50] Similarly, equatorial positions and distances (≥3.45 Å) of the H8 and H8' w.r.t the neighboring carbazole rings highly indicate that both the protons lie close to the deshielding region of the neighbouring carbazole units (see Figure 5.11). The observed downfield shift of ~0.6 ppm for the H8' proton compared to H8 most likely results from the cumulative contribution of the deshielding due to the ring currents of the neighbouring carbazole unit, the shielding due to the $^{-}C{\equiv}N^{+}$─ moiety and the bonding interaction of H8' with the $^{-}C{\equiv}N^{+}$─ moiety(section 4.1). In the case of the N─H proton, the distance of the proton from the $^{-}C{\equiv}N^{+}$─ moiety is 2.7Å and the ∠HC≡N is 94^{o}. And, the distance of the proton from the neighbouring carbazole ring is 3.2Å and lies very close to the region directly above the plane of the ring (~0.9Å) (Figure 5.15c). Thus the N─H proton lies in the deshielding region of the $^{-}C{\equiv}N^{+}$─ moiety and in the shielding region of the aromatic ring. The rather upfield shift (by 3.0 ppm) of N─H proton and the downfield shift of H8' (by 0.6 ppm) show that influence of the ring currents of the carbazole unit are dominant over the influence of $^{-}C{\equiv}N^{+}$.

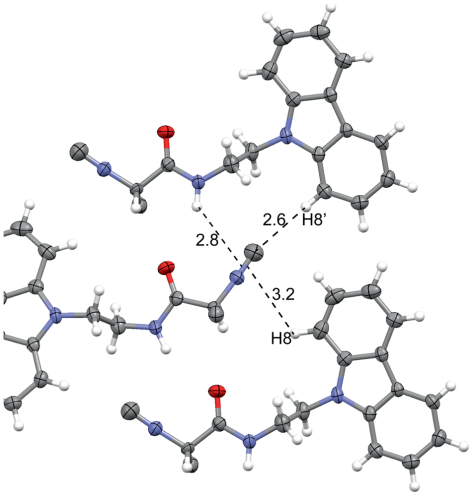

Figure 5.10 The position of H8, H8' and NH protons with respect to the $^{-}C{\equiv}N^{+}-$ group. The distances are in angstroms.

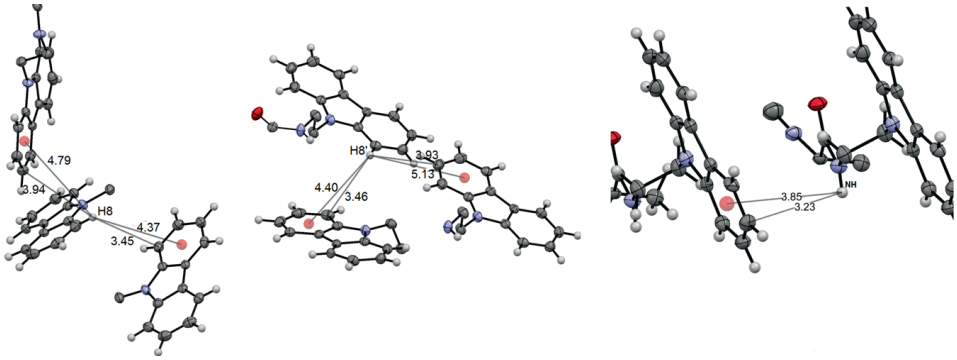

Figure 5.11 The position of H8, H8' and NH w.r.t the neighbouring carbazole rings.The distances are indicated in angstroms.

To further support the existence of hydrogen bonding in the monomer, Figure 5.13 shows the IR spectra of the monomer in the solid state[4]. The N─H stretch frequencies appear in the frequency range of 3000 cm^{-1} to 3600 cm^{-1} and the amide I frequency, comprising mainly the C═O stretch with an absorption near ~1620–1700 cm^{-1} are well studied in the literature and are known to be indicators of hydrogen bonding[51, 52] A free N─H stretch is commonly known to appear above ~3400cm^{-1} and a free amide stretch is known to appear in the range of ~1660-1700cm^{-1}. Strong hydrogen bonds show a large red shift in the N─H and C═O stretch frequencies giving rise to absorptions in low frequency region

of ~3200cm^{-1}-3370cm^{-1} and ~1620-1650 respectively.[51-54] The NH stretch frequency of 3377cm^{-1} of the monomer **1** lies in the weak bonding regime.[51] The broad width of the N─H stretch also suggests a N─H---O═C bonding. On the other hand, the amide I stretch frequency of 1683 cm^{-1} is indicative of a free C═O stretch as is widely seen in literature.[51, 53] It is highly intriguing and important to note that this frequency is identified extensively with amide-I stretching band of antiparallel-pleated β-sheets and recently also in β-sheets.[55, 56] We also compare this stretch frequency to related isocyanide i.e. L-Isocyanoalanyl-L-alanine methyl ester, which has strong N─H---O═C hydrogen bonds and has an amide-I stretch of 1669 cm^{-1}. [57] We further note that, a small red shift of about 5cm^{-1} in the amide-I stretch is observed in the solid-state as compared to the liquid state C═O stretch frequency in the monomer **1.**[4] The IR data therefore support the formation of weak hydrogen bonds in the monomer.

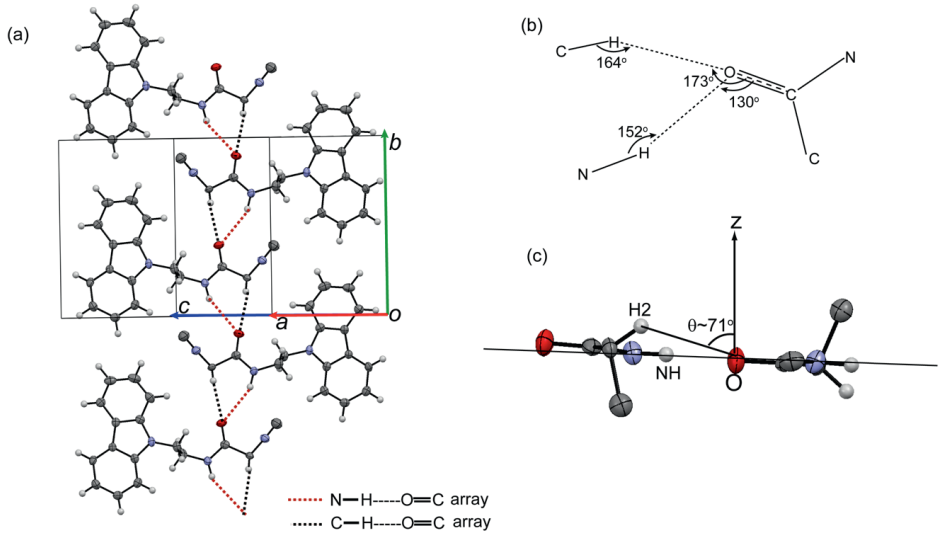

Figure 5.12 (a) Zig-zag array of C═O and N─H groups and C═O and C─H groups in the crystal structure of monomer 1(CH3 groups are hidden for clarity). (b) Top view of the N─H---C═O and C─H---C═O moiety. It shows the projections of atoms onto the C4-O-N-C2 plane of alanine. (c) Side view: θ is the polar angle subtended by H2 with the z- axis perpendicular to the C4-O-N-C2 plane at O. (only neighboring atoms near the atoms of interest are shown so as to not obstruct the view of the atoms involved in the bonding)

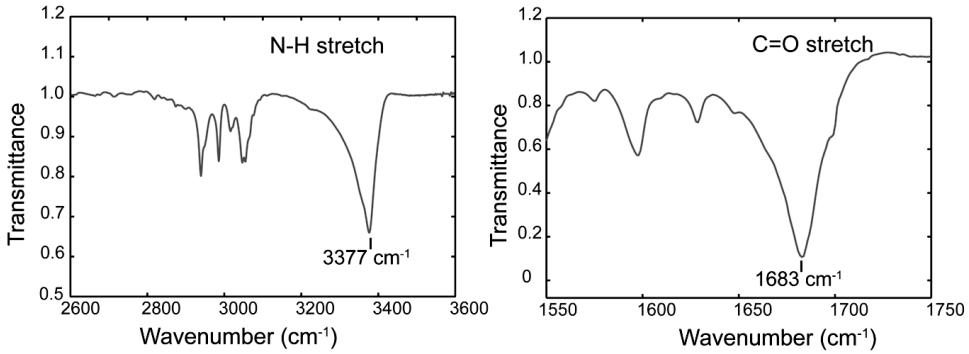

Figure 5.13 Infrared Spectrum of monomer **1** showing the N─H and amide I (C═O) stretch frequencies.

5.5.3 The σ-π/XH-π weak interactions

The monomer **1** crystal packing shows a herringbone type (T-shaped) arrangement of the molecules in the crystal as shown in Figure 5.15a. The view of the molecules shown in Figure 5.15b and Figure 5.15c show clearly that the protons H10', H11', H2 and NH lie in close proximity to the face of the π-rings. This suggests the σ–π interactions involving H10', H11' and H2 and the carbazole π systems. σ–π/XH-π interactions are known to stabilize several organic and inorganic compounds, biological molecules such as proteins, organo-metallic complexes, supramolecular systems, and host guest complexes.[58-61] Unlike hydrogen bonds, which can be strong, σ–π interactions are very weak.[62-64] Database studies of weak interactions use constraints on the distance and angular parameters of the atoms involved in σ–π/XH–π interactions which can be represented as shown in Figure 5.14.

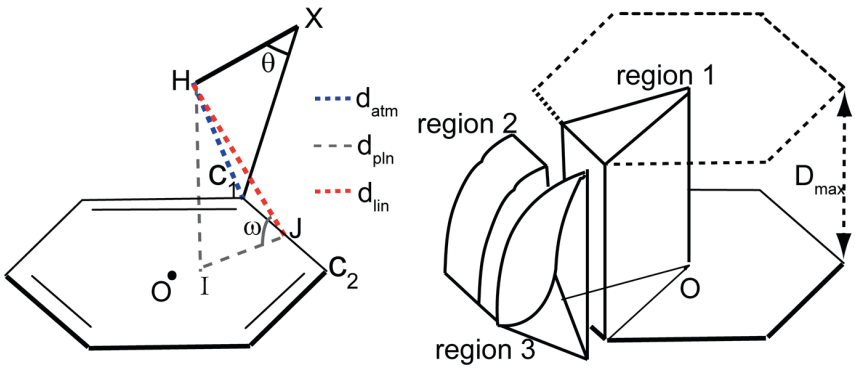

Figure 5.14 Pictorial representation of distance and angular constrains used in database searches of the σ–π/CH–π interactions. The figure is adapted from reference [65]. C_1 and C_2 are the nearest and second nearest atoms for X on the ring. The distance d_{atm} represents the distance of X from the nearest atom on the ring; d_{pln} represents the perpendicular distance of the X-H proton to the plane of the ring; d_{lin} represents the distance from X-H to the bond C_1C_2 (J is the centroid of C_1C_2). Proton position with respect to the ring is divided into region 1: region directly above the ring 2, region 2 and region 3 where H is outside region 1 and are positioned near the edge and the corner respectively. D_{max} is the distance used as cut off value to determine d_{pln}.

The distance and angle parameters for the H10', H11', H2 and NH protons in the monomer **1** are tabulated in Table 5.4. [65-67] A comparison of these parameters to the database studies done earlier strongly conjure the presence of σ–π/CH–π interaction involving the H10', H11', and H2 protons in monomer **1**. The chemical shifts of the protons H10', H11', H2 are upfield shifted in the monomer as compared to that of the solution state shifts and also in comparison to that of the polymer **2**. Upfield chemical shifts have been good indicators of σ–π/CH–π interactions in several molecular systems such as host guest complexes.[58, 60, 68, 69] Also with the geometrical parameters associated with N─H and ring P (Figure 5.15c) a N─H---π interaction is potentially possible. The 5.4ppm could thus have a contribution from the increased shielding due to the N─H---π interaction, though much weaker than the C─H---π interactions discussed earlier due to larger distances of separation in the former case. This possibly can explain the weak N─H---O═C hydrogen bonding despite the proximity of the N─H protons to the C═O groups and the feasible hydrogen bonding angle (∠NCO) of 155°.

Table 5.4 CH–π interaction relevant parameters of monomer **1** involving H10' and H11' protons as determined from the X-Ray crystal structure. All distances are in nanometers. In $\angle HCX_1$, X_1 corresponds to the nuclei on the ring with closest distance to the H. d_{pln} is the distance from H to the plane of the aromatic ring. d_{atm} is the distance from H to X_1. d_{lin} is the distance from H to the center of the line X_1X_2 where X_2 is the nuclei on the ring that is second nearest to H.[65]

Constraint	d_{pln} (nm)	d_{atm} (nm)	d_{lin} (nm)	$\angle HCX_1$(deg)
	<0.305	<0.305	<0.305	<60°
H10'	0.272	0.301	0.293	31.91°
H11'	0.290	0.302	0.298	39.5°
H2	0.288	0.299	0.295	20.43°
NH	0.316	0.326	0.340	67°

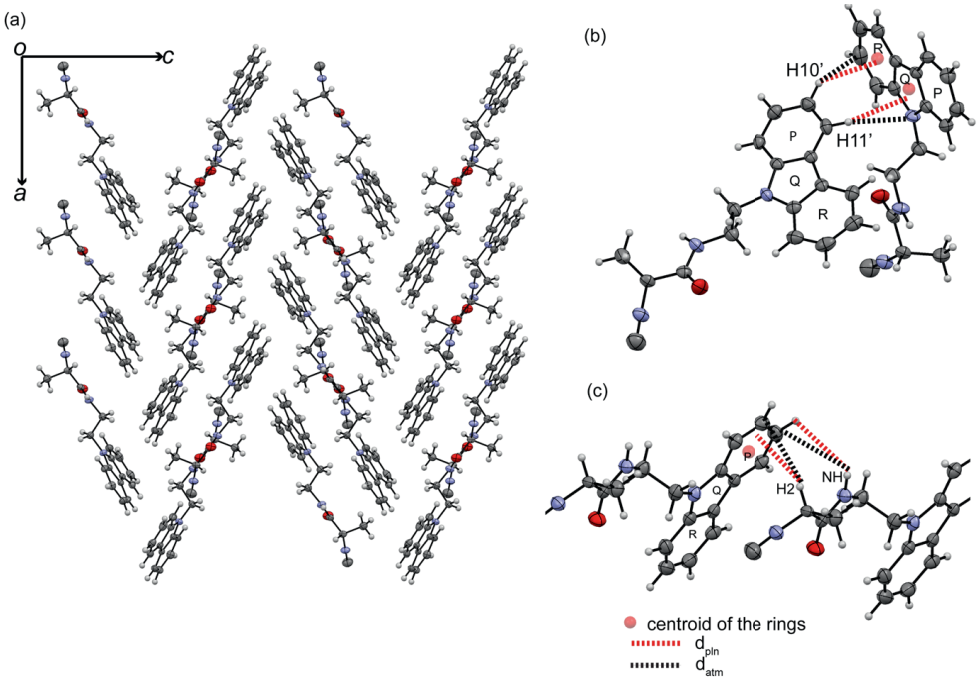

Figure 5.15. (a) Herringbone stacking of the molecules in the monomer 1 crystal structure. (b) The edge-to-face alignment of molecules (c) The H2 and NH proton orientation showing the proximity to the aromatic ring. For the d_{pln}, d_{atm} and other relevant distance and angular parameters see Table 5.4.

5.6 Chemical shift analysis of the polymer

The solid-state NMR chemical shifts of the polymer **2** are very broad showing large structural heterogeneity. Yet certain conclusions regarding the side chain conformations can be made by comparison of the polymer chemical shifts to those of the monomer. The T-shaped alignment of the molecules in the crystal packing induce upfield shifts for protons such as H10', H11', and H2. The H2 proton of the polymer has a chemical shift of 4.0 ppm, which is very similar to the chemical shift in the liquid state of the monomer **2**. This is expected as the carbazole units in the polymer face away from the backbone and hence aromatic interactions with the H2 proton are not possible. The key feature of interest is the interaction between the carbazole units. The proton chemical shifts of the carbazole unit of polymer **2** do not show any unusual upfield shifts, as shown in Figure 5.6 and Figure 5.7. This indicates that the aromatic interactions in the monomer crystal packing and the polymer are completely different. The edge-to-face (T-shaped) interactions of the carbazole rings are clearly absent in the polymer **2**. The carbonyl carbon chemical shifts are known to show a downfield shift when it is involved in N─H---O═C hydrogen bonding.[70, 71] The carbonyl carbon of the polymer **2** shifts downfield by a substantial magnitude of 5.1 ppm from that of the monomer **1**, and the N─H protons now appear at 8.1 ppm indicating N─H---O═C hydrogen bonding. These hydrogen bonds occur between different sidechains of the polymer close to the backbone so that they aid in stabilizing the (helical) backbone of the polymer **2**.

5.7 Conclusions

Complete and unambiguous ^{1}H and ^{13}C chemical shift assignment of the monomer **1** has been made using the combination of solid-state NMR and DFT calculations. This is the first herringbone type structure for which complete proton and carbon chemical shift assignments are made in the solid state. In view of the intriguing interplay of interactions leading to such structures this can aid in understanding the structure directing forces. The combined experimental and theoretical study has revealed multiple hydrogen bonding interactions in the monomer crystal. The NICS analysis clearly shows that the ─N─H, ─C─H and O═C moieties form a bifurcated hydrogen bond. The expected deshielding of the proton resonances in the bifurcated hydrogen bond is masked by ring current effects resulting from the aromatic units of the neighbouring molecules. On the basis of this

analysis we conclude that the crystal structure of monomer **1** is defined by two types of interactions. First is the array of N─H---O═C and C─H---O═C hydrogen bonding which gives the extended alignment of molecules (almost parallel to the molecular plane) in one dimension and the second is the weak σ-π interactions that give rise to the herringbone arrangement. The σ–π interactions however, are too weak to be detectable through the chemical shift data. In case of the polymer **2** the side chains are stabilized by an extended array of N─H---O═C hydrogen bonds present between two different sidechains. The absence of upfield shifts for the protons in the carbazole unit of the polymer proves that the carbazole moieties do not have a T-shaped alignment in the polymer. From literature, given that polyisocyanides form stable helical structures[3] it is most likely that the carbazole units in the side chains of the polymer **2** are reoriented to maximize π–π overlap. The rearrangement of the carbazole units in the polymer can be attributed to the steric hindrances due to the bulky carbazole groups in the side chains. Our study also shows that the semi-empirical interpretation of NH proton chemical shift as an indicator of hydrogen bonding runs into problems especially in scenarios where proton chemical shifts are influenced by ring currents etc. This study demonstrates that solid-state NMR data combined with advanced DFT calculations can be exploited to understand the structure stabilizing interactions in supra molecular systems and large bio-molecular assemblies.

The CIF file for the monomer **1** is available at the Cambridge Crystallographic Data Centre with the CCDC reference number 755663.

5.8 References

[1] J.M. Lehn, Toward self-organization and complex matter, Science, 295 (2002) 2400-2403.

[2] G.M. Whitesides, J.P. Mathias, C.T. Seto, Molecular Self-Assembly and Nanochemistry - a Chemical Strategy for the Synthesis of Nanostructures, Science, 254 (1991) 1312-1319.

[3] J.J.L.M. Cornelissen, J.J.J.M. Donners, R. de Gelder, W.S. Graswinckel, G.A. Metselaar, A.E. Rowan, N.A.J.M. Sommerdijk, R.J.M. Nolte, β-Helical Polymers from Isocyanopeptides, Science, 293 (2001) 676-680.

[4] E. Schwartz, et.al., Synthesis, Characterization, and Surface Initiated Polymerization of Carbazole Functionalized Isocyanides, Chemistry of Materials, 22 (2010) 2597-2607.

[5] E. Salager, G.M. Day, R.S. Stein, C.J. Pickard, B.n.d. Elena, L. Emsley, Powder Crystallography by Combined Crystal Structure Prediction and High-Resolution 1H Solid-State NMR Spectroscopy, Journal of the American Chemical Society, 132 (2010) 2564-2566.

[6] F. Mauri, B. Pfrommer, S. Louie, Ab initio theory of NMR chemical shifts in solids and liquids, Physical review letters, 77 (1996) 5300-5303.

[7] C. Pickard, F. Mauri, All-electron magnetic response with pseudopotentials: NMR chemical shifts, Physical Review B, 63 (2001) 245101.

[8] J.R. Yates, S.E. Dobbins, C.J. Pickard, F. Mauri, P.Y. Ghi, R.K. Harris, A combined first principles computational and solid-state NMR study of a molecular crystal: flurbiprofen, Physical Chemistry Chemical Physics, 7 (2005) 1402-1407.

[9] A.C. Uldry, J.M. Griffin, J.R. Yates, M. Perez-Torralba, M.D.S. Maria, A.L. Webber, M.L.L. Beaumont, A. Samoson, R.M. Claramunt, C.J. Pickard, S.P. Brown, Quantifying weak hydrogen bonding in uracil and 4-cyano-4 '-ethynylbiphenyl: A combined computational and experimental investigation of NMR chemical shifts in the solid state, Journal of the American Chemical Society, 130 (2008) 945-954.

[10] M. Profeta, F. Mauri, C.J. Pickard, Accurate first principles prediction of O-17 NMR parameters in SiO2: Assignment of the zeolite ferrierite spectrum, Journal of the American Chemical Society, 125 (2003) 541-548.

[11] N. Forler, F. Vasconcelos, S. Cristol, J.-F. Paul, L. Montagne, T. Charpentier, F. Mauri, L. Delevoye, New insights into oxygen environments generated during phosphate glass alteration: a combined 17O MAS and MQMAS NMR and first principles calculations study, Phys Chem Chem Phys, 12 (2010) 9053-9062.

[12] D. Ceresoli, T. Thonhauser, D. Vanderbilt, R. Resta, Orbital magnetization in crystalline solids: Multi-band insulators, Chern insulators, and metals, Physical Review B, 74 (2006) 24408.

[13] T. Thonhauser, D. Ceresoli, A. Mostofi, N. Marzari, R. Resta, D. Vanderbilt, A converse approach to the calculation of NMR shielding tensors, The Journal of Chemical Physics, 131 (2009) 101101.

[14] D. Ceresoli, N. Marzari, M. Lopez, T. Thonhauser, Ab initio converse NMR approach for pseudopotentials, Physical Review B, 81 (2010) 184424.

[15] S.A. Joyce, J.R. Yates, C.J. Pickard, S.P. Brown, Density functional theory calculations of hydrogen-bond-mediated NMR J coupling in the solid state, Journal of the American Chemical Society, 130 (2008) 12663-12670.

[16] E. Schwartz, Et.al., "Helter-Skelter-Like" Perylene Polyisocyanopeptides, Chemistry- A European Journal, 15 (2009) 2536-2547.

[17] A.E. Bennett, C.M. Rienstra, M. Auger, K.V. Lakshmi, R.G. Griffin, Heteronuclear decoupling in rotating solids, The Journal of Chemical Physics, 103 (1995) 6951-6958.

[18] B.J. van Rossum, H. Förster, H.J.M. de Groot, High-Field and High-Speed CP-MAS13C NMR Heteronuclear Dipolar-Correlation Spectroscopy of Solids with Frequency-Switched Lee-Goldburg Homonuclear Decoupling, Journal of Magnetic Resonance, 124 (1997) 516-519.

[19] A. Bielecki, A.C. Kolbert, M.H. Levitt, Frequency-switched pulse sequences: Homonuclear decoupling and dilute spin NMR in solids, Chemical Physics Letters, 155 (1989) 341-346.

[20] M.H. Levitt, A.C. Kolbert, A. Bielecki, D.J. Ruben, High-resolution 1H NMR in solids with frequency-switched multiple-pulse sequences, Solid State Nuclear Magnetic Resonance, 2 (1993) 151-163.

[21] D.J. States, R.A. Haberkorn, D.J. Ruben, A two-dimensional nuclear overhauser experiment with pure absorption phase in four quadrants, Journal of Magnetic Resonance (1969), 48 (1982) 286-292.

[22] P.K. Madhu, E. Vinogradov, S. Vega, Multiple-pulse and magic-angle spinning aided double-quantum proton solid-state NMR spectroscopy, Chemical Physics Letters, 394 (2004) 423-428.

[23] S.P. Brown, A. Lesage, B. Elena, L. Emsley, Probing Proton−Proton Proximities in the Solid State: High-Resolution Two-Dimensional 1H−1H Double-Quantum CRAMPS NMR Spectroscopy, Journal of the American Chemical Society, 126 (2004) 13230-13231.

[24] A. Brinkmann, V.M. Litvinov, A.P.M. Kentgens, Environmentally friendly flame retardants. A detailed solid-state NMR study of melamine orthophosphate, Magnetic Resonance in Chemistry, 45 (2007) S231-S246.

[25] A. Samoson, T. Tuherm, Z. Gan, High-Field High-Speed MAS Resolution Enhancement in 1H NMR Spectroscopy of Solids, Solid State Nuclear Magnetic Resonance, 20 (2001) 130-136.

[26] D. Sebastiani, M. Parrinello, A New ab-Initio Approach for NMR Chemical Shifts in Periodic Systems, The Journal of Physical Chemistry A, 105 (2001) 1951-1958.

[27] P.E. Blochl, Projector augmented-wave method, Physical Review B, 50 (1994) 17953.

[28] G. Kresse, J. Furthmüller, Efficiency of ab-initio total energy calculations for metals and semiconductors using a plane-wave basis set, Comput. Mat. Sci., 6 (1996) 15.

[29] G. Kresse, J. Hafner, Ab initio molecular dynamics for liquid metals, Phys. Rev. B, 47 (1993) 558.

[30] G. Kresse, J. Hafner, Ab initio molecular-dynamics simulation of the liquid-metal-amorphous-semiconductor transition in germanium, Phys. Rev. B, 49 (1994) 14251.

[31] G. Kresse, J. Furthmüller, Efficient iterative schemes for ab initio total-energy calculations using a plane-wave basis set, Phys. Rev. B, 54 (1996) 11169.

[32] G. Kresse, D. Joubert, From ultrasoft pseudopotentials to the projector augmented-wave method, Physical Review B, 59 (1999) 1758.

[33] J.P. Perdew, K. Burke, M. Ernzerhof, Generalized Gradient Approximation Made Simple, Phys. Rev. Lett., 77 (1996) 3865.

[34] J.P. Perdew, K. Burke, M. Ernzerhof, Erratum: Generalized Gradient Approximation Made Simple, Phys. Rev. Lett., 78 (1997) 1396.

[35] P. von Ragué Schleyer, C. Maerker, A. Dransfeld, H. Jiao, N. van Eikema Hommes, Nucleus-independent chemical shifts: a simple and efficient aromaticity probe, J. Am. Chem. Soc, 118 (1996) 6317-6318.

[36] ChemBioOffice 2008- CambridgeSoft Life Science Enterprise Solutions. http://www.cambridgesoft.com/software/ChemBioOffice/, in.

[37] Y. Suzuki, R. Takahashi, T. Shimizu, M. Tansho, K. Yamauchi, M.P. Williamson, T. Asakura, Intra- and Intermolecular Effects on 1H Chemical Shifts in a Silk Model Peptide Determined by High-Field Solid State 1H NMR and Empirical Calculations, The Journal of Physical Chemistry B, 113 (2009) 9756-9761.

[38] Y.K. Lee, N.D. Kurur, M. Helmle, O.G. Johannessen, N.C. Nielsen, M.H. Levitt, Efficient dipolar recoupling in the NMR of rotating solids. A sevenfold symmetric radiofrequency pulse sequence, Chemical Physics Letters, 242 (1995) 304-309.

[39] R. Taylor, O. Kennard, W. Versichel, Geometry of the imino-carbonyl (N-H...O:C) hydrogen bond. 1. Lone-pair directionality, Journal of the American Chemical Society, 105 (1983) 5761-5766.

[40] G.A. Jeffrey, An introduction to hydrogen bonding, Oxford University Press, New York ; Oxford, 1997.

[41] G.A. Jeffrey, W. Saenger, Hydrogen bonding in biological structures, Springer-Verlag, Berlin ; New York, 1991.

[42] G.R. Desiraju, T. Steiner, The weak hydrogen bond : in structural chemistry and biology, Oxford University Press, Oxford, 1999.

[43] G.R. Desiraju, Supramolecular Synthons in Crystal Engineering—A New Organic Synthesis, Angewandte Chemie International Edition in English, 34 (1995) 2311-2327.

[44] R. Vargas, J. Garza, D.A. Dixon, B.P. Hay, How Strong Is the Cα−H···OC Hydrogen Bond?, Journal of the American Chemical Society, 122 (2000) 4750-4755.

[45] G.F. Fabiola, S. Krishnaswamy, V. Nagarajan, V. Pattabhi, C-H...O hydrogen bonds in beta-sheets, Acta Crystallogr D Biol Crystallogr, 53 (1997) 316-320.

[46] T. Steiner, W. Saenger, Geometry of carbon-hydrogen.cntdot..cntdot..cntdot.oxygen hydrogen bonds in carbohydrate crystal structures. Analysis of neutron diffraction data, Journal of the American Chemical Society, 114 (1992) 10146-10154.

[47] G.R. Desiraju, The C−H···O Hydrogen Bond: Structural Implications and Supramolecular Design, Accounts of Chemical Research, 29 (1996) 441-449.

[48] R. Taylor, O. Kennard, Crystallographic evidence for the existence of CH.cntdot..cntdot..cntdot.O, CH.cntdot..cntdot..cntdot.N and CH.cntdot..cntdot..cntdot.Cl hydrogen bonds, Journal of the American Chemical Society, 104 (1982) 5063-5070.

[49] K. Yamauchi, S. Kuroki, K. Fujii, I. Ando, The amide proton NMR chemical shift and hydrogen-bonded structure of peptides and polypeptides in the solid state as studied by high-frequency solid-state 1H NMR, Chemical Physics Letters, 324 (2000) 435-439.

[50] R.G. Viglione, R. Zanasi, P. Lazzeretti, Are Ring Currents Still Useful to Rationalize the Benzene Proton Magnetic Shielding?, Organic Letters, 6 (2004) 2265-2267.

[51] W. Klemperer, M.W. Cronyn, A.H. Maki, G.C. Pimentel, Infrared Studies of the Association of Secondary Amides in Various Solvents, Journal of the American Chemical Society, 76 (1954) 5846-5848.

[52] D.T. McQuade, S.L. McKay, D.R. Powell, S.H. Gellman, Indifference to Hydrogen Bonding in a Family of Secondary Amides, Journal of the American Chemical Society, 119 (1997) 8528-8532.

[53] B. Kaczmarczyk, S. Danuta, Hydrogen bonds in poly(ester amide)s and their model compounds, Polymer, 36 (1995) 5019-5025.

[54] D.J. Skrovanek, S.E. Howe, P.C. Painter, M.M. Coleman, Hydrogen bonding in polymers: infrared temperature studies of an amorphous polyamide, Macromolecules, 18 (1985) 1676-1683.

[55] T. Miyazawa, E.R. Blout, The Infrared Spectra of Polypeptides in Various Conformations: Amide I and II Bands1, Journal of the American Chemical Society, 83 (1961) 712-719.

[56] J. Bandekar, S. Krimm, Vibrational analysis of peptides, polypeptides, and proteins: Characteristic amide bands of β-turns, Proceedings of the National Academy of Sciences of the United States of America, 76 (1979) 774-777.

[57] J.J.L.M. Cornelissen, W.S. Graswinckel, P.J.H.M. Adams, G.H. Nachtegaal, A.P.M. Kentgens, N.A.J.M. Sommerdijk, R.J.M. Nolte, Synthesis and characterization of polyisocyanides derived from alanine and glycine dipeptides, Journal of Polymer Science Part A: Polymer Chemistry, 39 (2001) 4255-4264.

[58] P. Soncini, S. Bonsignore, E. Dalcanale, F. Ugozzoli, Cavitands as versatile molecular receptors, The Journal of Organic Chemistry, 57 (1992) 4608-4612.

[59] G. Tarkanyi, P. Kiraly, S. Varga, B. Vakulya, T. Soos, Edge-to-face CH/pi aromatic interaction and molecular self-recognition in epi-cinchona-based bifunctional thiourea organocatalysis, Chemistry-a European Journal, 14 (2008) 6078-6086.

[60] P. Sozzani, A. Comotti, S. Bracco, R. Simonutti, Cooperation of multiple CH center dot center dot center dot pi interactions to stabilize polymers in aromatic nanochannels as indicated by 2D solid state NMR, Chemical Communications, (2004) 768-769.

[61] T. Steiner, G. Koellner, Hydrogen bonds with pi-acceptors in proteins: Frequencies and role in stabilizing local 3D structures, Journal of Molecular Biology, 305 (2001) 535-557.

[62] G.R. Desiraju, Hydrogen bridges in crystal engineering: Interactions without borders, Accounts of Chemical Research, 35 (2002) 565-573.

[63] O. Takahashi, Y. Kohno, S. Iwasaki, K. Saito, M. Iwaoka, S. Tomoda, Y. Umezawa, S. Tsuboyama, M. Nishio, Hydrogen-Bond-Like Nature of the CH/π Interaction as Evidenced by Crystallographic Database Analyses and Ab Initio Molecular Orbital Calculations, Bulletin of the Chemical Society of Japan, 74 (2001) 2421-2430.

[64] C.A. Hunter, J.K.M. Sanders, The nature of .pi.-.pi. interactions, Journal of the American Chemical Society, 112 (1990) 5525-5534.

[65] Y. Umezawa, S. Tsuboyama, H. Takahashi, J. Uzawa, M. Nishio, CH/[pi] interaction in the conformation of organic compounds. A database study, Tetrahedron, 55 (1999) 10047-10056.

[66] H. Suezawa, S. Ishihara, Y. Umezawa, S. Tsuboyama, M. Nishio, The Aromatic CH/pi Hydrogen Bond as an Important Factor in Determining the Relative Stability of Diastereomeric Salts Relevant to Enantiomeric Resolution - A Crystallographic Database Study, European Journal of Organic Chemistry, 2004 (2004) 4816-4822.

[67] H. Suezawa, T. Yoshida, Y. Umezawa, S. Tsuboyama, M. Nishio, CH/pi Interactions Implicated in the Crystal Structure of Transition Metal Compounds - A Database Study, European Journal of Inorganic Chemistry, 2002 (2002) 3148-3155.

[68] K. Kobayashi, Y. Asakawa, Y. Kikuchi, H. Toi, Y. Aoyama, CH-.pi. interaction as an important driving force of host-guest complexation in apolar organic media. Binding of monools and acetylated compounds to resorcinol cyclic tetramer as studied by proton

NMR and circular dichroism spectroscopy, Journal of the American Chemical Society, 115 (1993) 2648-2654.

[69] J. Dupont, P.A.Z. Suarez, R.F. De Souza, R.A. Burrow, J.P. Kintzinger, CH-π Interactions in 1-n-Butyl-3-methylimidazolium Tetraphenylborate Molten Salt: Solid and Solution Structures, Chemistry – A European Journal, 6 (2000) 2377-2381.

[70] Y. Wei, D.K. Lee, A. Ramamoorthy, Solid-State 13C NMR Chemical Shift Anisotropy Tensors of Polypeptides, in, 2001, pp. 6118-6126.

[71] K. Tsuchiya, A. Takahashi, N. Takeda, N. Asakawa, S. Kuroki, I. Ando, A. Shoji, T. Ozaki, Hydrogen-bonding effect on 13C NMR chemical shifts of amino acid residue carbonyl carbons of some peptides in the crystalline state, Journal of Molecular Structure, 350 (1995) 233-240.

Summary

Polyisocyanides are polymers consisting of repeat units of isocyanide monomer with a variable side chain group attached to each of the isocyanide unit. The side chain variation consisting of the alanyl-alanine dipeptide units were found to form highly stable, rod-like helical structures. It was proposed that inter-chain hydrogen bonds formed between the alanine moieties stabilized the backbone structure of the polymers. This imparted stability has in turn motivated substitution of the sidechains consisting of alanine units with functional moieties such as the carbazoles, porphyrins and pyridines etc. The polyisocyanides carrying functional groups have been shown to possess charge-carrying capabilities or to be optically active. Careful design and optimum structural modifications are essential for the efficient functioning of these polymers that will enable their use in diverse areas of applications.

The exact structure and conformation of polyisocyanides has been subject of discussions over many years. Several structural models have been proposed based on evidence from different analytical and theoretical methods. Due to lack of strong experimental evidence for the proposed models the debate regarding the actual conformation of these polymers persists. Attaching different chemical groups as side-chains influences the backbone conformation and the arrangement of the side-chains in the polymer. The experimental determination of the conformation of these polymers will help in the innovation of better and sophisticated materials. In this thesis we present the results that were obtained in the study of the poly(L-isocyanoalanyl-D-alanine methyl ester (L,D-PIAA) polymer, stereoisomers of the dipeptide polymer namely L,L-PIAA, D,L-PIAA and D,D-PIAA and also the carbazole-functionalized polyisocyanide using solid-state NMR techniques.

Two-dimensional solid-state NMR experiments such as the separated-local-field (SLF) and double-quantum single-quantum (DOQSY) spectroscopic methods have been used to obtain structural constraints in the poly(L-isocyanoalanyl-D-alanine methyl ester (L,D-PIAA). The backbone structure of the L,D-PIAA polymer is determined to be a 15_4 helix. The ^{1}H NMR chemical shifts of the amide protons in the sidechains show the presence of strong hydrogen bonding interactions between the alanine moieties of the n and n+4 side-

chains. The narrow lines of the carbon spectra of the polymer show that the polymer has a well-defined rigid structure.

The alanyl-alanine dipeptide moiety has two chiral centers leading to the formation of four stereoisomers namely LD, LL, DL and DD polymers. The isotropic chemical shift and chemical shift tensor analysis of the stereoisomers of the four stereoisomers of the polyisocyanodipeptide has enabled us to compare the similarities and differences in the structures. The high-resolution carbon and proton chemical shifts reveal that the different stereoisomers of the polyisocyanodipeptides exhibit similar backbone conformations. The structures of the enantiomeric polymers (L,D-PIAA and D,L-PIAA as well as the L,L-PIAA and D,D-PIAA) are identical to each other whereas the structures of the diastereoisomers(L,D/D,L-PIAA and L,L/D,D-PIAA) exhibit minor differences. The spectra of the polymers L,L-PIAA/D,D-PIAA seem to be show higher structural regularity compared to that of the L,D-PIAA/D,L-PIAA polymers. The sidechains in the L,D/D,L-PIAA show minor local structural irregularity. However the backbone conformation remains well defined and regular in all the stereoisomers of the polyisocyanodipeptides.

During the course of this study we realized that one of the limitations of studying these polymers by solid-state NMR is the low-sensitivity of the two-dimensional experiments even by solid-state NMR standards. We have provided a sensitivity enhancement technique by introducing the Hahn-solid-Hahn Carr-Purcell-Meiboom-Gill (HSHCPMG) echo acquisition that boosts the sensitivity of the experiments by approximately a factor of four. The spikelet spectrum acquired with optimum experimental setup preserves the angular information contained in the static spectrum.

Structure stabilizing interactions in the molecular structures of the carbazole functionalized isocyanides have been determined by combining experimental solid-state NMR experimental data with Density Functional Theory (DFT) based calculations. Array of bifurcated hydrogen bonds of N─H---O═C and C─H---O═C and the aromatic σ–π interactions are shown to coexist in the monomer crystal lattice of carbazoles. For the first time the high-resolution ^{1}H and ^{13}C chemical shifts have been provided for a herringbone lattice of the carbazole monomer. The chemical shift data help in understanding the packing of the functional moieties with aromatic entities in the polymer chains where the

X-ray diffraction analysis is not always possible. The carbazole functionalized polyisocyanopeptide is again shown to be stabilized by hydrogen bonds. However, the bulky aromatic groups influence the strength of the hydrogen bonding between the alanine moieties in the sidechains. The arrangement of the carbazole units in the polymer differ from that of the monomer crystal lattice as is shown by the ^{1}H NMR chemical shifts. The absence of T-shaped stacking in the polymer is convincingly proven. It is likely that the carbazole units in the side chains of the polymer reorient to form a face-to-face stacking to maximize π–π overlap.

As is clearly shown in this thesis, the structure of polyisocyanides can be determined accurately using solid-state NMR methods independent of the pendant groups used in the polymer. Chemical shift and CSA tensor analysis have enabled structural comparison of the various stereoisomers of the polyisocyanodipeptides. The study here shows that in the presence of bulky, functional groups the combined role of hydrogen bonding, steric interactions and aromatic interactions influence the overall structure of the functionalized polyisocyanides. Further studies of complex materials using similar approach will enable reliable structure elucidation that is pivotal for the design and synthesis of molecules with functionalities.

Samenvatting

Polyisocyanides bestaan uit een backbone gevormd door herhaling van isocyanide monomer eenheden met aan elke isocyanide een variabele zijketen gebonden. In de literatuur zijn de isocyanide polymeren veel bestudeerd door chemici en theoretici, omdat ze een stabiele en starre helixstructuur zouden vertonen. Er is uitgevonden dat de zijketenvariatie bestaande uit alanyl-alanine dipeptide eenheden stabiele, staaf-achtige structuren vormen. Er wordt gesteld dat de waterstofbruggen die worden gevormd tussen de alanine groepen van de verschillende ketens extra stabiliteit geven aan de backbone van de peptide-afgeleide polymeren. De gepostuleerde rigide helix structuur van de polymeren maakt ze interessant voor het ontwerp van innovatieve functionele materialen materialen. Polyisocyanodipeptiden gesubstitueerd met andere functionele groepen in de zijketens zoals carbazolen, porphyrines, en pyridines, hebben de mogelijkheid om een lading te dragen of zijn optisch actief. Polymeren met zulke zijketens hebben commerciele potentie als functionele materialen. Secuur ontwerp en optimale structuurmodificaties zijn essentieel voor het efficiënt functioneren van deze polymeren in een grote variëteit aan toepassingen.

De exacte structuur en conformatie van polyisocyaniden is gedurende vele jaren een onderwerp van discussie geweest. Er zijn diverse structuurmodellen voorgesteld op basis van verschillende analytische en theoretische methoden. Vanwege gebrek aan hard bewijs voor de voorgestelde modellen, blijft het debat over de conformatie van deze polymeren voortduren. Het inbrengen van verschillende functionele groepen aan de peptide zijketens, kan invloed hebben op de conformatie van de backbone en de organisatie van de zijketens in het polymeer. Het experimenteel bepalen van de conformatie van deze polymeren kan derhalve helpen bij de innovatie van betere en slimmere materialen.

In dit proefschrift presenteren we de resultaten die zijn verkregen uit vaste-stof NMR onderzoek aan polyisocyanodipeptides en carbazole-gefunctionaliseerde polyisocyanides. Er is gebruikt gemaakt van twee-dimensionale vaste-stof NMR technieken zoals "separated-local-field" (SLF) en "double-quantum single-quantum spectroscopy" (DOQSY) om de structurele randvoorwaarden voor de bepaling van de backbone-structuur in handen te krijgen. De op deze wijze vastgestelde backbone structuur van het poly(L-isocyanoalanyl-D-alanine methyl ester (L,D-PIAA) blijkt een 15_4 helix met waterstofbruggen tussen zijketenes n en n+4 te zijn.

De alanine dipeptide zijketens hebben twee chirale centra. Dit resulteert in de formatie van twee stereoisomeren, namelijk LD, LL, DL en DD polymeren. De structuren zijn in detail vergeleken door de analyse van de isotrope chemische verschuiving en de chemische verschuivingstensor van de stereoisomeren van de polyisocyanodipeptiden. Hoge resolutie metingen van de koolstof en proton chemische verschuivingen laten zien dat de backbone conformaties van de verschillende stereoisomeren van de polyisocyanodipeptiden gelijk zijn. De structuren van de enantiomere polymeren zijn gelijk, terwijl de structuren van de diastereoisomeren subtiele verschillen vertonen. We hebben laten zien dat de zijketens aan de buitenzijde, ver van de backbone, structurele onregelmatigheden vertonen, terwijl de backbone conformatie identiek is voor de vier stereo polymeren. De sterkte van de waterstofbruggen is kennelijk de voornaamste stabiliserende kracht en deze is, gebaseerd op de proton chemische verschuiving, vergelijkbaar in alle polymeren.

Een van de beperkingen voor het bestuderen van de eigenschappen van deze polymeren is de lage gevoeligheid van vaste stof NMR, in het bijzonder voor twee dimensionale experimenten die gebruik maken van multiple quantum coherenties. Daarom hebben we een methode ontwikkeld waarmee de gevoeligheid met een factor vier kan worden vergroot, namelijk de Hahn-solid-Hahn Carr-Purcell-Meiboom-Gill (HSHCPMG) echo. De resulterende toename in gevoeligheid die wordt verkregen door poeder spectra te beschrijven als een serie bijeenhorende smalle resonanties (spikelets) laat desondanks de bepaling van de volledige anisotrope informatie uit de NMR lijnvormen toe.

De interacties die de moleculaire structuur stabiliseren van carbazole gefunctionaliseerde isocyanides zijn bepaald door de combinatie van experimentele vaste stof NMR data en Density Functional Theory (DFT) berekeningen. Voor de eerste keer zijn hoge resolutie 1H en 13C chemische verschuivingen bepaald voor de visgraat organisatie van de moleculen van het carbazole monomeer. Deze data helpen in het begrijpen van de stapeling van functionele helften met aromatische entiteiten in de polymeerketens, wanneer röntgen diffractie analyse niet mogelijk is. We hebben laten zien dat de carbazole functionele polyisocyanopeptide wederom wordt gestabiliseerd door waterstofbruggen. Deze data suggereert een mogelijke face-to-face stapeling van carbazole eenheden in de polymeer ketens.

Zoals in dit proefschrift is beschreven kan de structuur van funtionele polyisocyanides uitstekend bepaald worden met behulp van vaste stof NMR methoden. Dit leidt tot een beter begrip van de structuur van de materialen in relatie tot hun functionaliteit en draagt zo bij aan het verbeteren van het ontwerp en de synthese van deze soort functionele materialen.

Curriculum Vitae

June 2012-present	Scientific Assistant at ETH Zurich, Switzerland.
June 2006-2011	PhD research in Physical Chemistry (NMR) Radboud University Nijmegen, The Netherlands.
2004- 2006	Project Assistant, NMR Research Center (SIF), Indian Institute of Science, Bangalore.
2003 –2001	Master of Science Degree (Physics), Christ College, Bangalore.
2001 – 1998	Bachelor of Science (Physics, Chemistry & Mathematics), St. Josephs's college of Arts and Science, Bangalore.

List of Publications

- Erik Schwartz, Eunhee Lim, **Chandrakala M. Gowda**, Andrea Liscio, Oliver Fenwick, Guoli Tu, Vincenzo Palermo, Rene de Gelder, Jeroen J. L. M. Cornelissen, Ernst R. H. Van Eck, Arno P. M. Kentgens, Franco Cacialli, Roeland J.M. Nolte, Paolo Samori, Wilhelm T. S. Huck, and Alan E. Rowan, *Synthesis, Characterization, and Surface Initiated Polymerization of Carbazole Functionalized Isocyanides* Chem. Mater. 2010, 22, 2597–2607 2597.

- **Chandrakala M. Gowda**, Filipe Vasconcelos, Erik Schwartz, Ernst R. H. van Eck, Martijn Marsman, Jeroen J. L. M. Cornelissen, Alan E. Rowan, Gilles A. de Wijs and Arno P. M. Kentgens, *Hydrogen bonding and chemical shift assignments in carbazole functionalized isocyanides from solid-state NMR and first-principles calculations.* Phys. Chem. Chem. Phys., 2011, **13**, 13082–13095

- **Chandrakala M. Gowda**, Ernst R. H. van Eck, Arend M. van Buul, Erik Schwartz, Gijsbrecht W. P. van Pruissen, Jeroen J. L. M. Cornelissen, Alan E. Rowan, Roeland J. M. Nolte, and Arno P. M. Kentgens, *Direct backbone structure determination of polyisocyanodipeptide using solid-state nuclear magnetic resonance*. Macromolecules 2012, vol. 45, pg. 2209−2218.

- **Chandrakala M. Gowda**, Vipin Agarwal and Arno P. M. Kentgens, *Sensitivity Enhancement of Double Quantum NMR Spectroscopy by modified CPMG,* Journal of Magnetic Resonance 2012, vol. 223, pg. 11-19

- **Chandrakala M. Gowda**, Ernst R.H. van Eck, Vipin Agarwal, Sander Weezenberg, Jeroen J. L. M. Cornelissen, Alan E. Rowan, Roeland J. M. Nolte, Arno P. M. Kentgens, *Structural insight to the stereoisomers of polyisocyanodipeptides using solid-state NMR chemical shift and tensor analysis*, Manuscript to be submitted

Acknowledgements

It is a pleasure to thank all those who made this thesis possible. I would like to express my deep gratitude to my supervisor, **Prof. Arno P.M. Kentgens,** for providing me an opportunity to work in your group. Thank you for the stimulating discussions and the guidance through my thesis work. The several projects I worked involved interesting and important questions to be answered in the world of polymers and I feel a sense of fulfillment in my PhD work.

Many thanks to **Dr. Ernst R. H van Eck** for your entire essential help with spectrometers, software programming and discussions through the projects.

My work in the NMR lab was impossible without the help of **Jan van Os, Gerrit Janssen and Hans Janssen**. "If something is broken-it can be fixed", was the valuable lesson I learned from them. When the technicians were on a vacation it was worry time for me!

Special thanks to **Dr. Andreas Brinkmann** for helping me with the phase cycling of some sequences, software related problems and explaining to me some of the NMR concepts.

I thank **Prof. Roeland J.M. Nolte, Prof. Alan Rowan and Prof. J.J.L.M Cornelissen** of the *Cluster for Molecular Chemistry* group for the fruitful collaboration with the study of polyisocyanides. Many thanks are also due to **Dr Gilles de Wijs** for nice collaboration with the hydrogen bond studies of the carbazole compounds.

I express my thanks to **Sjaak van Asten** for recovering my data from the crashed computer disk.

I extend my thanks to **Prof. K.V. Ramanathan** (Indian institute of science Bangalore) for encouraging me to pursue a career in the field of NMR.

I thank **Dr. Vipin Agarwal** for providing me with new ideas in the projects I did and providing broader and clearer insight into the research world. I thank you for the laborious and thorough manuscript reading, correcting, and rearranging you did for each of my papers.

The nice samples to work with were provided by **Dr. Erik Schwartz** and other PhD students form the cluster for Molecular Chemistry group. Erik, it was nice working with

you as not only you provided samples you also did excellent reviewing work with the manuscripts until the submission point. I appreciate it very much.

The five year long stay in Nijmegen was filled with fun and frolic and this is due to the wonderful and very cheerful friends in the lab. I thank Paul, Margriet, Ramon, Otmar, Mark, Kirsten, Agnieszka, Suresh, Gijs, Jorge (pronounced as GGORRGGE…it's the Mexican thing), Ard, Dennis, Mithun, Jacob, Anna-Jo for many NMR discussions and software related help. I thank prof. Sybren Wijmenga, Aafke, Frank, Jan van Bentum and the several master students who came and left the lab during my stay for their nice company during the coffee breaks. I thank Marian de With for being so helpful in making all the office related work go smooth. I express my gratitude to the two friends, Ramon and Margriet, who transformed the thesis 'summary' into 'samenvatting'. I also thank my friends Shoba, Nethra, Veena, Yogitha-Deepak, Partha, Deepak, Alokta, Chandan, Ashim, Rajashekar, Gautam, Pragnya, Pradnya, Sachin and many others for your company and fun time during my stay in Nijmegen. Finally I thank my family for being always there for me. My Mother and Father brought me up in a peace loving home and provided me a good education to the best of their abilities. I thank my sisters for their precious love and care. I would love to remember my nieces my nephews here who have given me the chance to live the childhood and teenage once again. Talking to them over the phone across the border was something I awaited every weekend. I thank my second family (my-in-laws) for their understanding, love and care. Lastly, I thank my husband, Vipin Agarwal, for being a loving and caring friend throughout.

Chandrakala Gowda